6-15-2011

Quantifying Multiple Types of Damping Acting on Bronze-Wound Guitar Strings

Jonathan Christian
Purdue University, christjw@purdue.edu

Graduate School ETD Form 9
(Revised 12/07)

PURDUE UNIVERSITY
GRADUATE SCHOOL
Thesis/Dissertation Acceptance

This is to certify that the thesis/dissertation prepared

By Jonathan Wesley Christian

Entitled
Quantifying Multiple Types of Damping Acting on Bronze-Wound Guitar Strings

For the degree of Master of Science

Is approved by the final examining committee:

Richard M. French
Chair

Nancy L. Denton

Nicholas J. Giordano

To the best of my knowledge and as understood by the student in the *Research Integrity and Copyright Disclaimer (Graduate School Form 20)*, this thesis/dissertation adheres to the provisions of Purdue University's "Policy on Integrity in Research" and the use of copyrighted material.

Approved by Major Professor(s): Richard M. French

Approved by: Gary R. Bertoline 06/15/2011
Head of the Graduate Program Date

Graduate School Form 20
(Revised 9/10)

PURDUE UNIVERSITY
GRADUATE SCHOOL

Research Integrity and Copyright Disclaimer

Title of Thesis/Dissertation:

Quantifying Multiple Types of Damping Acting on Bronze-Wound Guitar Strings

For the degree of Master of Science

I certify that in the preparation of this thesis, I have observed the provisions of *Purdue University Executive Memorandum No. C-22,* September 6, 1991, *Policy on Integrity in Research.**

Further, I certify that this work is free of plagiarism and all materials appearing in this thesis/dissertation have been properly quoted and attributed.

I certify that all copyrighted material incorporated into this thesis/dissertation is in compliance with the United States' copyright law and that I have received written permission from the copyright owners for my use of their work, which is beyond the scope of the law. I agree to indemnify and save harmless Purdue University from any and all claims that may be asserted or that may arise from any copyright violation.

Jonathan Wesley Christian

Printed Name and Signature of Candidate

06/15/2011

Date (month/day/year)

*Located at http://www.purdue.edu/policies/pages/teach_res_outreach/c_22.html

QUANTIFYING MULTIPLE TYPES OF DAMPING ACTING ON BRONZE-WOUND GUITAR STRINGS

A Thesis

Submitted to the Faculty

of

Purdue University

by

Jonathan W. Christian

In Partial Fulfillment of the

Requirements for the Degree

of

Master of Science

August 2011

Purdue University

West Lafayette, Indiana

ACKNOWLEDGEMENTS

I would like to thank all of those who have supported this study and have encouraged me during my graduate work. I would like to thank my committee members Dr. Mark French, Dr. Nick Giordano, and Professor Nancy Denton for their valuable time and advisement throughout my graduate and undergraduate work. I would especially like to thank my chair Dr. Mark French for inspiring me as a sophomore to think critically and for bringing my coursework to life. Thank you for answering my stream of endless questions and for advisement in my career pursuit and in married life as well.

I would also like to thank Fan Tao and Ray Keogh of D'Addario strings for their support of this research. Thanks also go out to Christopher Wiegandt, Shawn Kleinpeter, Gail Guynn, and Tom Rohm of Faurecia Emissions Control Technologies in their flexibility and support as I finish my thesis before beginning employment there. I look forward to being in Columbus soon.

I would like to thank my amazing wife for her patience, love, and support as I finished my graduate work. Thank you for listening to me ramble about technical things and for chuckling when I made engineering jokes that I knew weren't that funny. Thank you to my parents who gave me every opportunity to succeed and for supporting me in the choices I made. Thank you also to my soon-to-be-born son for being a motivating factor to finish my work quickly so I can spend time getting to know you. Praise be to God for giving me life each day and the ability to comprehend the wonderful universe He created.

TABLE OF CONTENTS

LIST OF FIGURES

Figure Page

LIST OF TABLES

ABSTRACT

Christian, Jonathan W. M.S., Purdue University, August 2011. Quantifying Multiple Types of Damping in Bronze-Wound, Steel Guitar Strings. Major Professor: Mark French.

The goal of this study was to quantify the contributions of multiple damping types acting on guitar strings for each mode over a wide frequency range so that design variables could be identified to one day create frequency based damping in guitar strings. Structural dynamic testing was used to obtain the time-response of a vibrating string in open air and in a vacuum. From this signal, each harmonic was filtered and the decay envelope was curve-fitted with a function that was a linear summation of decay functions. From the curve-fits, the damping coefficients for aerodynamic, friction, and material damping were calculated and used in the equation of motion for a single degree-of-freedom spring-mass-damper system.

The curve-fit and the spring-mass-damper model were primarily sensitive to the aerodynamic damping parameter, which allowed the other damping parameters to take on a wide range of values, some of which contradicted the laws of physics. The curve-fit and model response was more representative of mathematical convenience rather than physical relevance, as both were influenced by the summation effect of the multiple damping functions. This method shows promise in its analytical simplicity; however, future areas of study are outlined so that this method may be further refined before being used in industry.

CHAPTER 1. INTRODUCTION

1.1. Overview

To a musician, damping is arguably one of the most important aspects to a vibrating guitar string; however, very little research has been done to identify and quantify the individual contributions of multiple types of damping that affect a string's dynamic response. This chapter provides an overview of the background and significance of the research performed, as well as an outline of the research's focus.

1.2. Scope

Damping is responsible for dissipating energy in a vibrating system and prevents perpetual oscillation and infinite amplitude response. While a high amount of damping may be preferred in some mechanical systems, this is not the case in the field of musical acoustics. For guitar strings, ideally there would be no damping. While this is not physically possible, the primary goal of guitar string makers is to minimize the amount of damping in their strings.

Damping in guitar strings comes from a variety of mechanisms, some of which are linear and some of which are non-linear. The amount of energy lost per cycle of oscillation can be dependent on the frequency, mode, velocity, displacement, amplitude, temperature, stress levels, or time (Beards, 1996). The energy loss mechanisms occur not only on the macro scale, but also on the atomic scale.

The current methods used to measure damping in guitar strings only measure the resultant damping, which reflects the contributions of all types of damping. Little research has been done to experimentally isolate and quantify the

individual contributions of multiple types of damping acting simultaneously on guitar strings. This study identifies and quantifies the contributions of material, fluid, and friction damping in bronze-wound, steel guitar strings across a wide frequency range.

1.3. Significance

With the advances in manufacturing processes and dynamic measurement tools, a question now being asked in the guitar string manufacturing industry is, “Can the damping in a guitar string be ‘tuned’?” More specifically, “Can a guitar string be made in a way such that energy loss in general, or at specific frequencies, can be controlled and minimized?” Positive answers to these questions would profoundly impact the guitar string industry. The differences between newly engineered strings and traditional strings would be significant. The decay times and overtones heard from strummed chords would be noticeably different, potentially changing the overall tone of the guitar.

In order to adjust design variables that would precisely control the damping in a wound guitar string, manufacturers must have an accurate understanding of which type of damping is dominant at a given frequency. The inspiration for this study comes from comparing two similar types of bronze-wound, steel guitar strings. The first type of string is wound with a brass wrap-wire consisting of 80% copper and 20% zinc, while the wrap-wire of the other string is made of 90–92% copper and 8–10% tin. Both strings have the same overall diameter and the same core-wire, but musicians have commented that the string with 20% zinc wrap-wire sounds brighter than the other string. The word “brighter” implies that this string is perceived to have less damping in the higher harmonics than the other string. This comparison gives the first hint at the possible results of being able to control damping in a guitar string. This study takes an in-depth look at the influences of several types of damping in wound guitar strings in order to provide insights as to what design variables can someday be altered to provide controlled damping.

1.4. Research Question

The primary research question for this study is:

1. Can structural dynamic testing and optimization techniques be used to quantify the individual contributions of multiple types of damping acting simultaneously on bronze-wound guitar strings?

1.5. Assumptions

The following assumptions are made in this study:

1. The impedance at the boundaries of the guitar string fixture is high enough such that there are no energy losses.
2. The steel guitar string fixture causes negligible change in magnetic field produced by the magnetic pickup.
3. Friction damping caused by the string rubbing on the boundaries, on the nut and the saddle, are assumed to be negligible.
4. Temperature fluctuations in the ambient environment are negligible due to climate control in the laboratory.

1.6. Limitations

The following limitations are present in this study:

1. Only bronze-wound, acoustic guitar strings are used in this study.
2. Only the contributions of aerodynamic, material, and friction damping are studied.

1.7. Delimitations

The following delimitations are present in this study:

1. Other musical instrument strings such as violin strings, electric guitar strings, bass strings, etc. are not examined.

2. The physical damping mechanisms behind each type of damping are not studied in depth.
3. The effects of acoustic radiation damping and thermoelastic damping are not studied.
4. Amplitude dependent damping is not considered in this study.

1.8. Definitions of Key Terms

Real Normal Mode – a natural deflection shape of a structure at a given frequency in which the response in each section of the structure reaches a maximum amplitude at the same point in time. For guitar strings, this is often visualized as a standing wave (Ewins, 2000).

Complex Mode – a natural deflection shape of a structure at a given frequency in which the response in each section of the structure reaches a maximum amplitude at different points in time. For guitar strings, this is often visualized as a traveling wave (Ewins, 2000).

1.9. Abbreviations

IFFT – Inverse Fast Fourier Transform

FFT – Fast Fourier Transform

FRF – Frequency Response Function

MDOF – Multiple Degrees of Freedom

RMS – Root Mean Square

SDOF – Single Degree-of-freedom

1.10. Summary

This chapter provided an overview of the focus and significance of the research to be performed in this study. The next chapter examines a variety of damping types and their mathematical representation and physical manifestation. In the Chapter 2, the most relevant types of damping for a vibrating guitar string are selected. The chapter concludes with an overview of several techniques for experimentally identifying and quantifying damping.

CHAPTER 2. REVIEW OF RELEVANT LITERATURE

2.1. Overview

Damping in vibrating systems has been studied as far back as 1897 in the works of Lord Rayleigh and still remains one of the least known areas of vibration analysis. Damping is not well understood because it is unclear which state variables are relevant for the damping forces and because current experimental techniques cannot accurately identify the actual damping mechanisms (Woodhouse, 1998). Without this knowledge, the physics behind damping mechanisms cannot always be clearly defined, making it difficult to create an accurate damping model. This chapter examines many types of damping and identifies the most relevant types of damping for guitar strings. This chapter also examines experimental techniques used to identify and quantify different types of damping and damping parameters.

2.2. Viscous Damping

In general, any cause-and-effect damping model that makes energy dissipation non-negative is a feasible candidate (Adhikari & Woodhouse, 2001a). Viscous damping is the most common model that describes energy loss in a system. Viscous damping is a linear model in which the only relevant state variable is the instantaneous velocity. In 1850 Stokes studied the drag force of a column passing through fluid and stated that the drag force was proportional to the velocity. Similarly in 1897, Lord Rayleigh introduced a dissipation function that included the product of the instantaneous velocity and a constant damping coefficient. This function is commonly used in Lagrange's method for deriving

equations of motion. Rayleigh developed a special form of this damping in which the damping coefficient is a linear combination of mass and stiffness; this type of damping is formally known as “Rayleigh damping” or “proportional damping.” Rayleigh noted the mathematical convenience in this method, in that for a multiple degree-of-freedom (MDOF) system, the damping matrix is diagonalizable when transformed into modal coordinates. The zero off-diagonal terms in the damping matrix imply that the resulting modes are not coupled by the damping forces (Hasselman, 1972). These modes are considered real normal modes and are identical to those of an undamped system (Ewins, 2000). In reality, most systems contain complex modes that are seen in systems with non-proportional damping.

Non-proportional viscous damping is perhaps the most physically realizable type in that it can be created by using a fluid-filled dashpot. Viscous dampers are widely used in vibration textbooks when considering the damped, SDOF, spring-mass-damper system as shown below.

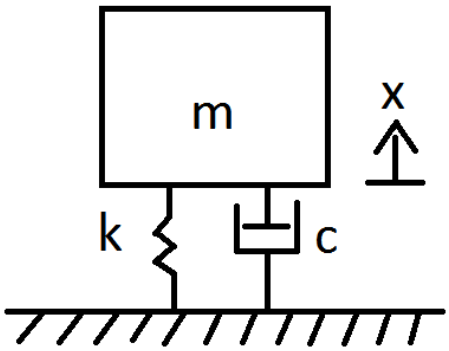

Figure 2-1: Spring Mass Damper

For this system, consider the well-known homogenous equation of motion below; note that the relevant state variable for the damping force is the instantaneous velocity as developed by Stokes.

$$m\ddot{x} + c\dot{x} + kx = 0 \qquad \text{Eq. 2.1}$$

Here, *m* is the mass, *c* is the viscous damping coefficient, and *k* is the stiffness. Commonly a complex trial solution is assumed and has the form:

$$x(t) = Xe^{st} \quad \text{Eq. 2.2}$$

Where *s* is a complex variable, *t* is time, and *X* is the amplitude. When substituting Eq. 2.2 into Eq. 2.1 and solving, the roots become:

$$s_{1,2} = \frac{-c}{m} \pm \frac{\sqrt{c^2 - 4km}}{2m} \quad \text{Eq. 2.3}$$

These roots can be rewritten in terms of the natural frequency (ω_n) and viscous damping ratio (ξ):

$$s_{1,2} = -\omega_n \xi \pm i\omega_n \sqrt{1 - \xi^2} \quad \text{Eq. 2.4}$$

$$\omega_n = \sqrt{\frac{k}{m}} \quad \text{Eq. 2.5}$$

$$\xi = \frac{c}{2\sqrt{km}} \quad \text{Eq. 2.6}$$

Eq. 2.4 can be simplified to:

$$s = \sigma \pm i\omega_d \quad \text{Eq. 2.7}$$

This complex expression is commonly referred to as the modal frequencies, where ω_d is the damped natural frequency. The complex solution for the displacement of the mass is now of the form:

$$x(t) = Xe^{(\sigma \pm i\omega_d)t} \quad \text{Eq. 2.8}$$

This equation is often written in the real form:

$$x(t) = Xe^{\sigma t}\cos(\omega_d t + \theta) \quad \text{Eq. 2.9}$$

The real exponential containing σ in Eq. 2.9 represents the exponential decay associated with viscous damping. The unit amplitude time decay envelope for viscous damping can be expressed as:

$$a_v(t) = e^{-\omega_n \xi t} \quad \text{Eq. 2.10}$$

The purpose and importance of the decay envelope will be examined in detail in section 2.7.

2.3. Quadratic Damping

While the earlier works of Stokes implied that the drag force on a column due to the viscosity of the fluid is proportional to the velocity, Giordano (1998) and Smith and Wereley (1999) noted that the force on a structure due to drag in air is actually proportional to the velocity squared– which, by definition, is quadratic. Air damping was successfully represented as quadratic in the study done by Smith and Wereley (1999) and the governing homogenous equation of motion for a SDOF system is of the form:

$$\ddot{x} + \epsilon|\dot{x}|\dot{x} + {\omega_n}^2 x = 0 \qquad \text{Eq. 2.11}$$

Here, ϵ is the quadratic damping ratio. Smith and Wereley (1999) give the following equation for the quadratic damping time decay envelope:

$$a_q(t) = \frac{2\pi a_0}{3\pi + 4\epsilon\omega_n a_0 t} \qquad \text{Eq. 2.12}$$

2.4. Coulomb Damping

While quadratic and viscous damping represents damping due to fluid interactions, Coulomb damping is a mechanical type of damping that arises from the sliding contact of surfaces. Charles Augustin Coulomb first observed and published a report on the laws of friction in 1779 and is considered as the first person to quantify the friction force that opposes the motion of an object sliding across a surface (Silva, 2007). This friction force is proportional to the normal force exerted by the object on the surface and directly opposes the velocity vector of the object (Nashif, Jones, & Henderson, 1985). Smith and Wereley (1999) give the governing homogenous equation of motion for a SDOF system with Coulomb damping to be:

$$\ddot{x} + \mu \frac{\dot{x}}{|\dot{x}|} + {\omega_n}^2 x = 0 \qquad \text{Eq. 2.13}$$

Here, μ is the Coulomb damping ratio. In the same study, Smith and Wereley give the following equation for the Coulomb damping time decay envelope:

$$a_c(t) = \frac{-2\mu}{\pi\omega_n} t + y_0 \qquad \text{Eq. 2.14}$$

Appendix A proves with a SDOF spring-mass-damper system that the decay functions in Eq. 2.10, Eq. 2.12, and Eq. 2.14 given by Smith and Wereley (1999) are of the correct general form. An exponential decay function describes a system with damping that is proportional to the velocity by a damping constant. A function of the form 1/t accurately describes a system with quadratic damping. Last, a linear decay function accurately describes a system with system with damping that is proportional to the sign of the velocity by a damping constant. Appendix B proves that the decay functions Eq. 2.10 and Eq. 2.14 are each valid solutions to the individual equations of motion seen in Eq. 2.1 and Eq. 2.13.

In the validation of these functions as documented in Appendix B, it was found that the decay function, Eq. 2.12, for aerodynamic (quadratic) damping consistently differed from the solution of the response of the SDOF model in Eq. 2.11. The error was found to be in the magnitude of the damping coefficient in the denominator; it was consistently high by a factor of a_0. When this constant was removed, the decay function perfectly matched the solution to the SDOF model, now making the decay function of the form listed below.

$$a_q(t) = \frac{2\pi a_0}{3\pi + 4\epsilon\omega_n t} \qquad \text{Eq. 2.15}$$

Appendix C proves that a for SDOF spring-mass-damper system with all three of these types of damping, the resulting decay envelope can be fitted using a linear summation of all three of these decay functions- Eq. 2.10, Eq. 2.14, and Eq. 2.15.

2.5. Hysteretic Damping

The word “hysteresis” is of Greek origin and means “to come late” (Silva 2007). This term is most commonly observed in cyclical tests in which a material or structure is displaced in a positive direction, returned to its original position, displaced in the negative direction, and cycled repeatedly. When examining a stress-strain curve, an ideal curve-fit would produce a purely linear trend. In reality, the ends of this stress-strain curve actually create cusps, hence, coining the name hysteresis “loops.” The area inside of this hysteresis loop represents the amount of non-recoverable work done per cycle. While the energy-loss mechanism is not readily recognizable as in the case of viscous or Coulomb damping; this mechanism is generally referred to as “internal friction” (Silva 2007).

Internal friction is a rather vague term. A more descriptive mechanism that explains why strain lags stress in a hysteresis loop can be attributed to dislocations and internal slip planes within a material’s atomic lattice structure. A dislocation is “a region of misaligned atoms existing between otherwise properly aligned atoms” (Dalton, 1994). As a material is deformed, an internal shear force is created as adjacent rows of atoms attempt to slide past each other. In elastic deformation, the atoms of a lattice structure return to their equilibrium state. In plastic deformation, these atoms slip and are permanently moved to a new location. This movement occurs in properly aligned atoms or in dislocations that can progress through the lattices. When metals slip at stresses below the yield stress, this is often attributed to dislocations moving (Dalton, 1994).

Hysteretic damping most commonly occurs with sinusoidal loadings and can be referred to in a temporal or spatial context according to Banks and Inman (1991). Time hysteresis includes mechanisms such as slip and dislocations that cause stress to be proportional to the strain plus the past time history of the strain. Spatial hysteresis can be interpreted as local differential movement between sections of a member that causes “internal friction” (Banks & Inman, 1991). Based on the previous paragraph’s definition of internal friction, these two

categories of hysteretic damping are describing the same energy-loss mechanism. Perhaps this is why many vibration textbooks, as well as this study, do not distinguish between the two types and only mention the following forms that are listed below.

For the case of a SDOF system with hysteretic damping the homogenous equation of motion given by Silva (2007) is:

$$\ddot{x} + \frac{h}{m\omega}\dot{x} + {\omega_n}^2 x = 0 \qquad \text{Eq. 2.16}$$

Here *h* is the hysteretic damping coefficient. In this equation it is interesting to note that damping force is inversely proportional with frequency; this implies that the magnitude of the damping forces will decrease with frequency. In Appendix B, it was found that for a single degree-of-freedom (SDOF) spring-mass-damper system, this is indeed what happens which is contradictory to what actually happens with a vibrating string. Rao (2004) noted that this equation of motion can be expressed in another form if the excitation is sinusoidal:

$$F(t) = F_0 \sin(\omega t) \qquad \text{Eq. 2.17}$$

For Eq. 2.16, let there be a sinusoidal excitation force of the form given above with a steady state solution of the form:

$$x(t) = X sin(\omega t - \theta) \qquad \text{Eq. 2.18}$$

After substituting this expression into Eq. 2.16, the magnitude of the corresponding transfer function is obtained:

$$\left|\frac{X}{(F_0/k)}\right| = \frac{1}{\sqrt{\left(1 - \frac{\omega^2}{\omega_n^2}\right)^2 + \left(\frac{h}{k}\right)^2}} \qquad \text{Eq. 2.19}$$

The phase of the transfer function is:

$$\theta = \tan^{-1}\left[\frac{h/k}{\left(1 - \frac{\omega^2}{\omega_n^2}\right)}\right] \qquad \text{Eq. 2.20}$$

From Eq. 2.20 it can be seen that at a value of $\omega = 0$ the phase is not zero. This implies that for hysteretic damping, the response will never be in phase with the forcing function (Rao, 2004). If the excitation force and response is of the form:

$$F(t) = F_0 e^{i\omega t} \qquad \text{Eq. 2.21}$$

Then the homogenous equation of motion can be expressed in the following form:

$$m\ddot{x} + k(1 + i\beta)x = 0 \qquad \text{Eq. 2.22}$$

In this equation, the damping term is denoted by $\beta k = h$. Notice now that the combined stiffness/damping term is actually complex and can be simplified as:

$$\ddot{x} + {\omega_n}^2(1 + i\beta)x = 0 \qquad \text{Eq. 2.23}$$

Inaudi and Kelly (1995) commented that, while this expression for hysteretic damping is convenient, it is neither physically nor mathematically valid. In this model, mathematically, response occurs before any excitation is applied, creating a problem in that the initial conditions cannot be accurately defined. In Appendix B, it was shown that the numerical solution to Eq. 2.23 results in an unstable system that has negative damping and whose response exponentially approaches infinity.

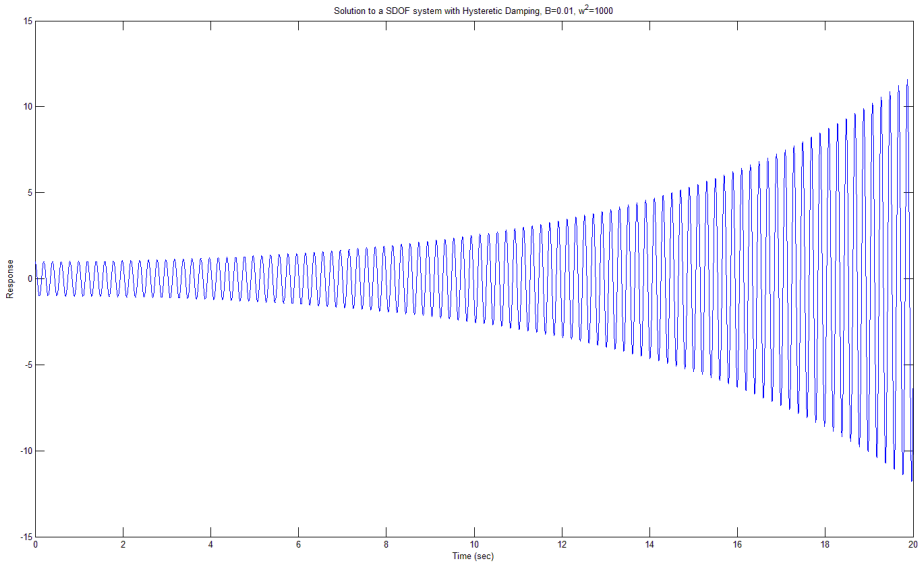

Figure 2-2: Unstable Hysteretic Damping Model (Eq. 2.23) Solved in Matlab

Inaudi and Kelly (1995) proposed another equation of motion that contains a hysteretic damping force listed below.

$$f(t) = k\Delta(t) + k\eta\widehat{\Delta}(t) \qquad \text{Eq. 2.24}$$

Here the Hilbert transform of the deformation history is defined as:

$$\widehat{\Delta}(t) = -\frac{1}{\pi}\int_{-\infty}^{\infty}\frac{\Delta(\tau)}{t-\tau}d\tau \qquad \text{Eq. 2.25}$$

The Hilbert transform now properly characterizes the primary characteristic of (temporal) hysteretic damping in that the future response of the system depends on its deformation history. This response of this model is difficult to solve even using numerical solvers. A solution for a system with this type of damping could not be obtained using the differential equation solver in Matlab or in Mathcad. Consequently, this type of damping will be left for further study in the future.

2.6. Other Damping Types and Considerations

Viscous, quadratic, Coulomb, and hysteretic damping are not the only types of damping that cause energy losses in a system. A non-comprehensive list of other types of common damping include: acoustic radiation damping, damping from air pumping, constrained layer damping, Kelvin-Voigt damping, and thermoelastic damping.

Acoustic radiation damping describes energy lost from a vibrating structure in the form of sound waves in the surrounding medium (Beards, 1996). This occurs when an unbounded volume of fluid mass-loads the structure as a result of pressure fluctuations that are close to the vibrating surface (Norton & Karczub, 2003). This is commonly visualized by a small mass of fluid that stays attached to the vibrating structure, causing the natural frequencies to decrease. This type of damping most commonly affects thin, lightweight structures with a large cross-sectional area such as aircraft panels and some loudspeakers. Acoustic radiation damping depends on the density of the fluid and is much higher in dense fluids such as water and oil than in air (Beards, 1996). Because a

guitar string is considered a relatively stiff structure with a small cross-sectional area, and because the primary fluid medium is air (whose density is many orders of magnitude smaller than that of water or oil), acoustic radiation damping is considered negligible in this study.

Damping from air pumping involves fluid movement through a gap or a hole as a result of differing stiffness between adjacent members of a structure (Beards, 1996). Energy loss occurs as a result of the change in volume acting on the vibrating member. Some air may escape, but in the case of a partially enclosed cavity, the volume of fluid may provide a reactive stiffness on the vibrating member. Because the strings in this study will be tested in an open-air or vacuum environment, damping from air pumping is not a consideration

Constrained layer damping occurs when layers of different materials are bonded together in order to obtain a balance between stiffness and damping properties. When the composite member vibrates, the damping layers dissipate energy, often in the form of heat, as they shear (Beards, 1996). Usually the damping materials are made of polymers and have viscoelastic material properties. Because the guitar strings used in this study are metal and do not contain viscoelastic properties, constrained layer damping is not considered in this study. It should be noted that for the case of wound steel guitar strings, the type of damping that arises from the windings rubbing on each other and the core-wire is more accurately represented as Coulomb damping instead of constrained layer damping.

Kelvin-Voigt damping, also known as strain-rate damping, is similar to hysteretic damping in that it tries to describe energy loss resulting from internal friction. The primary difference is that strain-rate damping is more mathematically convenient as it is a type of proportional damping. This type of damping is plausible when attempting to describe amplitude-dependent material energy loss because this type of damping is dependent on the strain experienced by the material. When Banks and Inman (1991) tried to match experimental time-responses for vibrating beams using a variety of theoretical material damping

models, they noted that hysteretic damping more accurately matched the experimental results rather than Kelvin-Voigt damping. Because of the results of Banks and Inman (1991), and because hysteretic damping is a more widely used model in vibration textbooks, Kelvin-Voigt damping is not considered in this study.

Thermoelastic damping is important for materials with large thermal coefficients and good thermal conductivity; this applies only when there is a net volume change associated with adiabatic vibrations (Silva, 2007). Thermoelastic dissipation is especially relevant for high-frequency compression vibrations. A common example of thermoelastic energy loss occurs in a rubber band that heats up from rapid, repeated stretching. Thermoelastic damping is not considered in this study due to small displacement amplitudes and insignificant volume changes, resulting in negligible energy losses in the form of heat.

In summary, the types of damping that seem most relevant for the case of a vibrating string include quadratic, hysteretic, and Coulomb damping. These three types of damping are the primary focus of this study. Should these models of damping be inadequate, other damping models may be considered.

2.7. Experimental Methods

Now that the relevant types of damping and their solutions have been identified, it is necessary to find a satisfactory method to quantify the amount of damping in a system. This section examines the different methods used to experimentally quantify damping in vibrating structure.

2.7.1. Logarithmic Decrement

The first widely used metric is the logarithmic decrement, or log decrement for short. The log decrement (δ) quantifies the amount of damping as a ratio of successive amplitudes in the time domain and is defined below.

$$\delta = \frac{1}{N}\ln\left(\frac{A_n}{A_{n+N}}\right) \quad \text{Eq. 2.26}$$

Here *A* is the amplitude of the peak and *n* signifies the reference peak and *N* denotes the peak of the subsequent cycle. The log decrement is most useful when dealing with one frequency from an oscillating SDOF system. An equivalent form of the log decrement for the viscously damping SDOF system as defined by Beards (1996) is:

$$\delta = \frac{2\pi\xi}{\sqrt{1-\xi^2}} \quad \text{Eq. 2.27}$$

When the damping is small, this can be simplified to:

$$\delta \simeq 2\pi\xi \quad \text{Eq. 2.28}$$

Because the log decrement is only a numerical ratio, its uses are limited in that it cannot classify which type of damping is acting.

2.7.2. System Loss and Quality Factors

The system loss factor *(η)*, as defined by Ewins (2000), is a metric used in frequency response functions (FRFs) that is expressed as the ratio of the half-power frequencies *(ω_1, ω_2)* divided by the resonant frequency (ω_n):

$$\eta = \frac{{\omega_2}^2 - {\omega_1}^2}{2{\omega_n}^2} \simeq \frac{\omega_2 - \omega_1}{\omega_n} \quad \text{Eq. 2.29}$$

The half-power frequencies are those frequencies for which the amplitude is $1/\sqrt{2}$ times the amplitude at the natural frequency. Nashif et al. (1985) noted that this measure of damping is constant for viscous and hysteretic damping; however, it is amplitude dependent in the case of Coulomb damping. The system loss factor is also referred to as the modal damping factor; and, when inverted, it is equal to the quality factor (Woodhouse, 2004a):

$$Q_r = \frac{1}{\eta_r} \quad \text{Eq. 2.30}$$

The subscript *r* indicates that the quality factor (or Q-factor for short) is unique for the r^{th} mode. If the structure is excited harmonically and steady-state conditions

are achieved, the Q-factor can be described as the ratio of the maximum dynamic response to the maximum static response (Beards, 1996). In the case of viscous damping, Beards (1996) illustrates that the Q-factor can also be written as:

$$Q = \frac{1}{\eta} = \frac{1}{2\xi} \qquad \text{Eq. 2.31}$$

Silva (2007) tabulated explicit expressions for Q-factors corresponding to a wide variety of damping types. Of that list, some interesting observations that Silva made include that 1) the Q-factor for viscous damping is directly proportional to frequency, while 2) hysteretic and Coulomb damping are directly proportional to frequency squared.

Most real systems have more than one energy-loss mechanism acting simultaneously, making the measured Q-factor actually a summation of the individual Q-factors due to each type of damping. Silva (2007) determined the following expression for the resultant Q-factor with Coulomb, hysteretic, and quadratic (fluid) damping acting:

$$\frac{1}{Q} = \frac{1}{Q_c} + \frac{1}{Q_h} + \frac{1}{Q_f} \qquad \text{Eq. 2.32}$$

This expression draws an interesting analogy to adding capacitors in series. A measure of a capacitor's ability to store energy is known as capacitance; similarly, damping capacity is a quantifiable measure that is used to describe an object's ability to absorb energy. The inverse summation seen above is exactly how capacitors in series add.

The Q-factor is used only for frequency domain analysis; and, while useful, it is not as informative as the decay functions mentioned earlier. If design variables can be identified, they will most likely be defined in relation to the time domain; because of this, the Q-factor is not the primary damping metric used in this study.

2.7.3. Damping Matrix Reconstruction

In the case of discrete systems, much research has been done in trying to reconstruct a damping matrix from experimental results. Hasselman (1972) proposed a method to reconstruct a damping matrix using complex modal frequencies (see Eq. 2.7), complex eigenvectors, and damping ratios obtained from modal analysis. Diagonal elements of the matrix were obtained by assuming proportional damping and having knowledge of the modal mass matrix. Off-diagonal elements were found using an expression containing the eigenvectors, natural frequencies, and elements in the modal mass matrix. In this study, the velocity was the only state variable that is deemed of interest for the damping term.

Adhikari (2006) performed a study that was similar to the work of Hasselman (1972); but, instead of a damping model that was proportional only to the mass and stiffness matrices, Adhikari proposed a generalized proportional damping expression. The Rayleigh damping that was proposed by Hasselman had limitations in that the damping factors did not reflect the natural variation with frequency as found in experimental results. The generalized proportional damping proposed by Adhikari involves fitting a function that characterizes the variation in damping factors with frequency and then using this function in reconstructing the damping matrix. Accurate knowledge of the mass and stiffness matrices are required in this procedure as well. This method is valid for linear structures, provided that the modes are not significantly complex.

Adhikari and Woodhouse (2001a) contributed to this line of study by proposing a method for reconstructing the viscous damping matrix and understanding the “spatial” distribution with respect to the modes used. This method used only the complex modal frequencies and eigenvectors to reconstruct the damping matrix for a series of SDOF spring-mass-damper systems. The spatial distribution refers to the distribution of damping with respect to the modes used in calculating the damping matrix. Essentially, this “visualization” technique creates a three-dimensional representation of the

damping matrix with the excitation and response degree-of-freedoms as the two independent axes and the damping coefficients as the out-of-plane axis. In this method, if the damping matrix is not symmetric, then a non-viscous damping model is needed. This method can also distinguish if the damping force in a system is locally or non-locally reacting.

Local reactive damping means that the dissipative force in a damping element depends on the absolute motion of the objects relative to some stationary point. Non-locally reactive damping means that the dissipative force in a damping element depends on the relative motion between two connected objects. In Adhikari and Woodhouse's study (2001a), the damping coefficient matrix depended on the distribution of the damping elements and how the dampers behaved as a function of time. In order to describe the damping function's behavior in time, an exponential or Gaussian function was used. This study found that an incorrect type of damping model with a different spatial distribution can still accurately reproduce a full set of transfer functions, making it impossible to identify the underlying damping mechanism (Adhikari & Woodhouse, 2001a).

Adhikari and Woodhouse (2001b) published a companion paper that involved reconstructing a damping matrix for a non-viscously damped system. This study was necessary because if viscous damping was the *a priori* selection, then any other types of damping were ruled out automatically. This study also used exponential and Gaussian functions, and introduced double exponential damping functions. To reconstruct the damping matrix, the complex natural frequencies and eigenvectors were needed as well as the undamped natural frequencies and mode shapes, the relaxation constant, and knowledge of the modal mass matrix. While the damping matrix of a discrete system could be reconstructed, this study reemphasized that the actual damping mechanism could not be identified by measuring the FRFs only.

Minas and Inman (1991) did a study on reconstructing a non-proportional damping matrix from incomplete modal test data. This method used an

incomplete set of eigenvalues and eigenvectors, a reduced form of the mass and stiffness matrices, and a least-squares algorithm to construct a viscous damping matrix. This was one of the earlier studies that began to couple the methods of structural testing and optimization techniques in order to determine damping parameters. The principles of combining these two methods are used and discussed more in depth in Chapter 3.

While these studies contain useful information about different types of damping, the primary limitation of all of those methods is that they all focused on numerical examples and one-dimensional systems. None of these methods were applied to two- or three-dimensional systems, and each of them were applied to situations where only one type of damping was present. Woodhouse (1998) summarized the problems with the damping matrix reconstruction methods in that they cannot identify the corresponding physical damping mechanisms, nor can they distinguish the contributions of multiple types of damping. This is because the damping matrix is actually a matrix of frequency-dependent functions that are being evaluated at only one frequency for a given mode, meaning that this matrix is now simply a matrix of coefficients. This describes nothing about the physical characteristics of the damping mechanism, such as whether or not it is amplitude-dependent; nor does it distinguish the magnitude of each different form of energy loss. In order to be able to experimentally identify different types of damping in real systems, a different method is needed.

2.7.4. Curve-Fitting Decay Envelopes

Smith and Wereley (1999) used the transient response of a system to identify the type of damping present based on the shape of the decay envelope in the time waveform. This was a purely numerical study, as an ordinary differential equation solver was used in Matlab to generate the time-responses for a SDOF system with Coulomb or quadratic damping. The decay envelopes were fitted with functions as seen earlier in Eq. 2.10, Eq. 2.12, and Eq. 2.15.

From these equations, the respective damping coefficients were found by minimizing the mean square-error function. These equations were deduced by using a moving block Fourier series analysis (FSMB) or a Hilbert damping analysis. In the FSMB analysis, the response signal is assumed to be sinusoidal and the Fourier series coefficients (A_1 and B_1 below) are calculated repeatedly for a progressing time window. The decay envelope was then estimated by the following relationship:

$$\hat{a}(t_k) = \sqrt{A_1(t_k)^2 + B_1(t_k)^2} \qquad \text{Eq. 2.33}$$

The Hilbert damping analysis is a linear integral transform that can be considered as a filter that causes a 90-degree phase shift of the response that leaves the magnitude unchanged (Smith & Wereley, 1999). In this study, quadratic damping was considered for this type of analysis and the response was assumed to be of the form:

$$y(t) = a_q(t)\cos(\omega_n t + \theta) \qquad \text{Eq. 2.34}$$

When the signal is shifted by 90 degrees, the response now becomes:

$$\tilde{y}(t) = a_q(t)\sin(\omega_n t + \theta) \qquad \text{Eq. 2.35}$$

The original and shifted signals then become the real and imaginary parts of a complex signal:

$$z(t) = y(t) + i\tilde{y}(t) \qquad \text{Eq. 2.36}$$

This function can be rewritten in phasor form:

$$z(t) = a_q(t)e^{i\theta(t)} \qquad \text{Eq. 2.37}$$

Here the envelope is the magnitude of the complex signal and can be written as:

$$a_q(t) = \sqrt{y(t)^2 + \tilde{y}(t)^2} \qquad \text{Eq. 2.38}$$

Smith and Wereley (1999) noted that the primary difference between these two methods is that the FSMB curve-fit contains less high-frequency content than the Hilbert damping analysis due to the averaging effects inherent in the process. The signal from the Hilbert damping analysis could be cleaned by passing it through a low-pass filter. While these methods have already been used to obtain the decay envelopes seen in Eq. 2.10, Eq. 2.12, and Eq. 2.14, these methods

may be needed to obtain an expression for the decay envelope for hysteretic damping.

Even though this type of damping analysis was performed in a purely numerical situation, Silva (2007) performed a very similar type of curve-fit analysis for the decay envelope of a time waveform from an oscillating pendulum in order to quantify the appropriate types of damping present. Similarly, Woodhouse (2004b) curve-fit the decay profiles from a frequency spectrum waterfall plot of a plucked guitar string to quantify the relative damping for each harmonic up to 2000Hz.

Although this section does not include an exhaustive list of all damping analyses, it contains the most relevant analyses for this study. The most promising experimental methods mentioned in this section involve using optimization methods and curve-fitting the decay profile of the time waveforms in order to distinguish the contributions of different types of damping. This is the approach used for this study and is outlined in more detail in Chapter 3.

2.8. Summary

In this chapter, a variety of damping types and their mathematical representation as well as their physical manifestation were discussed. It was deemed that quadratic, hysteretic, and Coulomb damping are the most potentially relevant damping types that act on a vibrating string. The purpose of studying these three damping types and the equations of motion of SDOF systems is that the response of these equations are a damped sine wave with unique decay envelopes that are identical to that of a harmonic of a vibrating string. These equations form the mathematical model with which the experimental results are compared. If the damping coefficients obtained experimentally from the decay envelopes given by Smith and Wereley (1999) in Eq. 2.10 , Eq. 2.12, and Eq. 2.15 match the damping coefficients in equations of motion in Eq. 2.1, Eq. 2.11, and Eq. 2.13 then these simple equations can be used to identify design variables that allows the response of the string to be predicted before it is manufactured. While these equations are discrete, if they match the experimental data, then these equations could be used to simulate a multiple degree-of-freedom lumped parameter system. An advantage of examining these discrete systems is that they are easier to solve numerically than continuous partial differential equations of motion.

Several different experimental techniques of quantifying damping were discussed in this chapter. Curve-fitting the decay envelopes of time-response signals in conjunction with least-square error calculations to obtain the damping coefficients was seen as the most relevant technique examined in this chapter. Throughout this chapter structural dynamic testing was used in conjunction with determining damping parameters. The next chapter discusses the experimental procedures performed to identify and quantify the contributions of multiple types of damping acting for a given mode.

CHAPTER 3. METHODOLOGY

3.1. Overview

The purpose of this research is to identify and quantify the different types of damping acting on bronze-wound guitar strings across a wide frequency range, as outlined in Chapter 1. If string manufacturers want to someday be able to control the damping for a specific frequency or frequency range, they must know which type of damping is dominant at that frequency of interest. The type of damping that is present will dictate what design variables can be adjusted in order to control that damping.

This chapter examines the methods that were used to identify the dominant damping types for a given frequency range. By changing the ambient and boundary conditions, different types of damping were isolated and quantified using optimization methods and curve-fitting the decay envelopes as discussed at the end of Chapter 2. In this study, two different types of bronze-wound acoustic guitar strings and their core-wire were tested. Structural dynamic testing was used in conjunction with altering the boundary conditions in order to isolate aerodynamic, material, and friction damping. All post-processing and curve-fitting was performed in Matlab. A single degree-of-freedom, mathematical model was created in Mathcad where the decay profiles from the numerical model were compared to those of the test data.

3.2. Specimens and Fixtures

Two different types of bronze-wound acoustic guitar strings were used in this experiment. The first string was designated as BW056 and had a 0.056″

nominal diameter with windings comprised of 80% copper and 20% zinc. The second string was designated as PB056 and had a 0.056″ nominal diameter with windings composed of 90% copper and 10% tin. Each of these wound strings contained a hexagonal, brass-plated, steel-core-wire. The baseline string was considered as the BW056 string, and the steel-core-wire was considered in order to identify the damping caused by the friction of the windings. The PB056 string was considered to see the differences in damping due to a different wrap-wire.

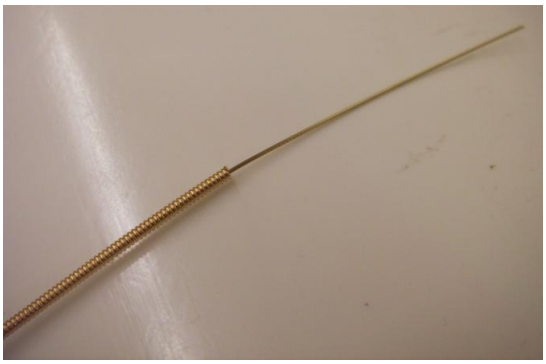

Figure 3-1: BW056, Wound String and Core-wire

The fixture used to mount the strings was made entirely of steel that emulated the natural mounting of a guitar string; a steel nut and saddle were welded to the base of the fixture and allowed for a normal string length of 25.5 in. This fixture was similar to that used by French (2009). The purpose of the fixture being completely steel was that the impedance at the boundaries was so high that no dynamic interaction between the string and the fixture occurred.

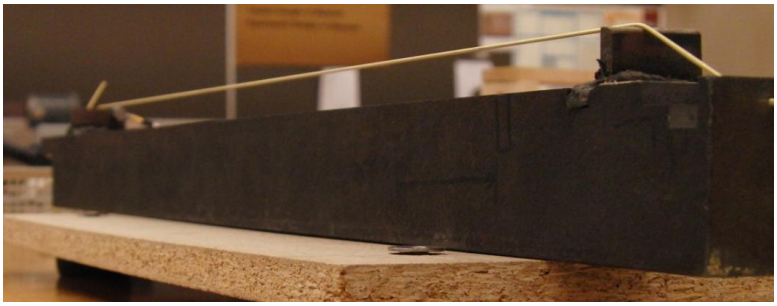

Figure 3-2: Steel Mounting Fixture

In order to verify that there was no interaction between the string and the fixture, a modal test was performed using a modal hammer (Entek IRD, model E086640). Drive-point FRFs were obtained in the axial, lateral, and vertical directions first without the string being mounted on the fixture, followed by a series of tests with the string mounted on the fixture. The first series of images below are drive point FRFs taken on the saddle of the fixture. Lateral is defined as parallel to the table and normal to the string– vertical is defined as normal to the table, and the longitudinal axis runs along the length of the string.

Figure 3-3: Saddle Excited in the Longitudinal (or Axial) Direction

The top graph in Figures 3-4, 3-5, and 3-6 is the phase angle– the middle is the magnitude, and the bottom is the coherence. The unit of measurement for the magnitude is dB, with 1g and 1N being the reference parameters. The phase angle is displayed in degrees, and the coherence is displayed as a percentage. The horizontal axis in each image shows frequency in Hz.

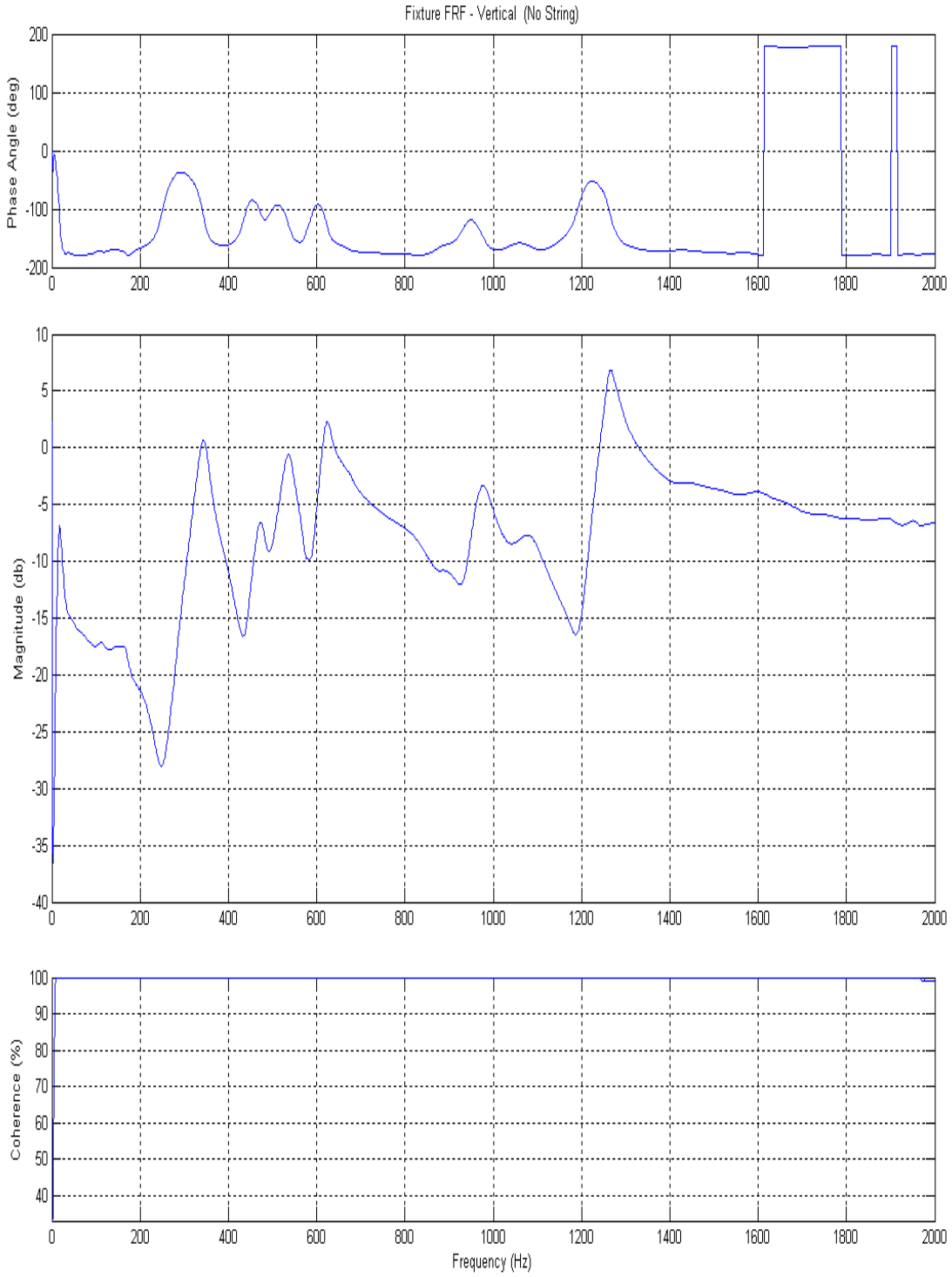

Figure 3-4: Vertical Drive-point FRF

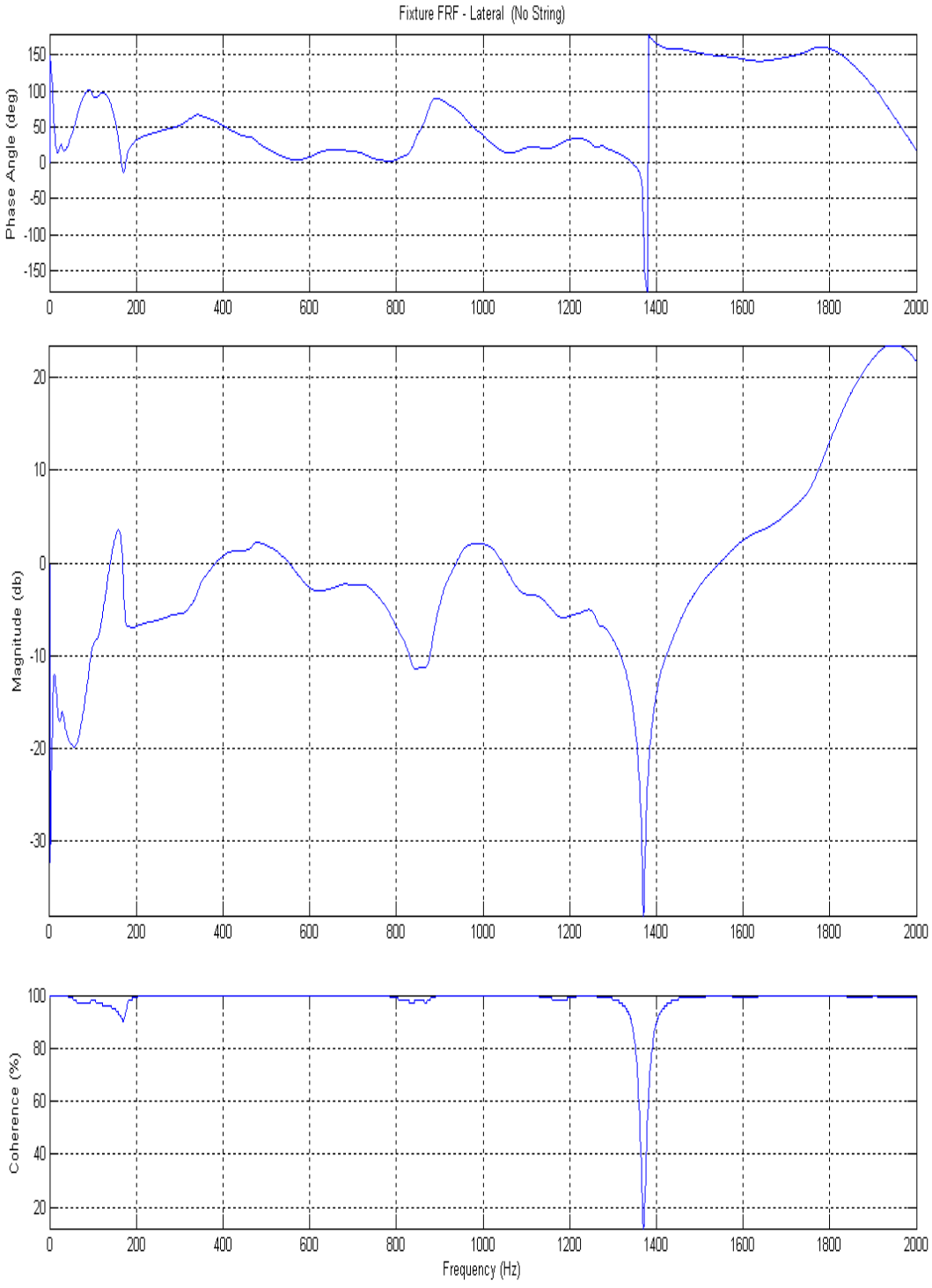

Figure 3-5: Lateral Drive-Point FRF

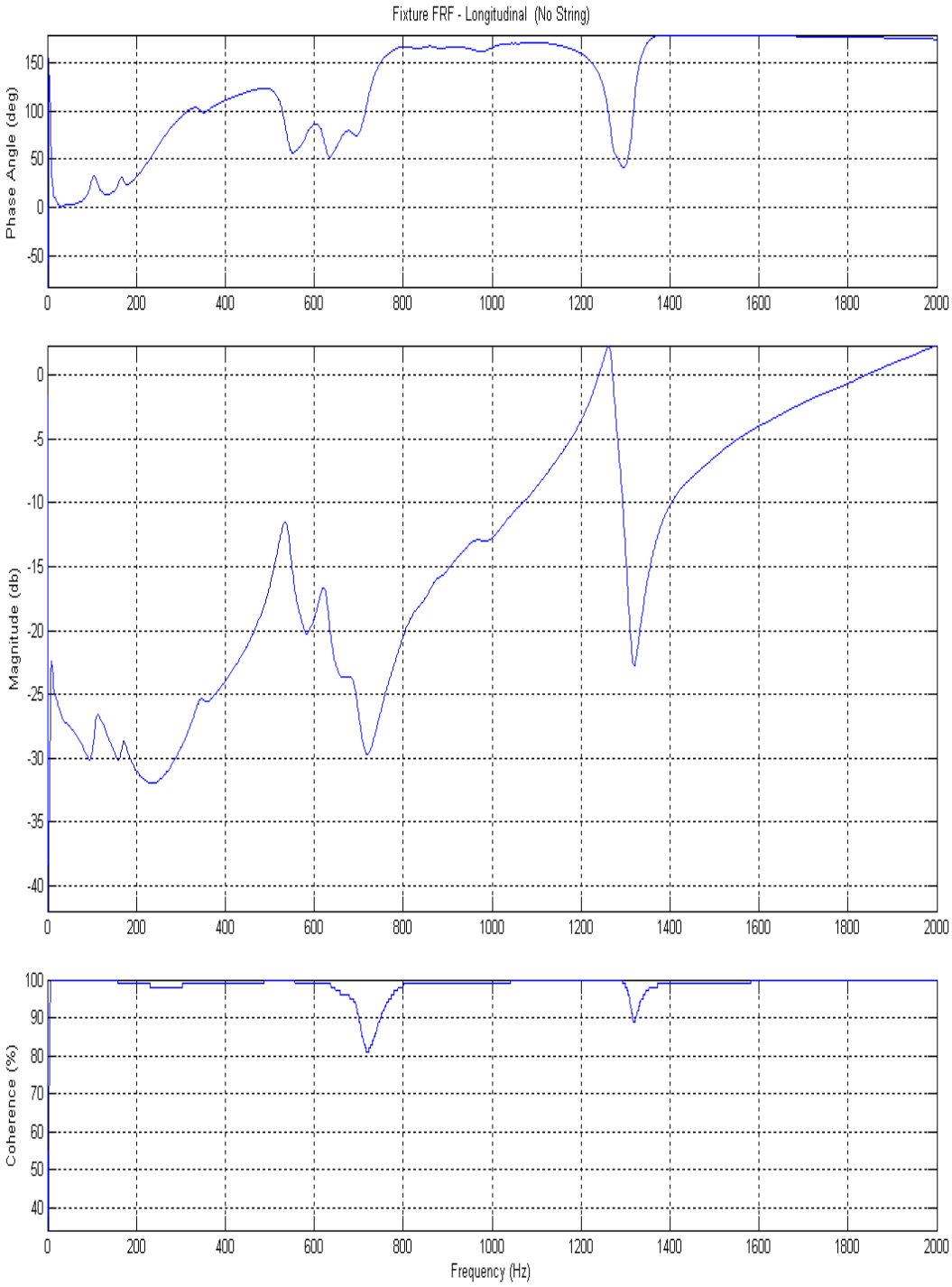

Figure 3-6: Longitudinal Drive-point FRF

The only significant response appeared to be in the vertical direction, as several modes could have influenced the motion of the string. This was significant because the response data that was curve-fitted was the response in the vertical direction. Next two FRFs with the string on the mounting fixture were obtained by measuring the response of the string when striking the string and when striking the saddle.

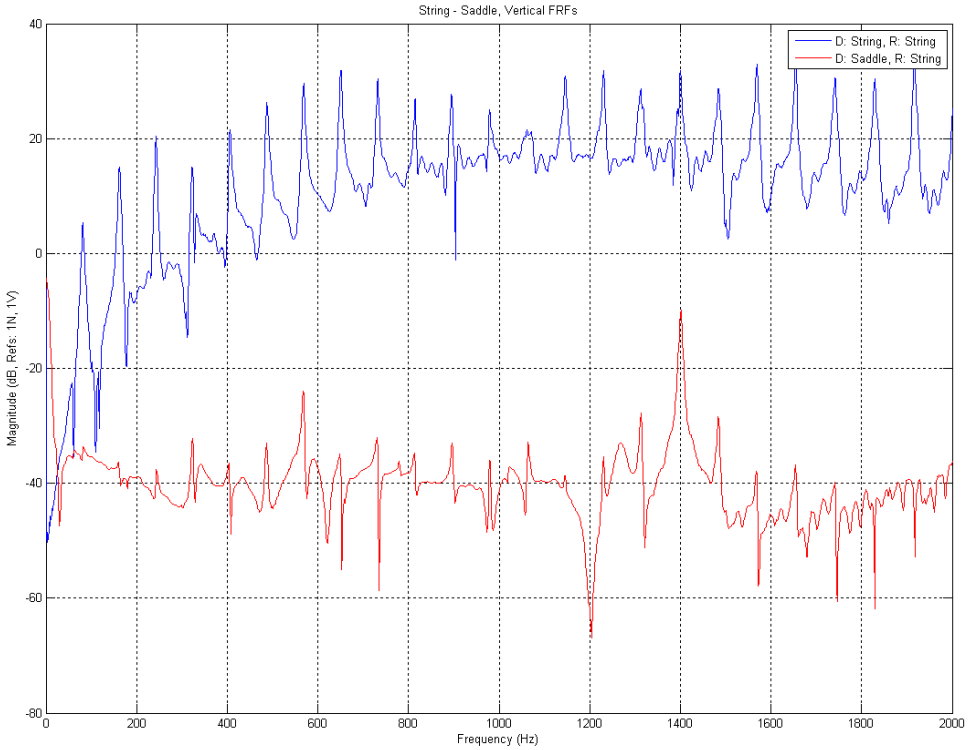

Figure 3-7: String response: string driven (top), saddle driven (bottom)

The only potential problem seen in these FRFs was at 1400Hz, which is clearly a string mode (16^{th} harmonic). Notice from Figure 3-4 that this is not a vertical saddle mode; however, to be safe, this harmonic was not used when curve-fitting the data.

While no structural interaction between the string and boundaries were found, the next item that was studied was the damping caused by the boundaries. Although the impedance of the boundaries was not quantified, its

effects were qualitatively studied. The goal was to create boundaries with such a high impedance that little to no energy was lost as the traveling wave hit the boundaries. This would match the acoustics concept of a traveling plane wave reflecting off a wall with very high acoustic impedance such that the reflection and transmission coefficients are one and zero, respectively. Similarly, the effects of friction at the boundaries were qualitatively studied. The goal was to minimize the amount of energy lost due to friction caused by the string rubbing on the saddle.

In creating boundaries with very high impedance, two different setups were created. The first setup involved resting a large steel block on the nut and the saddle. The added mass would in theory raise the mechanical impedance at the boundaries, causing the reflection coefficient to increase and the transmission coefficient to decrease. While this could not quantitatively measured, if the reflection coefficient increased, the effects could be identified by less damping in each of the string harmonics.

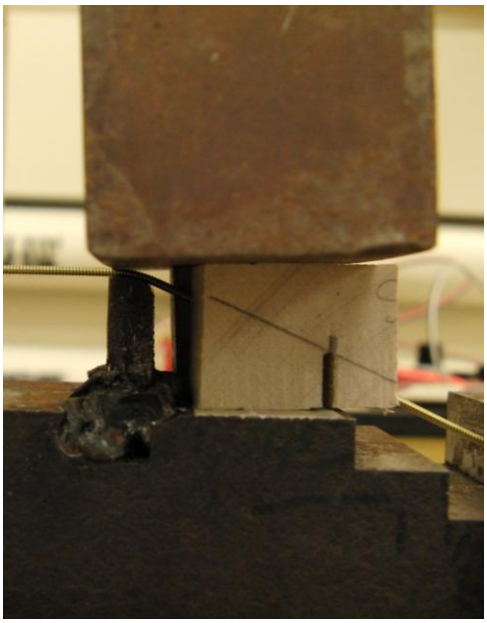

Figure 3-8: Steel Blocks at the Boundaries

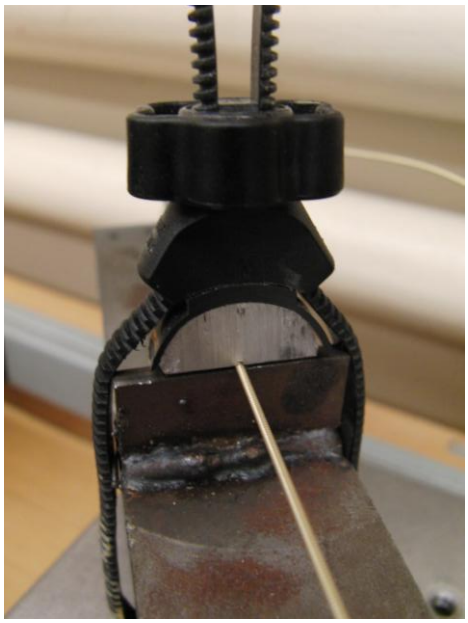

Figure 3-9: Aluminum Half-Rounds Clamped at the Boundaries

The addition of these blocks did not significantly alter the damping; if anything, they actually increased the damping across the frequency spectrum. To try to achieve a greater clamping force, half rounds of aluminum were cut and clamped to the nut and saddle using plastic hose clamps. A groove was cut in the half-rounds to keep the string from sliding laterally. The addition of these half-rounds resulted in an increase in damping as well. Because it seemed that any additional clamping force resulted in increased damping, no further methods were attempted to create higher impedance at the boundaries.

In order to minimize damping caused by the string rubbing on the nut and saddle, different materials were placed under the string and the effects in damping were noted. A piece of plastic cut from electrical wire shrink-wrap was placed under the string and it was observed that this increased the damping across the frequency spectrum. Next, a piece of packing tape was placed under the string, and it was observed that this also increased the damping. No fluids were used in this attempt to minimize friction losses at the boundaries because it could fill the small gaps in the windings of the strings and alter the concept of Coulomb damping, which is the rubbing of two dry surfaces.

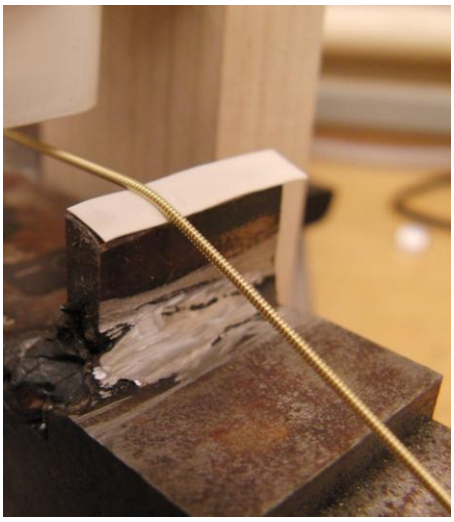

Figure 3-10: Plastic Layer Beneath the String

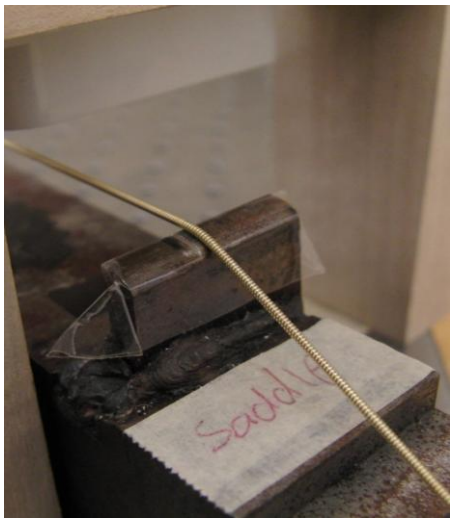

Figure 3-11: Packing Tape Beneath the String

In conclusion, none of these efforts were able to successfully decrease the amount of energy lost at the boundaries; instead, they actually increased the energy lost. Because the energy loss at the boundaries could not be minimized further, energy loss at the boundaries was considered to be negligible as stated in Chapter 2.

In order to eliminate the damping caused by aerodynamic drag two different vacuum chambers were designed. The first was made entirely of acrylic pieces bonded with Weld-On ©. Extensive ribbing and reinforcing was used along with a gasket lining around the top to create an airtight seal; however, at -50kPa, the bonded joints in the top started to come apart. Ultimately the top cracked in two places, so a second top was created using 2″-thick RenShape; however, even with this new top, the bonded joints in the sides started to come apart.

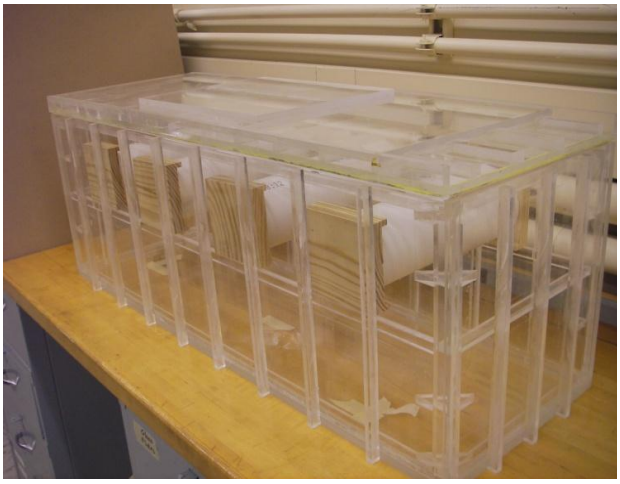

Figure 3-12: Acrylic Vacuum Chamber with Acrylic Top

Figure 3-13: Acrylic Vacuum Chamber with RenShape Top

A second vacuum chamber was created using 10″ schedule 40 PVC piping, vacuum bag tape, and hot glue. The pipe was rated to 140psi but the end caps were not rated; because of this, 2″-thick discs of RenShape were added to reinforce the end caps.

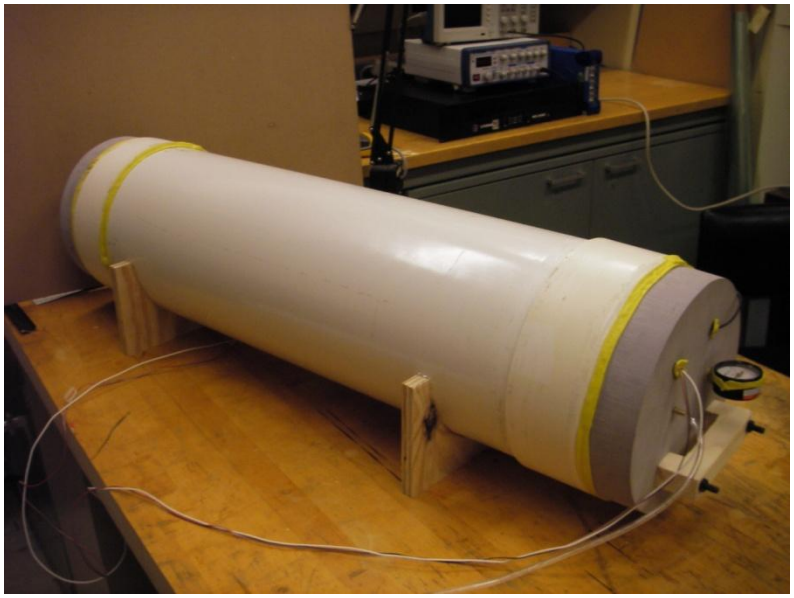

Figure 3-14: Final Vacuum Chamber Design

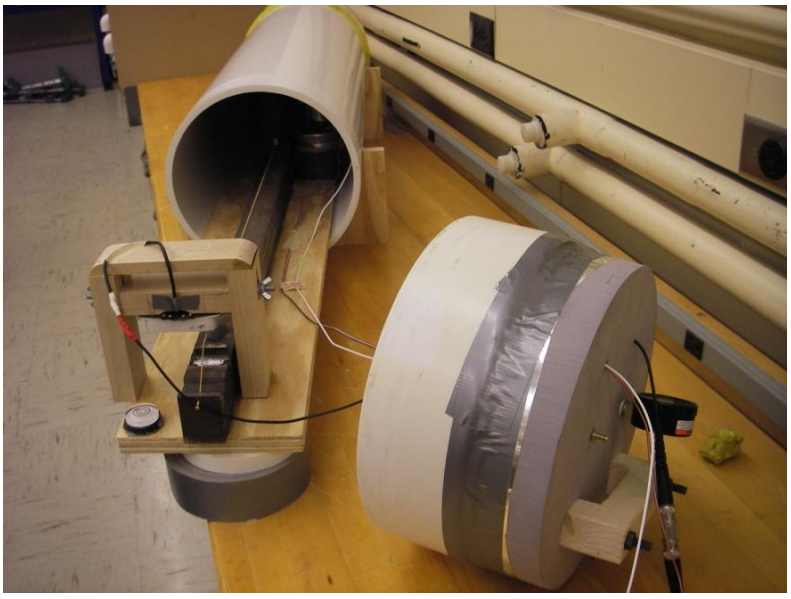

Figure 3-15: Mounting Fixture in the Vacuum Chamber

While this design was not quite as elegant and did not allow as easy access to the interior of the chamber, this design was very robust and could achieve a perfect vacuum (-100kPa on the analog vacuum gauge used). The shaker,

pickup, and steel mounting fixture were hot-glued onto a piece of five-ply plywood that was slid into the vacuum chamber when vacuum tests were performed.

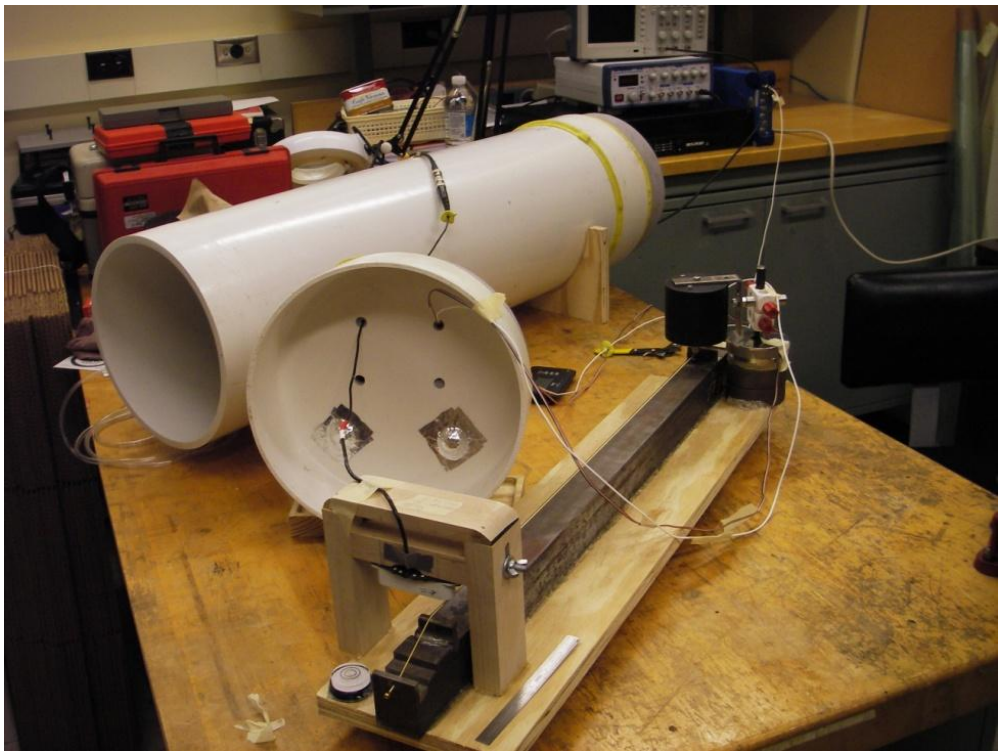

Figure 3-16: Slide Plate and Mounting Fixture

When air was drawn out of the vacuum chamber, the end caps mating with the tube created a fairly good seal, as a vacuum of -60kPa could be obtained without any additional sealant. To ensure a perfect seal, vacuum bag tape was used to line the edges between the end caps and the tube. This tape was very elastic; and, as air was drawn out of the chamber, this tape would fill the gaps between the end caps and the tube without tearing. This tape was also used to fill the electrical wire access holes. After the vacuum tests were finished, the vacuum bag tape was removed from one end cap, and pressurized air was pumped into the chamber in order to remove the end cap.

3.2.1. Excitation and Transducers

In order to excite the string, a small shaker was used in conjunction with a function generator and an amplifier. Counterweights were added to balance the shaker so that it did not rebound after striking the string. A force transducer was placed on the end of the shaker to measure the input force transmitted to the string. The function generator produced a repeatable impulse and the shaker was small enough that it easily fit inside the vacuum chamber. An impulse was desired in order to excite the higher harmonics (over 1kHz) of the string. When performing an FFT of the impulse excitation, the shorter the pulse, the more frequency content is present. One item that aids in creating a short, narrow pulse is the stiffness of the impact tip. In these experiments, the force transducer has an embossed tip and because the casing was metal, this created a good broad spectrum impulse.

. 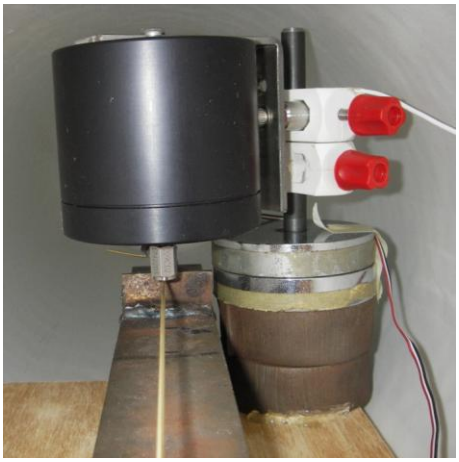

Figure 3-17: Shaker used to excite the string with an impulse

Transducers considered for measuring the response of the string included an accelerometer, a microphone, a laser vibrometer, and an electromagnetic pickup. A primary concern in choosing a transducer was that it would not alter the behavior of the vibrating string.

An accelerometer was not used because the only attachment location was either the nut or the saddle. Because of the high impedance of the steel nut and

saddle, a clean signal could not be obtained using this transducer. A microphone was a viable option only for open-air measurements since an elastic medium is needed to make measurements with a microphone. In order to be consistent from the open air to the vacuum tests, a microphone was not used. Another option was using a laser vibrometer. Laser vibrometers are an excellent transducer for non-contact measurements and do not alter the response of the structure at all. The laser vibrometer available for use was quite old and was extremely difficult to focus, making it not a time-efficient instrument to use.

An electromagnetic pickup is appropriate as long as it does not draw too much energy from the vibrating string as it cuts through the magnetic field. This was checked by taking time-response measurements with the pickup at a different height for each measurement. A pickup in a humbucking configuration was used with all of the magnets except for one being removed. A pickup in a humbucking configuration consists of two coils wound in opposite directions with opposite polarities. Having two coils results in more sensitive pickup, and the opposing polarities provide noise cancellation that is not available in a single coil pickup.

The string was excited with an impulse from a small electromagnetic shaker located 0.8″ from the nut, while the pickup was placed 0.8″ from the saddle and 1/16″ above the string. After each measurement the pickup was elevated 1/32″ higher up to a maximum height of 7/32″.

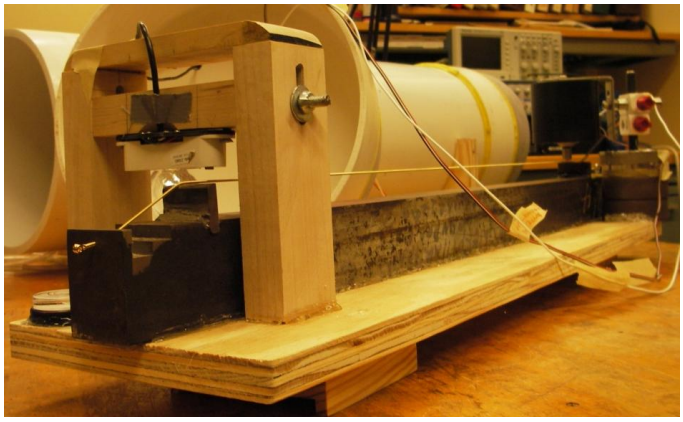

Figure 3-18: Wooden Pickup Fixture

The height of the pickup was controlled using a small wooden fixture, shown in Figure 3-18, and a small bubble level was used to ensure that the pickup was kept normal to the string for each measurement.

Each time-response signal was filtered with a third-order 4 Hz band-pass, Butterworth filter so that the decay rate of the fundamental frequency could be identified. The decay envelope of the fundamental frequency was curve-fitted with a pure exponential function and the constants of the exponential function for each measurement were plotted as a function of pickup height as shown in Figure 3-19, below.

The exponential function was used because it was the simplest to use for comparing the decay rates and it resulted in a good fit with the R^2 values being greater than 99.5% for each fit. R^2 is a statistics metric that is a ratio of errors. The numerator is the sum of squares error, which totals the distances between the data points and the best fit line. The denominator contains this error plus the sum of squares error between the data points and the mean value of the data points. Ideally the R^2 ratio is equivalent to a value of one, or 100%.

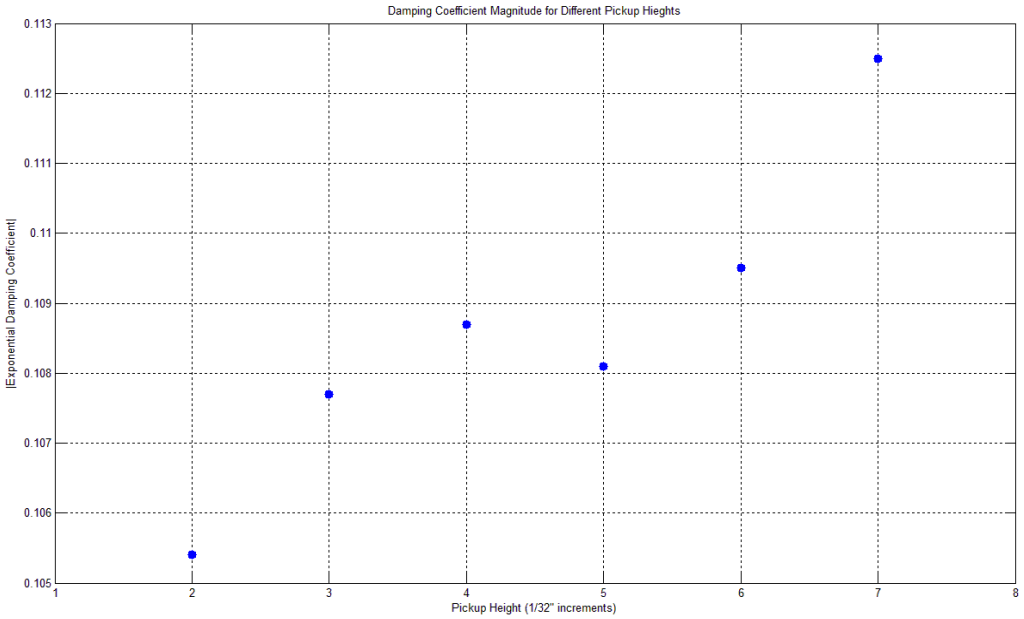

Figure 3-19: Damping Coefficients in Relation to Pickup Height

When choosing a height for the pickup, the two items of concern are creating artificial damping and measured frequency range. It was originally thought that because the core-wire of the string was ferromagnetic, positioning the pickup too close to the string would create artificial damping as a result of magnetic forces acting on the string. This data shows that as the pickup is moved higher above the string, the decay rate appears to increase. This is most likely due to a nonlinear response in the pickup itself. As the pickup is moved higher above the string, fewer magnetic field lines are cut, and the strength of the magnetic field decreases logarithmically, as documented by Horton and Moore (2009). While the pickup should be less sensitive to the amplitude of response, the decay rate should not change. Figure 3-20, below, shows that as the pickup height increases, the response amplitude decreases and the frequency content above 1 kHz becomes lost in the noise floor as expected.

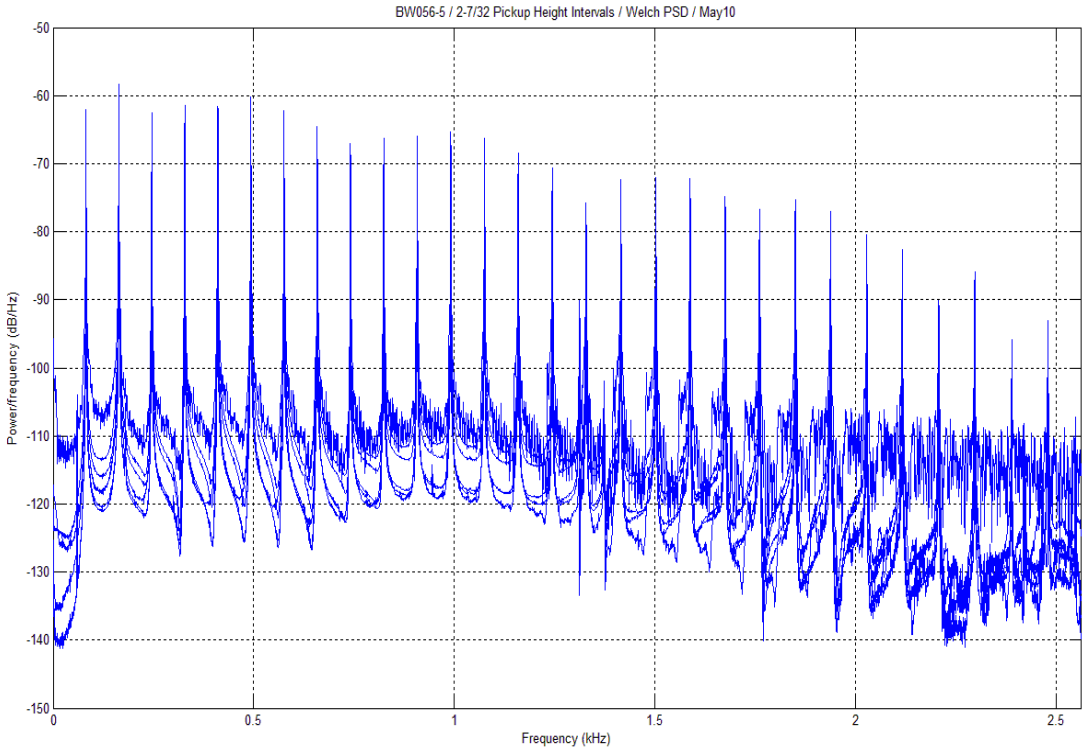

Figure 3-20: Power Spectral Density Plots, Varying Pickup Heights

Although a solution to this non-linearity could not be identified, it was decided that the pickup should be located 3/32″ above the string for future measurements because the smallest variation in damping coefficient lies in the 3–5/32″ range, and because this height showed good frequency resolution beyond 1 kHz without having to worry about creating artificial damping.

3.2.2. Data Collection

Before each data set was recorded, each string was tuned using a digital guitar tuner. The shaker, located 0.8″ inboard from the nut, then struck the string with an impulse and the response was measured with an electromagnetic pickup located 0.8″ inboard from the saddle.

Figure 3-21: Digital Tuner Used Before Each Test

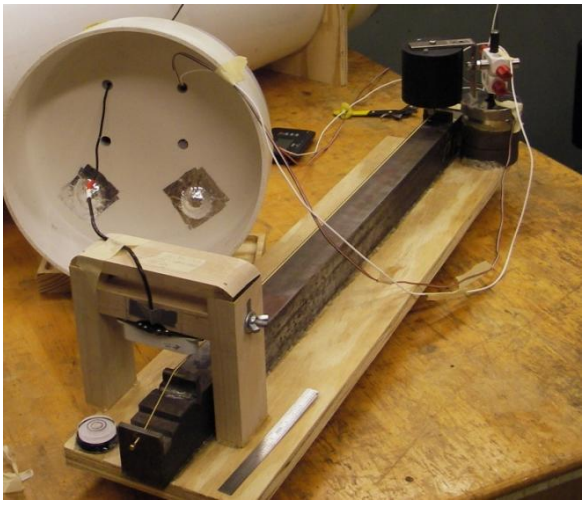

Figure 3-22: Excitation and Response Positions

This excitation location was chosen because the string is stiffer closer to the boundaries. This minimizes the concern that the string will rebound and hit the shaker multiple times and skew the damping measurements.

If the pickup was placed close above and toward the longitudinal center of the string, the magnetic field from the pickup would alter the motion of the string if the amplitude of motion was large. To minimize this interaction, the pickup was placed close to the saddle and the excitation was kept to small amplitudes. This location also was preferred because of the high-frequency content that could be measured. The number of harmonics that could be measured was a function of where the pickup was located. For example, if placed exactly in the longitudinal center of the string, the first harmonic could not be measured because that is a node location– a location with no response for that mode. By moving the pickup closer to the saddle, it was less likely to encounter nodal points.

Time-response signals from the pickup were recorded using a four channel OROS data acquisition module with a sample frequency of 5120 Hz. The recording time period was 20 seconds and the frequency range for the FFT was 2 kHz. Because frequency resolution is equal to the reciprocal of the sample time, this resulted in a frequency resolution of 1/20 Hz.

In order to eliminate aerodynamic damping each string (BW056, PB056, and the core-wire) was tested in open air as well as in a vacuum. The purpose of testing the core-wire by itself was to quantify the material damping which was assumed to come primarily from the core-wire and not the windings. Because material damping is related to the internal friction forces, the core-wire needed to have the same tension as the wound strings which was calculated using the equation below (French, 2009).

$$f = \frac{1}{2L}\sqrt{\frac{T}{\rho_L}} \qquad \text{Eq. 3.1}$$

In this equation f is the fundamental frequency, L is the length of the string (25.5″); T is the tension in the string and ρ_L is the linear mass. This expression is actually represented as a series to account for the effects of bending stiffness,

but the additional terms added more precision than was necessary. For this calculation the BW056 string was used as a baseline where the length, frequency, and linear mass were known. *T* was calculated (120.07 N) using Eq. 3.1, and was then used along with the known length and linear mass of the core-wire to calculate the frequency to which core-wire should be tuned (232.14 Hz). Because 232.14 Hz was not a chromatic pitch– the closest pitch was A# at 233.08 Hz– the tuning pegs were turned until this frequency was reached using the real-time FFT analyzer within the OROS software.

3.3. Post-processing and Data Analysis

All post-processing of the time-response signals was performed in Matlab. First, a power spectral density plot of the harmonic content of the time signal was created using the *pwelch* command. Then a lower and upper cutoff frequency limit was selected for each harmonic. Next, the *butter* command was used to create a third-order band-pass Butterworth filter with a bandwidth of 3–4Hz for each harmonic. The filter visualization tool in Matlab was used to ensure that the magnitude of the response was flat across the selected frequency range. It was found that for a 4 Hz band-pass filter, the magnitude remained constant up to a fifth-order filter, where there was significant ripple in the magnitude and phase as shown in Figure 3-23. Note that the magnitude and phase are shown on the y1 and y2 axes respectively.

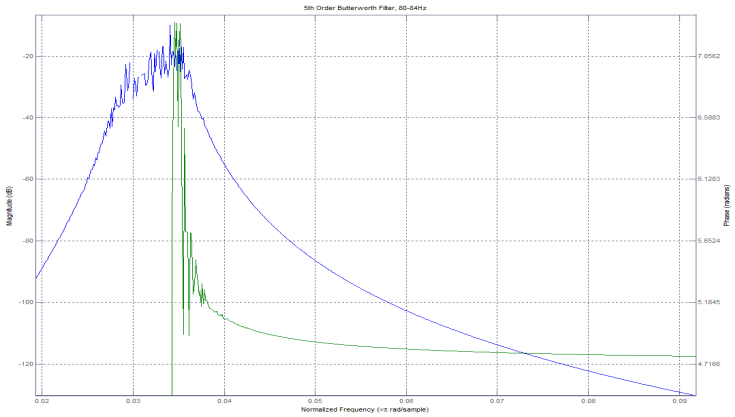

Figure 3-23: Fifth-order, 4 Hz Band-pass Butterworth Filter

The effects of filter bandwidth also were examined and were found to not create any artificial damping. To examine this, three third-order band-pass Butterworth filters with bandwidths of 2, 3, and 9Hz were created to filter the fundamental frequency. The filtered time-responses were plotted on top of each other look for any visual difference in decay rate. The plots showed that no artificial damping was created as a result of the bandwidth of the filters for this order and frequency range.

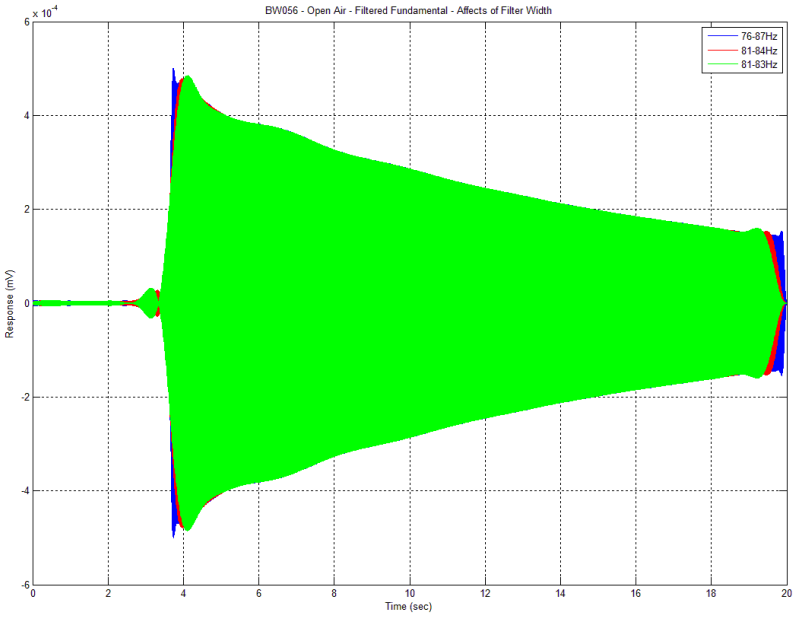

Figure 3-24: Third-Order Band-pass Butterworth Filters

After identifying a reliable order and bandwidth for the filter, the recorded time-response signal was then filtered using the *filtfilt* command for each harmonic.

The cursor tool was then used to select points along the decay envelope of the filtered harmonic. These points were exported to the workspace as a structure and this structure was then converted into two vectors using for loops. These two vectors represented the time and the response for each of the selected points. These vectors were then imported to the curve-fitting tool where the points from the decay envelopes of each harmonic were fitted using a linear summation of the decay functions mentioned early in Eq. 2.10, Eq. 2.12, and Eq. 2.15. Appendix C proves that for a SDOF spring-mass-damper system with multiple types of damping, a linear summation of these decay functions accurately describes the damped sinusoidal response. As mentioned in Chapter 2, the response of a filtered harmonic resembles that of this SDOF system.

The fitting function was given more generalized parameters that were calculated by Matlab as shown in Eq. 3.2.

$$F(t) = me^{-at} + \frac{2\pi a_0}{3\pi + ct} + dt + f \qquad \text{Eq. 3.2}$$

The arbitrary parameters *m, a, a_0, c, d,* and *f* in Eq. 3.2 were returned by Matlab when a best fit was obtained. In order to be considered the best fit, the R^2 value needed to be greater than 99%. From these fitted parameters, the aerodynamic (ε), coulomb (μ), and viscous (ζ) damping coefficients were calculated by the following equations:

$$\varepsilon = \frac{c}{4\omega} \qquad \text{Eq. 3.3}$$

$$\mu = \frac{-\pi\omega d}{2} \qquad \text{Eq. 3.4}$$

$$\zeta = \frac{-a}{\omega} \qquad \text{Eq. 3.5}$$

While *a, c,* and *d* are used to calculate the damping coefficients, a_0 is an offset term that is not explicitly described by Smith and Werely (1999).

3.4. Threats to Validity

The largest threat to validity lies in the correlation between the mathematical solutions to the equations of motion and the physics that actually describe the response of each harmonic. Because Eq. 3.2 is a linear summation of functions, the primary concern is the range of values that the calculated damping coefficients can assume. There likely is no absolute set of damping coefficients that match the decay of each harmonic because they are being summed linearly. With three variables in a linear equation one variable may increase in magnitude while another may decrease, keeping the final magnitude the same. Consider the very primitive example: $x + y + z = 0$. Here, there is nearly an infinite range of values that x, y, and z can be; the only condition that must be satisfied is that their summation must equal zero. The same is true in this method of curve-fitting the decay envelopes of each harmonic. The fitted parameters must result in the magnitude of the fitting function being equal to the magnitude of the data for each point in time. This threat was present in the results and is discussed more in depth in Chapters 4 and 5.

The second threat to validity lies in the nature of the pickup-string interaction. When matching the SDOF models to the fitted damping parameters, the assumption of the model is that the response is a damped sinusoidal solution. If the data set that is being fitted is not sinusoidal, then the SDOF models should not be used. This threat would manifest itself when performing the FFT of the time-response signals in that extra frequency content would be present near the peaks of the harmonics. This threat did manifest itself in the data; however, it did not affect the results of this study as it was either able to be identified and filtered or the affected harmonic was not curve-fitted. This threat is be discussed further in Chapters 4 and 5.

3.5. Summary

This chapter provided an overview of the instrumentation that was used, as well as the data collection and analysis methods that were performed. Structural dynamic testing has been used to identify damping parameters for many years; however, the individual contributions of multiple damping types acting simultaneously have not been successfully identified and quantified. This study uses structural dynamic testing and optimization techniques in order to quantify the individual contributions of several different types of damping in a vibrating guitar string. The next chapter describes the results that were seen from the methods mentioned in this chapter.

CHAPTER 4. RESULTS

4.1. Overview

This chapter examines the results using the methodology described in Chapter 3. Two rounds of testing were performed. The first involved testing the BW056, PB056, and core-wire in open air and in a vacuum. These time signals were filtered and several harmonics were curve-fitted in order to calculate the damping ratios. The second round of testing involved testing 10 BW056 strings in open air to see if this type of analysis can be used as a quality tool in which the amount of variation in damping across a batch of strings can be identified. Several obstacles were identified and overcome including the presence of beat frequencies in nearly every harmonic (due to the mounting fixture), differences in the vertical and lateral modes, and potentially string-pickup interaction.

4.2. Beat Frequencies

The string was excited with an impulse from an electromagnetic shaker located 0.8″ from the nut and the response was measured with an electromagnetic pickup located 0.8″ from the saddle. After having filtered each harmonic, a significant amount of these harmonics had apparent beat frequencies that could significantly affect the accuracy of the curve-fits. Figure 4-1 and Figure 4-2 show the type of beat frequencies seen in the filtered harmonics.

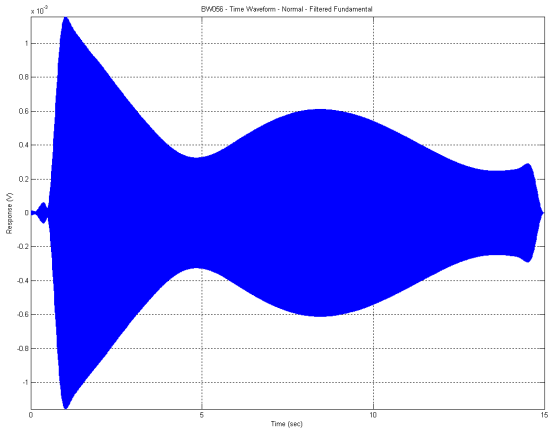

Figure 4-1: Filtered Fundamental, BW056

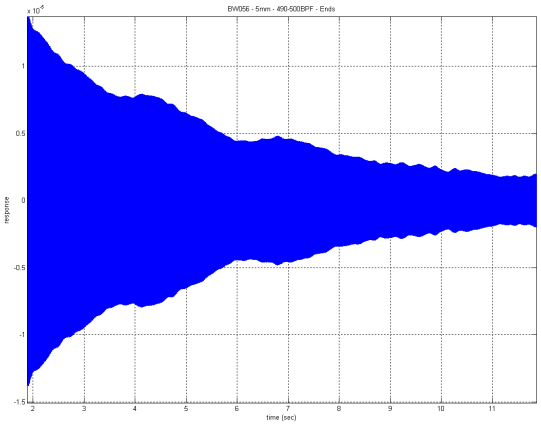

Figure 4-2: Filtered Fifth Harmonic, BW056

In the filtered time-response signals, up to three different beat frequencies could be present. The most common beat frequency that was seen was at ½ Hz. This implies that there is another frequency present that is extremely close to the frequency of the harmonic and identifying the source of this frequency was not easy. The first source of beat frequencies came from the fact that the lateral modes were not identical to the vertical modes; this was true across the entire frequency range.

The frequency spectrum plots in this section show two data sets obtained by measuring the response of a string in the vertical and lateral directions using a microphone to avoid any string-transducer interactions. The microphone (PCB I30D10) was placed 1/16″ from the string and a small piece of pickup wire (42 gage) was broken across the string in the vertical directions to create a repeatable impulse. The gauge wire was broken 0.8″ from the nut; the microphone was placed 0.8″ from the saddle and the time-response was recorded for 15 seconds.

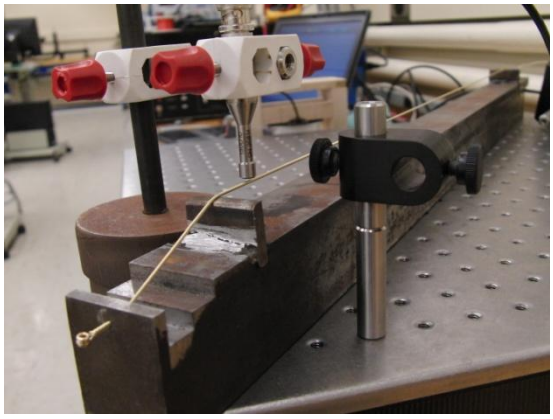

Figure 4-3: Vertical Microphone Positioning

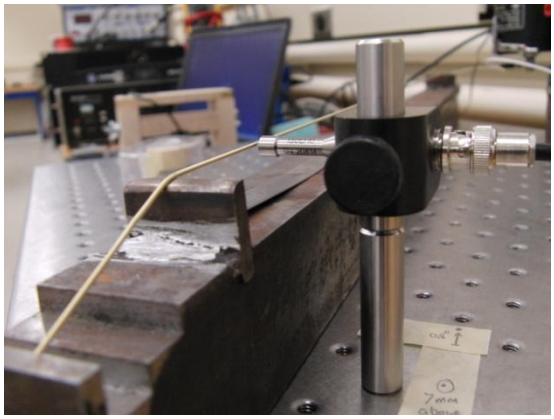

Figure 4-4: Lateral Microphone Positioning

The frequency spectra below show that both of these two peaks were seen when measuring the response in both the vertical and horizontal direction. It was clear from the frequency spectra that the second peak at each harmonic was higher when measuring in the lateral direction, implying that this is a lateral mode.

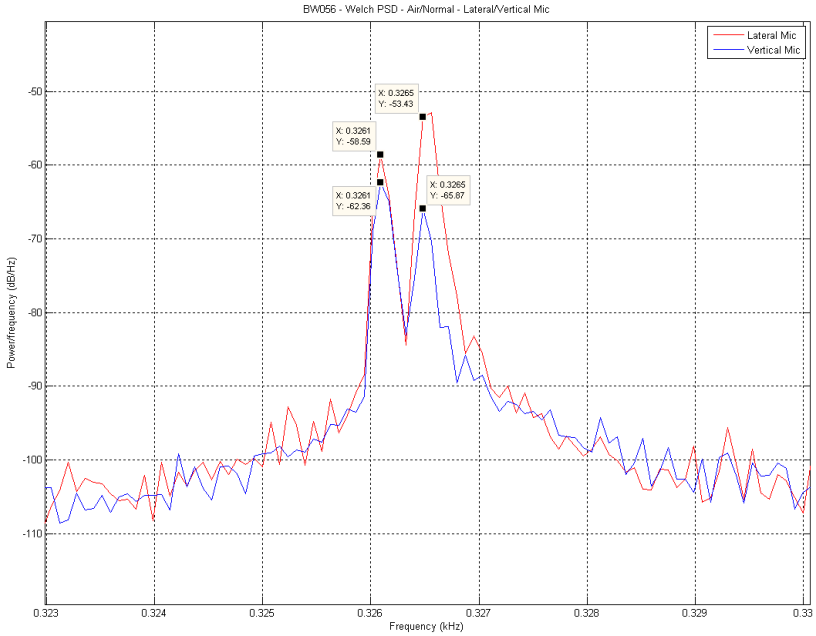

Figure 4-5: Third Harmonic, BW056 String

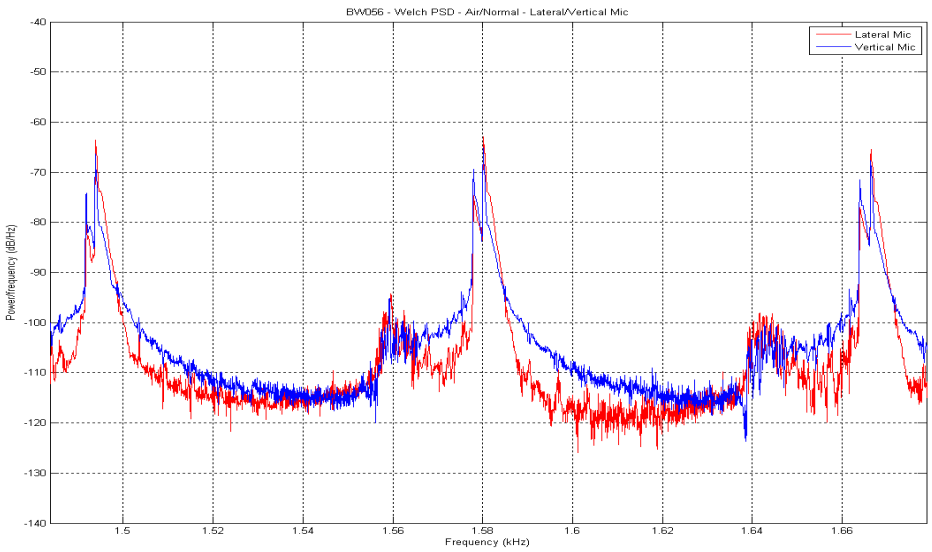

Figure 4-6: Harmonics 16-18 BW056 String

When filtering these peaks (third-order, 4Hz band-pass Butterworth Filter) and looking at the time-response of each harmonic, it was found that the vertical and lateral modes were 90 degrees out of phase, as shown in Figure 4-7. This explains the drastic contours of the filtered harmonics as seen in Figure 4-1 and Figure 4-2.

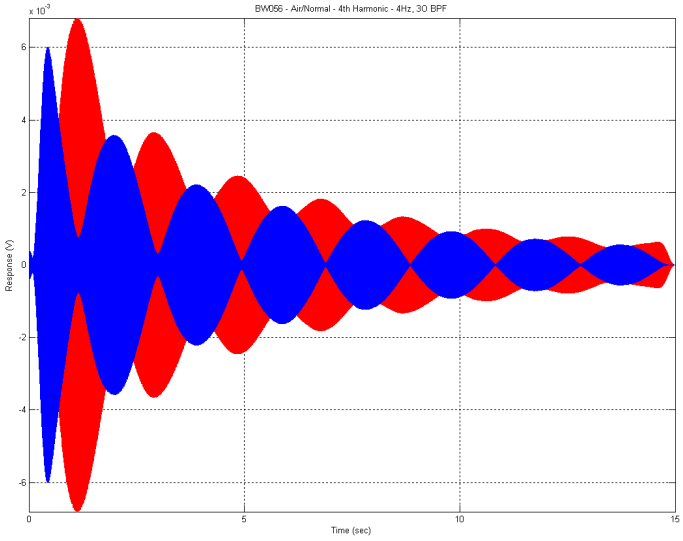

Figure 4-7: Fourth Harmonic, Vertical and Lateral Responses

For a driven vibrating string, the motion is not strictly planar as assumed in the ideal wave equation. From their study in 1994, Hanson et al. noted that a non-planar component of motion always exists. As the string is driven closer to its natural frequency, the magnitude of this component increases, resulting in a whirling motion as observed experimentally by Fang (2007). This was observed to be true experimentally not only for a driven string, but also for a plucked string as well. Even though the string was excited purely in the vertical or lateral direction, Elliott (1980) showed that one mode parametrically excites the other mode resulting in a whirling motion; hence, the microphone is actually measuring a component of the motion in both directions. The only problem here is that this is more common for large amplitude vibrations and the initial data had very small amplitudes of motion resulting from the shaker strike. This implies that there may be another source contributing to this beat frequency.

The next step was to examine the fixture itself. While the stiffness of the nut and saddle was high enough to prevent any significant motion in these directions (as seen in the FRF in Figure 3-5), the notches in the nut and saddle could possibly contribute to the beat frequency problem. The notches in the nut and saddle were cut shallower than the recommended depth (0.028″) for a low E string. This could allow for more lateral motion, especially if the string could hop or rock out of the notches. Typically the string rests on a flat surface on the saddle and in a groove cut in the nut. The tension and surface friction are usually high enough to keep the string from sliding or rocking on the nut. Another problem noticed with the fixture was that the grooves were not colinear, and the top faces of the nut and saddle were slightly sloped.

To try to eliminate the two peaks around each harmonic, the string was taken out of the grooves and displaced to the side. The string was then excited again with a shaker, and the response was measured by an electromagnetic pickup in the same locations mentioned previously. The resulting frequency spectra and time waveforms looked much cleaner. The two split peaks for each

harmonic disappeared as shown in Figure 4-8, and the beat frequencies were either eliminated completely or drastically reduced.

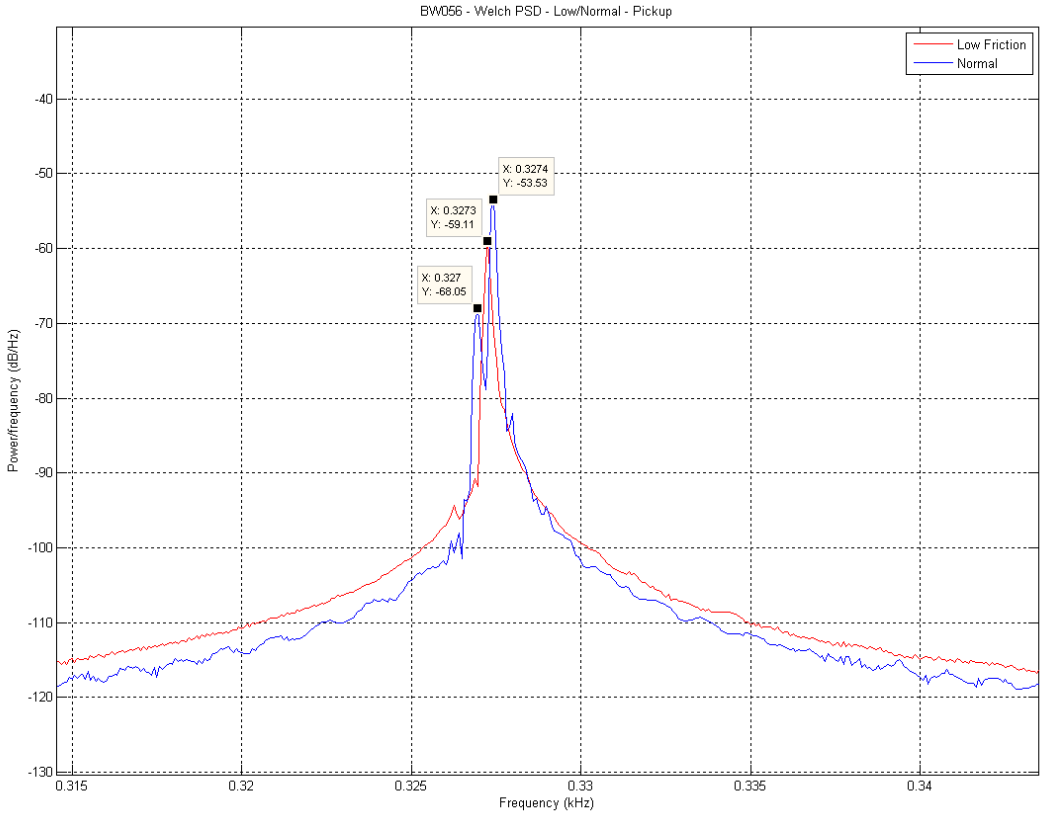

Figure 4-8: Third Harmonics, BW056, Out of the Grooves

The vertical and lateral measurements with the microphone were repeated to see if one of the modes was now suppressed and to see if the frequencies of the vertical and lateral modes still were significantly different. Figure 4-9 shows that the vertical and lateral frequencies are still slightly (< 1 Hz) different.

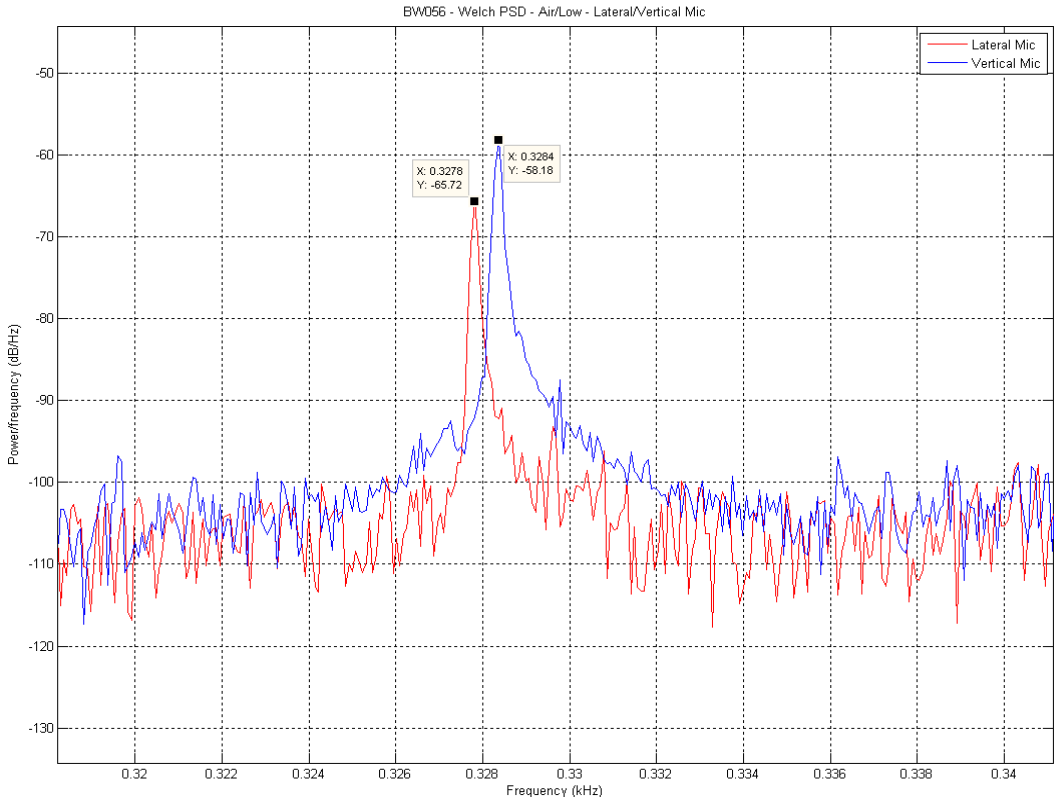

Figure 4-9: Harmonics 3, BW056 String

The most notable difference is that when the microphone is oriented vertically or horizontally, it now only “sees” the response in that respective direction (indicated by a single peak). The magnitude of response in the other direction is below the noise floor now. This was significant because now the response seen by the electromagnet will be the result of only one degree-of-freedom, allowing the data to be compared to the response of the SDOF model.

4.3. Curve-Fitting Functions

With the beat frequency problem resolved, 20 second time-response data (using the electromagnetic pickup) was obtained and filtered and curve-fitted using a variety of functions. The fundamental frequency for the BW056 string was used to identify which function, or combination of functions, were valid.

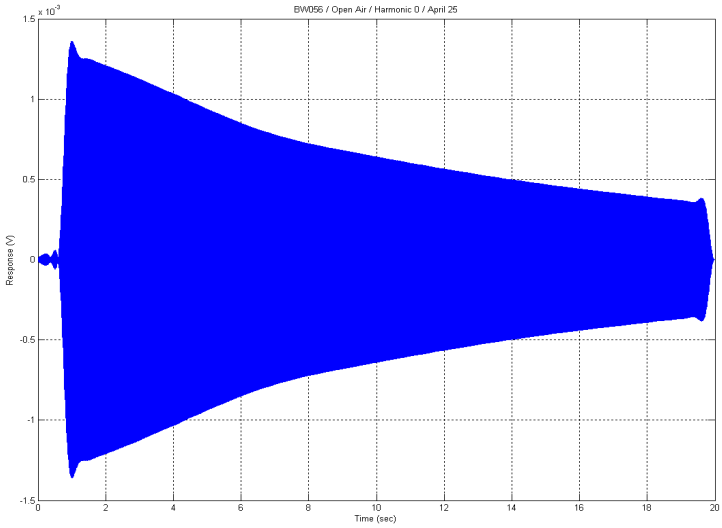

Figure 4-10: BW056, Open Air, Filtered Fundamental Frequency

It should be noted that two distinct decay rates appear to be present in this plot. This also was seen in another BW056 string as shown below.

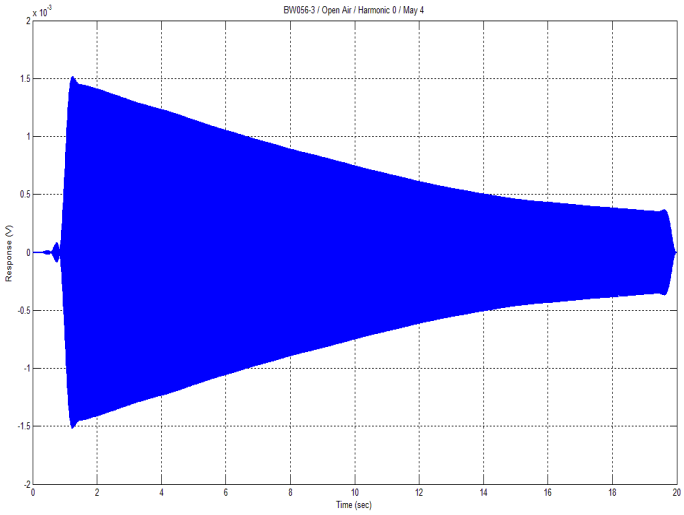

Figure 4-11: BW056, Open Air, Filtered Fundamental with Two Phase Decay

This apparent two-phase decay was not an anomaly and is discussed later in Section 5.2. Table 1 lists the results of using a variety of functions to curve-fit the decay profile of the fundamental frequency.

Table 1: BW056 Open Air, Fitting Functions

Model	Function	SSE	R^2
Exponential	F(t) = a*exp(-b*t)	6.679e-009	0.9912
Linear	F(t) = -p*t + k	4.134e-008	0.9455
Aero	F(t) = (2*pi*a0)/(3*pi + c*t)	4.338e-009	0.9943
Aero-Coulomb	F(t) = (2*pi*a0)/(3*pi + c*t) - p*t + k	1.167e-009	0.9985

From this table, it is clear that the Aerodynamic-Coulomb function best fits the data because it has the smallest sum of squares error (SSE) and the highest R^2 value.

4.3.1. Curve-Fitting, First Pass

In a first pass curve-fit, the lower and middle harmonics were fitted with just the aerodynamic and friction damping components.

$$F(t) = \frac{2\pi a_0}{3\pi + ct} - dt + f \qquad \text{Eq. 4.1}$$

This first pass method allowed for rapid curve-fitting because only four parameters were being matched. The limitations of this method became evident as the higher harmonics (above the 12th harmonic) could not be curve-fitted with this model; instead, the best curve-fit was an exponential function of the form below.

$$F(t) = me^{-at} \qquad \text{Eq. 4.2}$$

Tables 2–7 show the calculated damping coefficients for the BW056, PB056, and core-wire test in open air and a vacuum.

Table 2: BW056 Open Air, Damping Coefficients

Harmonic	Aerodynamic (ε)	Coulomb (μ)	Viscous (ζ)
0	5.122E-04	4.976E-04	0
1	6.855E-04	-3.757E-02	0
12	4.190E-04	-4.257E-01	0
14	0	0	1.139E-04
21	0	0	1.039E-04

Table 3: BW056 Vacuum, Damping Coefficients

Harmonic	Aerodynamic (ε)	Coulomb (μ)	Viscous (ζ)
0	0	4.796E-02	0
1	0	-3.771E-02	0
12	0	0	9.480E-05
14	0	0	1.030E-04
21	0	0	1.068E-04

Table 4: PB056 Open Air, Damping Coefficients

Harmonic	Aerodynamic (ε)	Coulomb (μ)	Viscous (ζ)
0	2.093E-04	-2.725E-03	0
1	2.167E-04	-4.770E-02	0
12	1.121E-04	-1.090E-01	0
17	0	0	3.785E-05
21	0	0	3.969E-05
22	0	0	3.877E-05

Table 5: PB056 Vacuum, Damping Coefficients

Harmonic	Aerodynamic (ε)	Coulomb (μ)	Viscous (ζ)
0	0	-1.192E+00	0
1	0	-5.255E+00	0
12	0	0	2.589E-05
17	0	0	2.947E-05
21	0	0	3.324E-05
22	0	0	4.222E-05

Table 6: BCW Open Air, Damping Coefficients

Harmonic	Aerodynamic (ε)	Coulomb (μ)	Viscous (ζ)
0	3.450E-04	7.249E-02	0
1	1.977E-04	2.366E-01	0
2	1.149E-04	2.139E-01	0
3	2.122E-04	3.417E-01	0
7	7.295E-04	1.358E+00	0

Table 7: BCW Vacuum, Damping Coefficients

Harmonic	Aerodynamic (ε)	Coulomb (μ)	Viscous (ζ)
0	0	0	8.664E-05
1	0	0	6.725E-05
2	0	0	6.453E-05
7	0	0	5.654E-05

Figure 4-12 to Figure 4-17 are the graphical representation of these results.

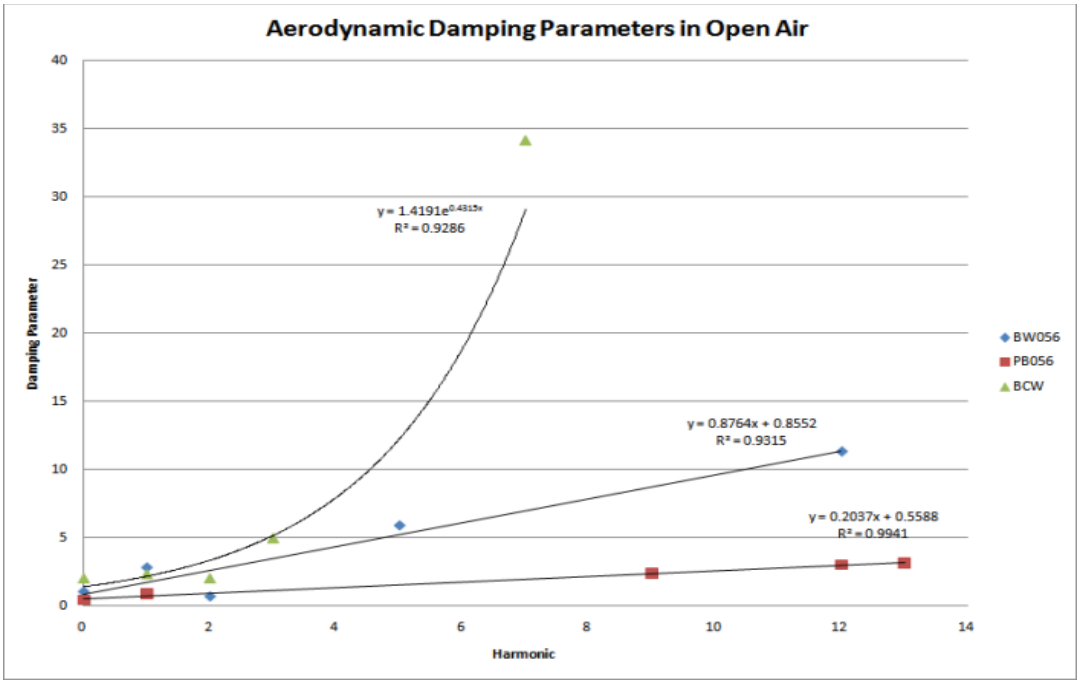

Figure 4-12: Aerodynamic Damping Parameters in Air

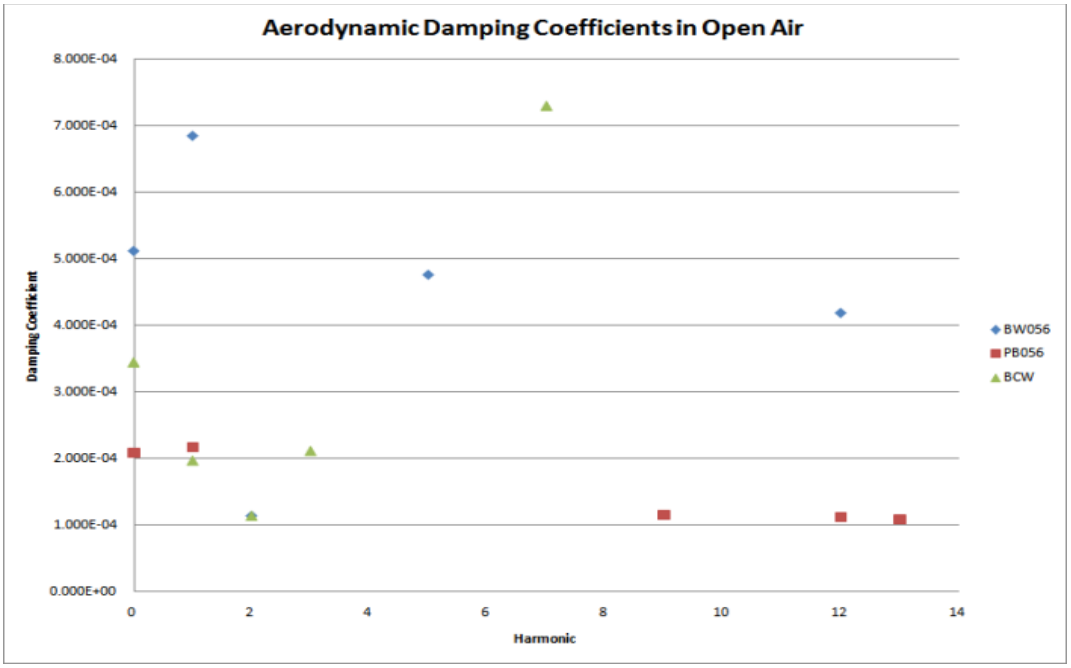

Figure 4-13: Aerodynamic Damping Coefficients in Air

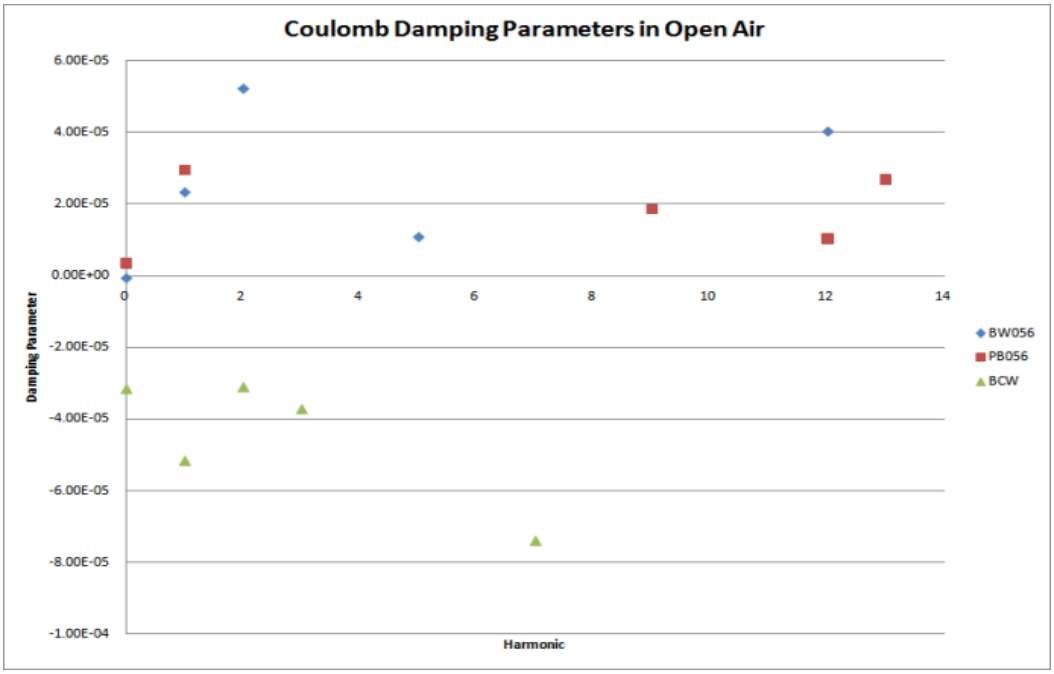

Figure 4-14: Coulomb Damping Parameters in Air

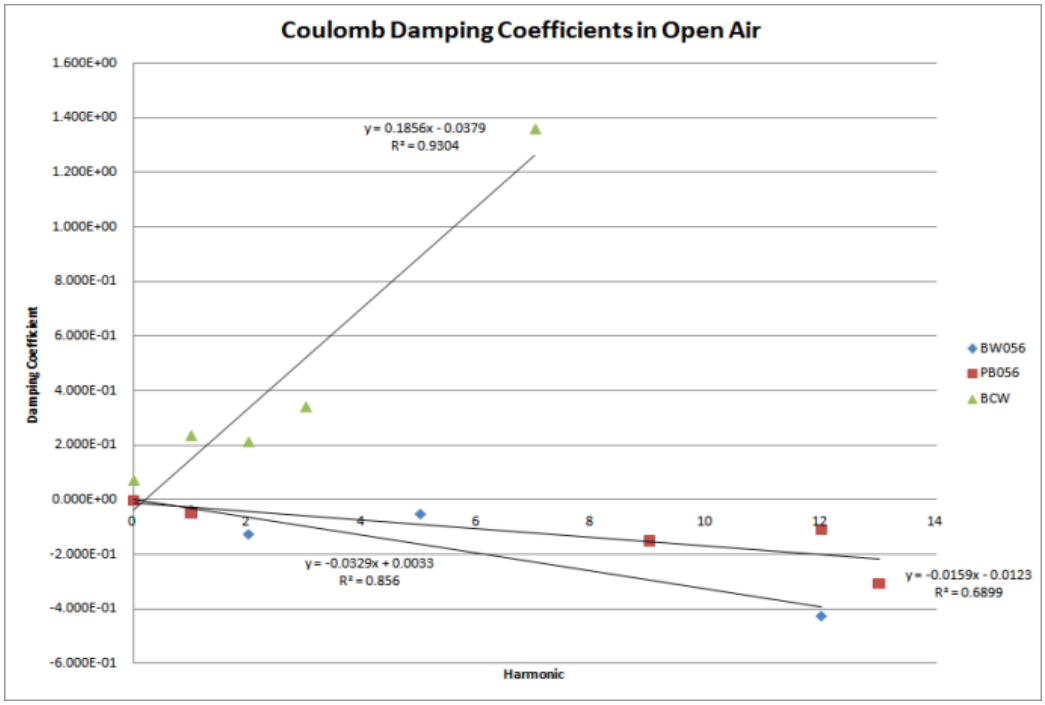

Figure 4-15: Coulomb Damping Coefficients in Air

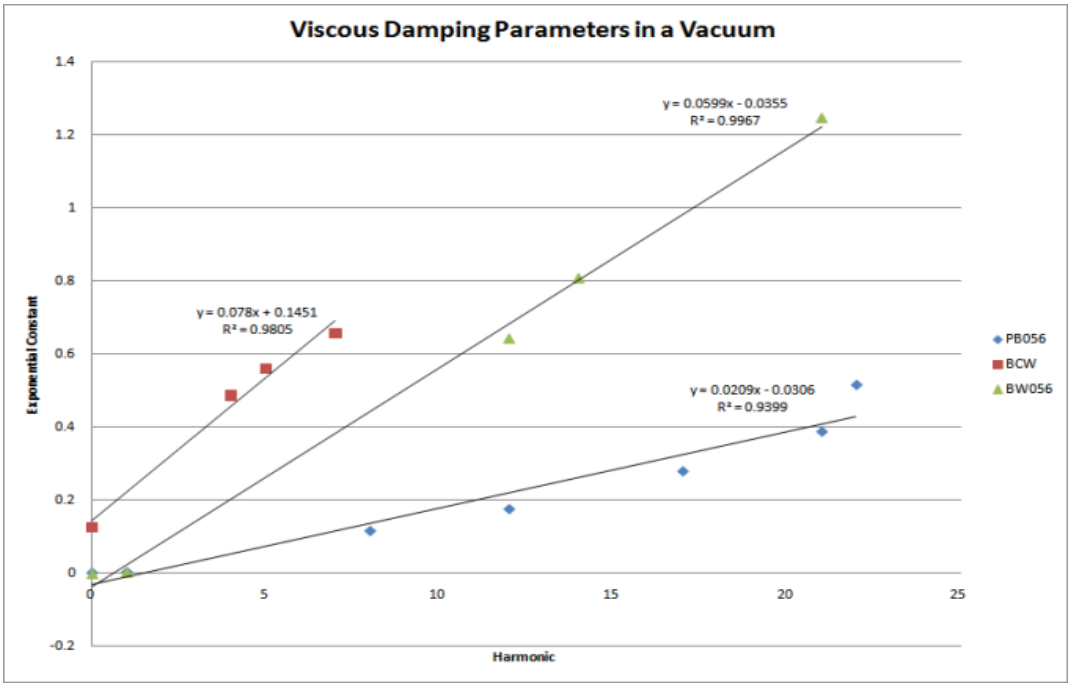

Figure 4-16: Viscous Damping Parameters in a Vacuum

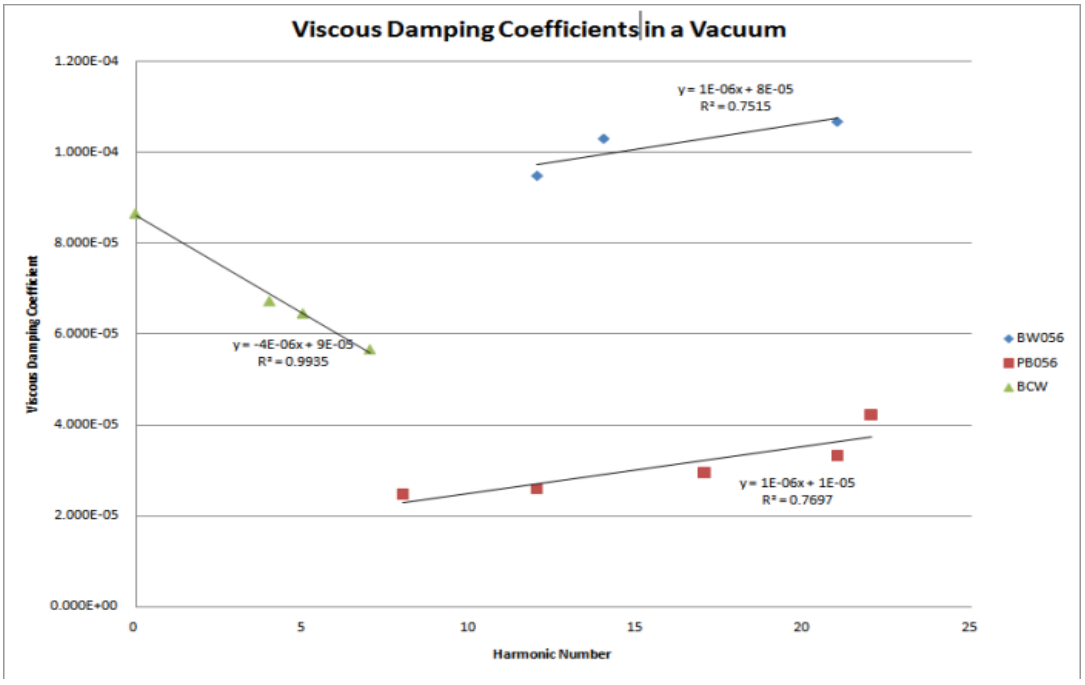

Figure 4-17: Viscous Damping Coefficients in a Vacuum

In Table 2 and Table 3, the sign of the Coulomb damping coefficient changed from the fundamental frequency to the first harmonic, indicating that the curve-fitting process is more that of mathematical convenience rather than physical relevance. Another interesting item to note is that in a vacuum, the viscous damping coefficient is shown to be relevant and significant. The few number of data points in Figures 4-12 through 4-17 are not of great concern since the presence and prominence of the viscous damping terms indicate that each data set needs to be refitted with all three damping parameters included. This will be discussed further in Section 4.3.3.

4.3.2. Damping Coefficient Variation

In order to identify how much the damping coefficients would vary from string to string, ten BW056 string were tested and curve-fitted using the same process listed above. The following figures show the variation of damping coefficients just for the fundamental frequency of the ten strings.

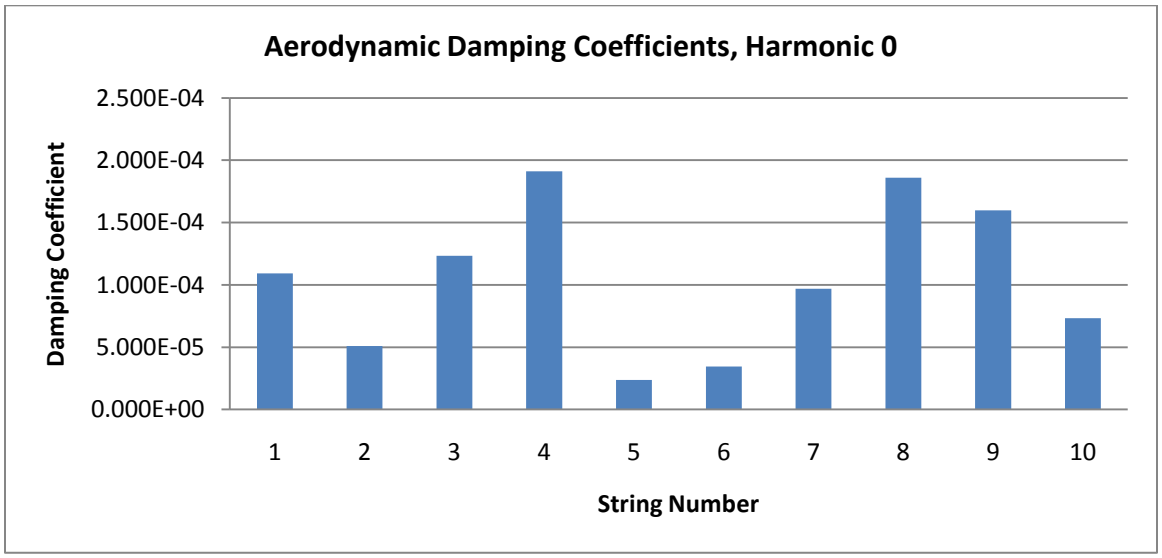

Figure 4-18: Variation in Aerodynamic Damping Coefficient for the Fundamental Frequency

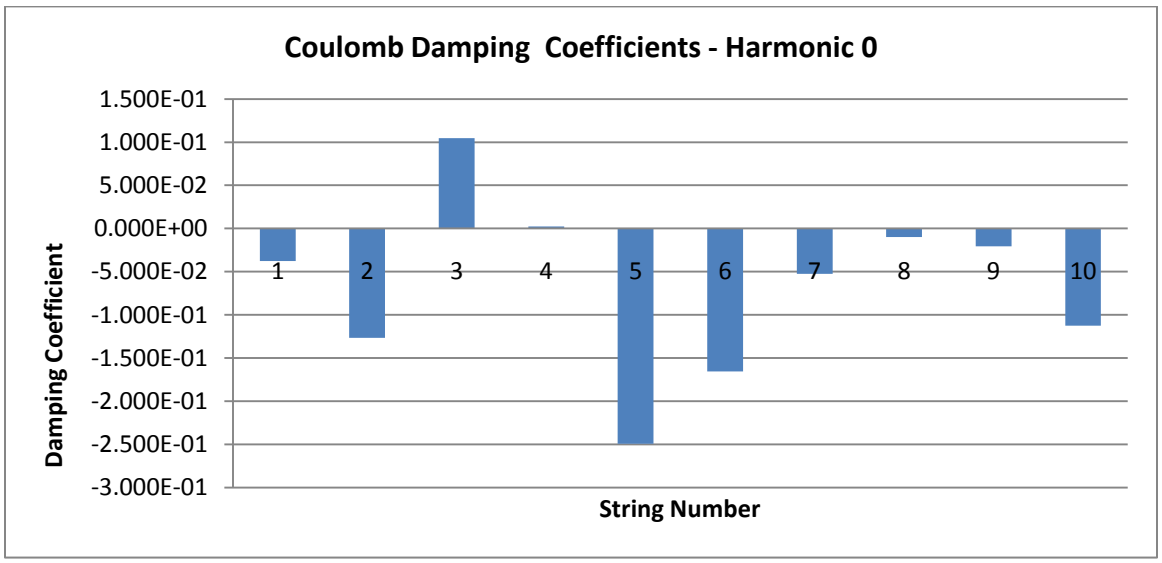

Figure 4-19: Variation in Coulomb Damping Coefficient for the Fundamental frequency

Figure 4-20 shows that for the 21st harmonic, there was little variation in the viscous damping coefficient.

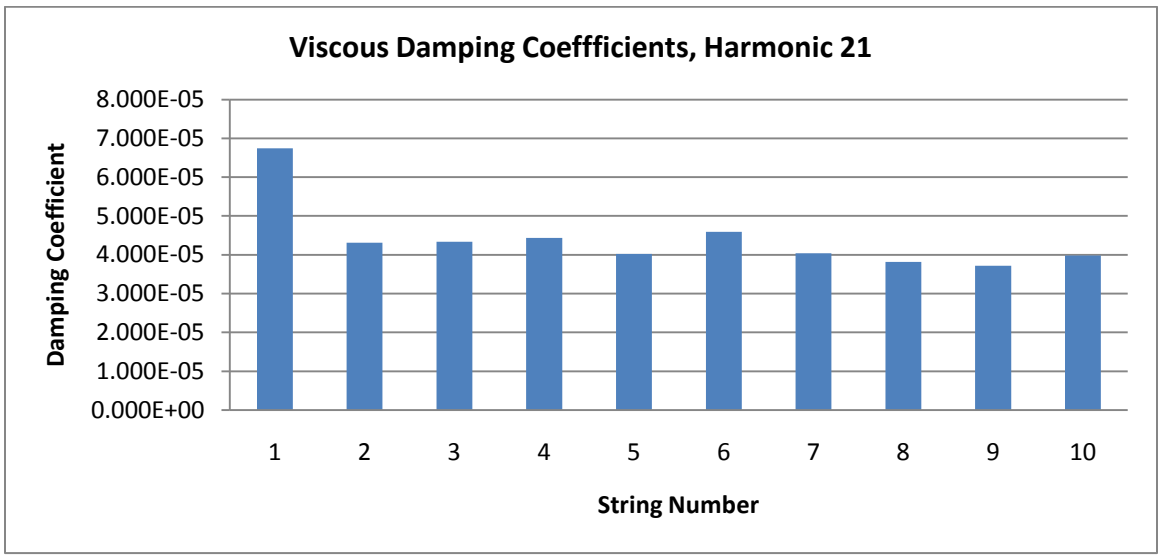

Figure 4-20: Variation in Viscous Damping Coefficient for the 21st Harmonic

When considering the damping variation across the frequency range, Table 8 shows that there is a significant amount of variation.

Table 8: BW056, Damping Coefficient Variation of 10 Strings

Harmonic	Aerodynamic (ε)	Coulomb (μ)	Viscous (ζ)
0	87.65%	338.58%	(n/a)
1	69.70%	3383.64%	(n/a)
12	86.37%	64.94%	(n/a)
21	(n/a)	(n/a)	44.86%

The variation in Coulomb damping across the frequency range is not physically possible. The significant variation in the Coulomb damping in the first harmonic is not caused by the change in signs of the damping coefficients as shown in Figure 4-19; rather, the coefficients are the same sign but there are two orders of magnitude difference between the minimum and maximum damping coefficient. The large variation in all three damping coefficients and the sign changes in the Coulomb damping coefficients deem this data as not physically relevant. Figure 4-19 shows that the Coulomb damping coefficient takes on any value that will positively influence a good mathematical curve-fit. Consequently, this does not reflect the probable physics acting on the system.

4.3.3. Curve-fitting, Second Pass

Originally it was thought that this viscous damping term was used out of mathematical convenience (see Section 2.2), and to approximate the fluid-structure interaction seen in aerodynamic damping. Appendix D shows that an exponential function can closely resemble the steady-state decay response of a system with quadratic damping by finding an appropriate amplitude term *(m)* and a decay term *(a)* that minimizes the square error between the two functions. The

primary difference between the two decay functions is the transient response. Because the function *1/t* has an asymptote at *t=0,* there is a very steep initial decay that the exponential function does not have. However, both functions approach 0 as *t* approaches infinity.

A more suitable approximation for a decay function *1/t* would be a logarithmic function. Appendix D also shows that a logarithmic function can be optimized such that the transient and steady-state responses can reflect that of the *1/t* function. Currently no type of damping is known to have a logarithmic decay envelope, limiting this information to purely a mathematical exercise.

For the BW056 and PB056 strings it is clear that an exponential function whose decay rate is directly proportional to frequency characterizes harmonics 12 and above both in open air and especially in a vacuum. In light of this, the BW056 open-air data was refitted with a function that includes all three damping components as seen in Eq. 3.2 and listed in Table 9.

Table 9: BW056 Open Air, Harmonic 0 Viscous-Aero-Coulomb Fit

Model	Function	SSE	R^2
Visc-Aero-Coul	F(t) = m*exp(-a*t) + (2*pi*a0)/(3*pi + c*t) -d*t + f	7.517e-010	0.999

When compared to the fits in Table 1, the fit with all three damping coefficients is superior. Table 10 shows the calculated damping coefficients using this new curve-fitting function.

Table 10: BW056 Open Air, Second Fit, Damping Coefficients

Harmonic	Aerodynamic (ε)	Coulomb (μ)	Viscous (ζ)
0	4.082E-04	-4.272E-03	1.365E-02
1	7.149E-04	-3.570E-02	8.976E-03
12	0	0	9.477E-05
21	0	0	1.039E-04

Table 11 compares the differences in damping coefficients obtained from the first and second pass curve-fitting methods.

Table 11: BW056 Open Air, First and Second Fit Comparisons

Harmonic	Aerodynamic (ε)	Coulomb (μ)	Viscous (ζ)
0	20.30%	958.40%	(n/a)
1	4.29%	4.99%	(n/a)
12	(n/a)	(n/a)	16.80%
21	(n/a)	(n/a)	0%

Curve-fitting the decay envelopes with the function listed in Eq. 3.2 was a very time-consuming process as the curve-fitting algorithm was sensitive to some variables and very insensitive to others. In the curve-fitting tool in Matlab, an initial guess could be specified and often the initial guess for a variable would be identical to the final fitted parameter. When observing changes in the fitted parameters, as a result of a different initial guess, it was found that the variable *c* (the aerodynamic damping parameter) was the most significant. This variable seemed to drive the rest of the fit in that if *c* was close to the optimal value the rest of the variables could take assume a wider range of values.

For example, in one curve-fit when *c* = 2, the value of *a* could range from 7–40 (a 471.4% variation) while *a0, d, f,* or *m* remained constant with no change in the SSE (1.094e-009) or R^2 (0.9986) values either. In another curve-fitting attempt when *c* = 1.5, *m* could assume values of 0.1–40 (a 39,900% variation) with 0.35% or less change in any of the other variables, no change in the R^2 (0.9989), and 0.064% change in the SSE.

Changing the value for *c* caused significant changes in *d* and *f* after every fit. For example, when trying to identify the optimal value for *c,* when *c* changed by 18%, *d* changed by 163% and *f* changed by 70%. This shows that the aerodynamic damping parameter is the driving factor in the curve-fit.

One variable that did not affect the goodness of the curve-fit was the magnitude of the exponential function, *m.* No matter what range of values this variable took on, it never affected the goodness of the curve-fit either positively or negatively. When an initial guess was used to fit this parameter, the fitted parameter always took on the value of the initial guess; this indicates that this variable is not meaningful in the fit and it was consequently omitted.

In the curve-fits in Table 10, the signs of the damping coefficients remained constant; however, there is still an issue with the Coulomb damping coefficients being negative. The problem lies when trying to use this damping coefficient in the SDOF models. Instead of energy being dissipated by a system in motion, negative damping implies that energy is being added to a system which is not physically possible with these given SDOF models.

4.4. SDOF Model Matching

From the three damping parameter curve-fit listed in Table 10, a SDOF model was created in order to try to match the response of the model to that of the data. If this model could match the data, then the next iteration of this model could lead to a MDOF lumped parameter model that is easy to solve and could replicate the harmonic content of a plucked string. From this lumped parameter

model, design variables could be identified from equivalent damping coefficients that commonly include terms pertaining to mass, stiffness, frequency, and amplitude. Eq. 4.3 is the equation of motion used for this SDOF model.

$$\ddot{x} + 2\zeta\omega\dot{x} + \varepsilon|\dot{x}|\dot{x} + \mu[sign(\dot{x})] + {\omega_n}^2 x = 0 \qquad \text{Eq. 4.3}$$

The *Odesolve* function in Mathcad was used to solve this equation with the following initial conditions.

$$x(0) = F(0) - 1 \qquad \text{Eq. 4.4}$$

$$\dot{x}(0) = 0 \qquad \text{Eq. 4.5}$$

The initial conditions defined in Eq. 4.4 apply to Eq. 3.2 (see below) with the fitted parameters *a, a_0, d,* and *f* coming from the curve-fit in Matlab.

$$F(t) = e^{-at} + \frac{2\pi a_0}{3\pi + ct} + dt + f \qquad \text{(Eq. 3.2)}$$

Because the value at time zero of the exponential function is equal to one, Eq. 4.4 subtracts one from the initial conditions because the response of the string very small.

The initial condition in Eq. 4.4 is equivalent to a system that is excited with an impulse in which the response is purely free response. Consider the impulse function below acting on a spring-mass-damper system.

$$I(t) = \left(\frac{1}{1 + e^{-rt}}\right)\left(\frac{1}{1 + e^{r(t-\delta)}}\right) \qquad \text{Eq. 4.6}$$

This function is the product of two sigmoid functions where *r* controls the curvature of the functions and δ controls the duration of the impulse. The time-response of this impulse function is shown in Figure 4-21.

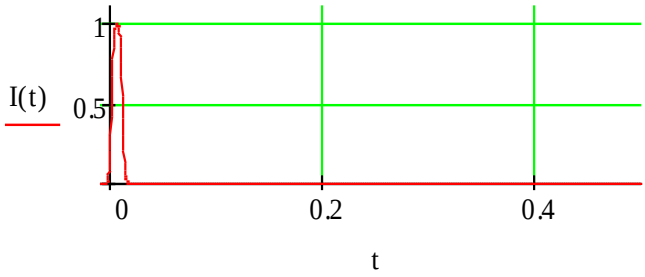

Figure 4-21: *Impulse Function*

When plotting the response of the spring-mass-damper and the impulse function on the same graph, it is easy to identify where the response is purely free response.

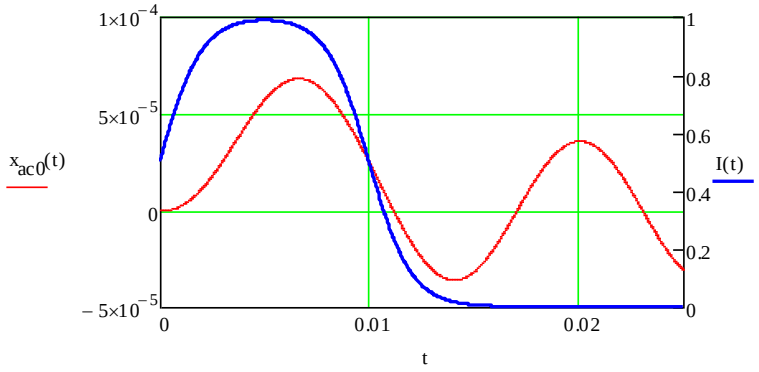

Figure 4-22: Impulse Response of a SDOF Spring-Mass-Damper System

Figure 4-22 shows that the free response of the system occurs after 0.015 seconds. At t = 0.02 seconds, the velocity is zero and the displacement is a constant value; this exactly resembles the initial condition used in Eq. 4.4.

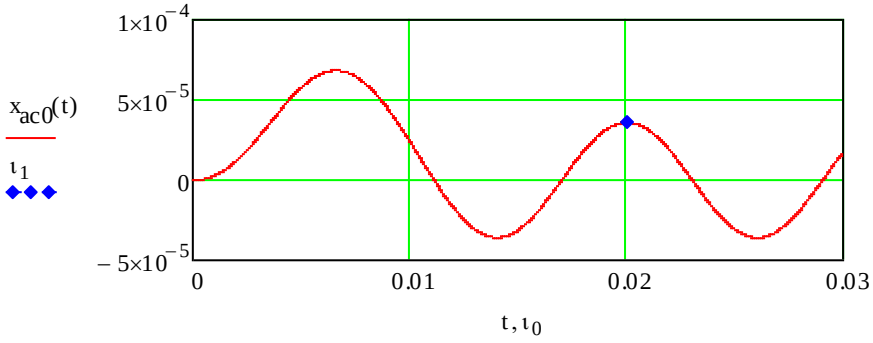

Figure 4-23: Initial Condition Point

In the equation of motion, Eq. 4.3, the calculated damping coefficients from the fitted data could not be used directly. In order to identify the appropriate damping coefficients in the equation of motion, the calculated coefficients from the data had to be scaled and then entered into the equation of motion. The

response was then plotted and visually matched to the decay profile function fitted from the data. Initially, aliasing in the SDOF response was a problem; then it was discovered that the default number of solution points in Mathcad is 1,000. In order to fix this aliasing problem, the number of solution points was increased to 150,000. Table 12 shows the calculated damping coefficients and the scaled coefficients used in the SDOF model for the fundamental frequency of the BW056 string.

Table 12: BW056, Harmonic 0, Scaled Damping Coefficients

	Aerodynamic (ε)	Coulomb (μ)	Viscous (ζ)
Calculated	4.082E-04	-4.272E-03	1.365E-02
Scaled Value	2.45E-01	2.443E-05	5.573E-05
Scale Factor	600	1/175	1/245

The figure below shows the SDOF response with these scaled damping coefficients and the decay function that was fitted from Matlab.

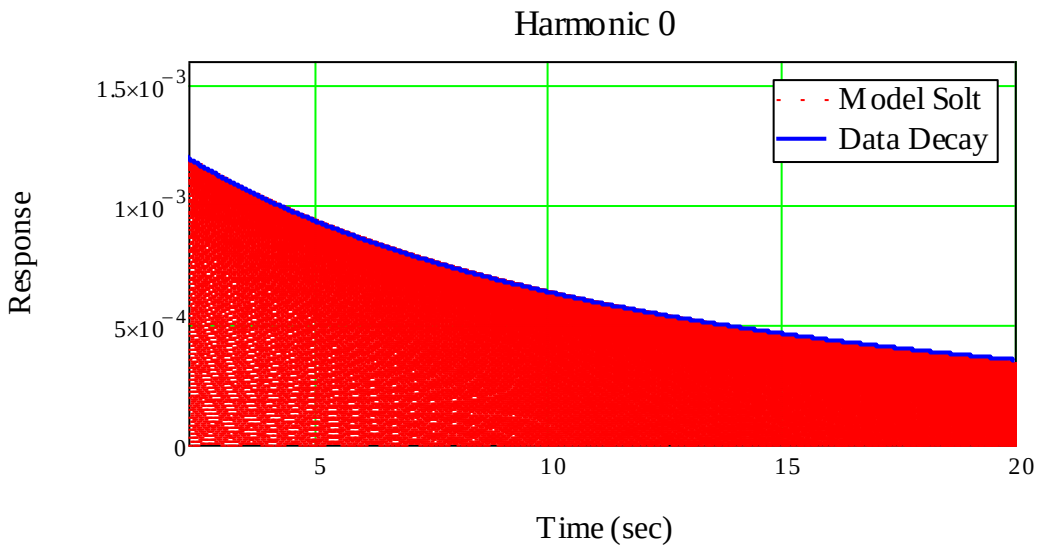

Figure 4-24: BW056, SDOF Model Response

This response was then exported to Matlab and curve-fitted using the same function listed in Eq. 3.2. The figure below shows the fitted decay envelopes from the data and from the SDOF model.

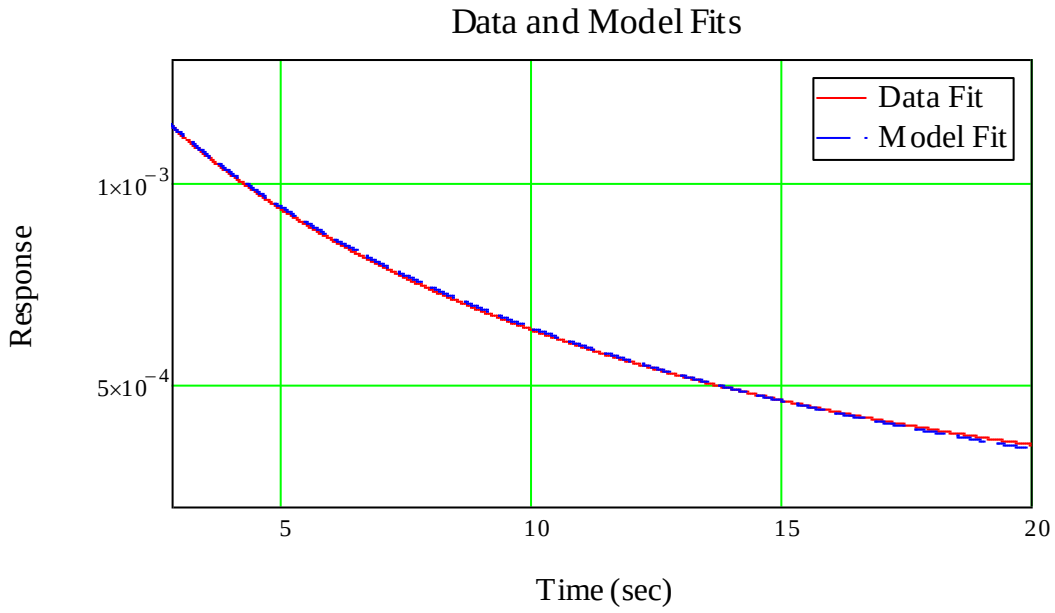

Figure 4-25: Data and Model Decay Envelopes

While the decay envelopes are visually identical, the numerical values of the damping coefficients show a great deal of variation.

Table 13: BW056, Harmonic 0, Damping Coefficient Comparisons

	Aerodynamic (ε)	Coulomb (μ)	Viscous (ζ)
Data	4.082E-04	-4.272E-03	1.365E-02
Model	4.17E-04	-1.455E-03	3.8E-02
Difference	2.16%	65.97%	175.02%

Given the difficulty in identifying scale factors, the wide range of variability in damping coefficients, and the limited amount of time left in this study, it was decided that further harmonics would not be fitted using this model.

This type of model was also used when trying to fit the data from Table 1 to Table 7; however, the three damping parameter curve-fit and model correlation produced superior results.

4.5. Differential Equation Solution Space

Another method to calculate the damping coefficients was attempted; it involved defining the homogenous equation of motion for SDOF system as a function and finding the roots of that function. A SDOF system with aerodynamic damping was considered in which the decay profile of the fundamental frequency was known from the curve-fit. The assumed solution used in the differential equation, Eq. 2.11, was a product of a sine wave of the fundamental frequency and this decay function, *f(t),* as shown below.

$$x(t) = \sin(\omega t) f(t) \qquad \text{Eq. 4.7}$$

$$Dx(t) = \dot{x}(t) \qquad \text{Eq. 4.8}$$

$$D2x(t) = \ddot{x}(t) \qquad \text{Eq. 4.9}$$

$$F(t, \varepsilon) = D2x(t) + \epsilon[Dx(t)]^2 + \omega^2 x(t) \qquad \text{Eq. 4.10}$$

The solution space of Eq. 4.10 is plotted in Figure 4-26.

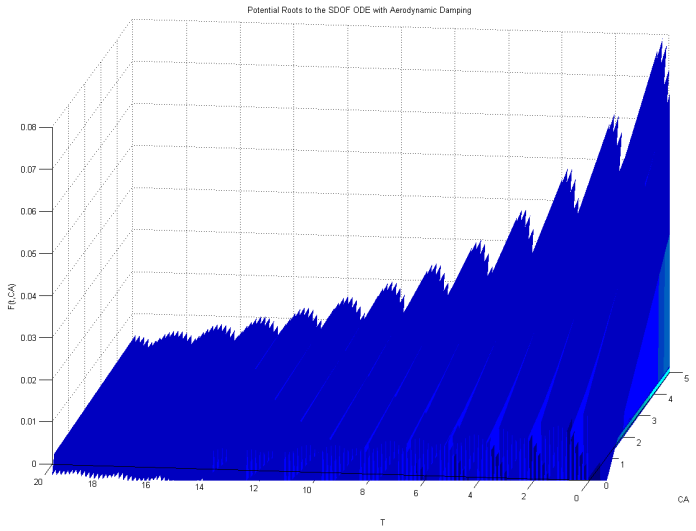

Figure 4-26: Solution Space, Aerodynamic Function

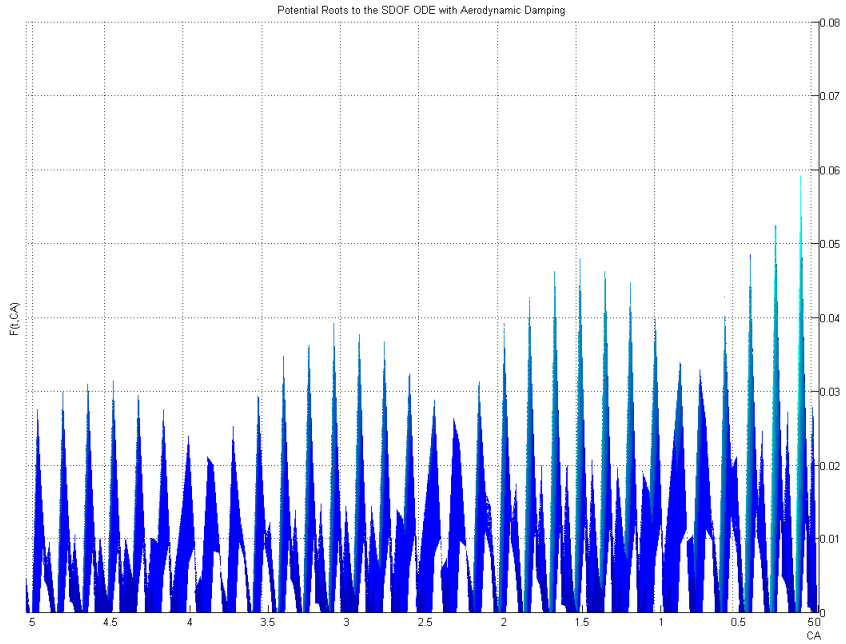

Figure 4-27: Solution Space, Aerodynamic Function Zoomed In

In order to satisfy the homogenous equation of motion, there must be a value for the aerodynamic damping coefficient such that, for all points in time, Eq. 4.10 equals zero. From Figure 4-26 and Figure 4-27 it can be seen that such a value does not exist. This method does not seem to be a practical option for finding the optimal damping coefficient, especially when three different types of damping are considered and the solution space becomes even more complex. This avenue of finding damping coefficients will be left for future study.

4.6. Summary

This chapter discussed the beat frequency complication and how it was resolved. This chapter also identified that the fitting function with aerodynamic, viscous, and Coulomb damping terms provided a more accurate fit than that of just the aerodynamic and Coulomb damping terms. A SDOF model was created using the calculated damping coefficients; however, in order to match the response from the data, the damping coefficients had to be scaled significantly. It appears that the aerodynamic damping parameters drive the curve-fit and the mathematical model as well. This enables the other damping coefficients to be able to take on a wide range of values that may not be physically accurate. A second method involving a math model of SDOF system with only aerodynamic damping was investigated, only to find that it could not provide a valid damping coefficient.

CHAPTER 5. CONCLUSIONS AND DISCUSSION

5.1. Overview

This chapter discusses the conclusions drawn from the study and suggests areas for future study. The causes behind the beating phenomenon seen in most of the harmonics are examined in detail, and the reliability of the curve-fitting routine and the SDOF model is addressed.

5.2. Beat Frequency Discussion

Throughout this study, the greatest obstacle that occurred was the presence of beat frequencies in the many of the string harmonics. Woodhouse (2004a) discussed this beating phenomenon and describes how each string mode consists of a pair of modes, one in the vertical and the other in the lateral plane. Due to low FFT resolution this pair of modes usually appears as one harmonic; in this experiment the FFT resolution was not an issue. Section 4.2 confirmed that the lateral and vertical modes are slightly different in frequency and could be caused by the structure on which the string was mounted. Woodhouse (2004a) described how the coupling between the body of a guitar and the string could change the string's rotational symmetry, causing the two frequencies to separate further. In Section 3.2, it was shown that the string and fixture have little to no dynamic interaction; however, this beating phenomenon was still prevalent. In this case, the rotational symmetry was not disrupted by string-fixture interaction; rather, it was caused by how the string was seated in the nut and saddle. When the string was in the shallow grooves of the steel nut

and saddle, the beating phenomenon worsened; but when the string was taken out of the grooves and laid to rest on the flat surface of the nut and saddle, the beating decreased.

It is interesting to note that the electromagnetic pickup was still able to measure both the vertical and lateral motion when the beating was most severe. Figure 4-9 shows that with the string out of the groove, there was still a difference between the vertical and lateral modes– either caused by geometric variations in the string or due to minor mounting differences. If the mounting point of the nut and the saddle are not colinear and flat, then the points where the string contacts the nut and saddle may be at slightly different angles, causing minor disruption in the rotational symmetry of the string. Figure 5-1, below, illustrates the angled point of contact; notice how the saddle slopes down from right to left.

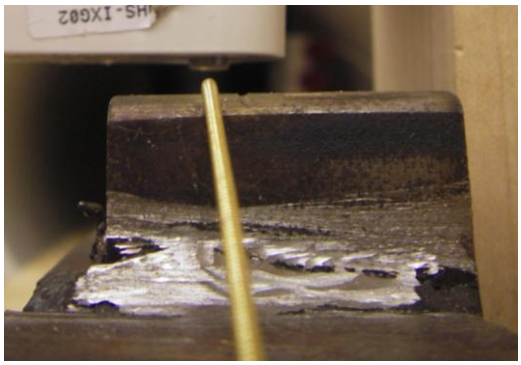

Figure 5-1: Sloped Surface on the Saddle

In the lower harmonics, a distinct two-phase decay was seen as shown in Figure 4-10. Woodhouse (2004a) theorized that this phenomenon is due to different amounts of damping in the two closely spaced orthogonal modes, but from the data in that study, the theory could not be prove. In this study, this phenomenon was observed with moderate regularity. The differences in contact point angles between the nut and the saddle could change the damping in the horizontal and vertical modes, giving this two-phase decay; but it is more likely that amplitude-dependent damping exists in the harmonics. When the amplitude of motion decreases to a certain level, a different type of damping dominates. In

Figure 4-10, the decay after six seconds is almost exclusively linear, indicating a transition from aerodynamic to Coulomb damping. Appendix G shows other instances of this two-phase decay in the time waveforms of a variety of harmonics.

In summary, removing the string from the grooves in the nut and saddle effectively minimized this beating phenomenon, allowing each harmonic to be filtered with confidence in knowing that it was a vertical mode as intended.

5.3. Viscous-like Damping in Upper Harmonics

When curve-fitting the vacuum data, the exponential decay function is prevalent in every harmonic; especially after the 12th harmonic where the decay envelope is exclusively exponential. When examining the viscous damping coefficients for the strings in a vacuum, the exponential decay constant increases with harmonic number.

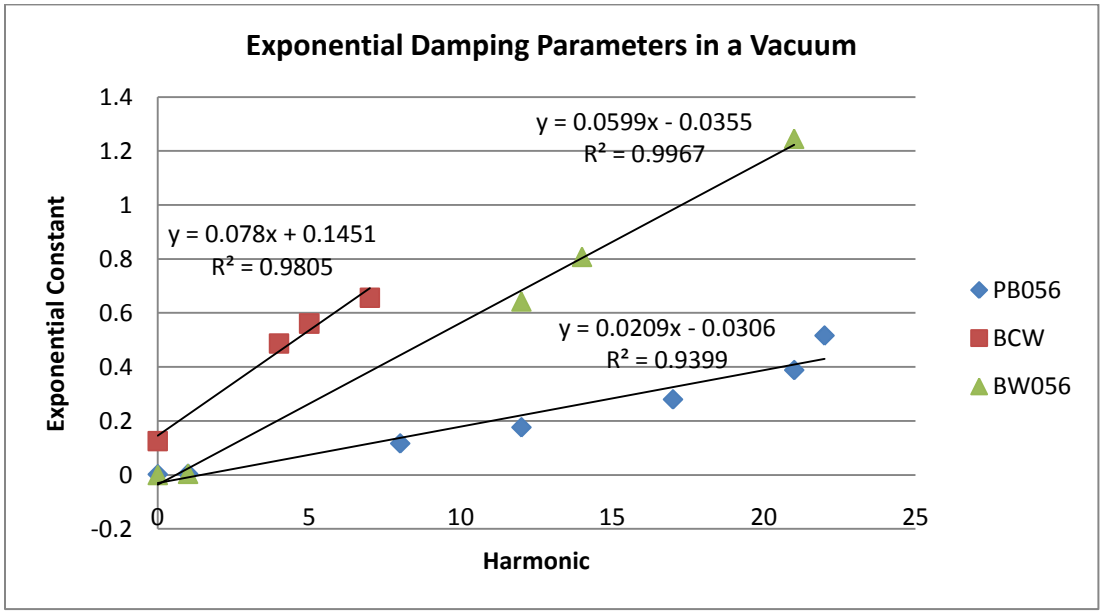

Figure 5-2: Exponential Damping Coefficients Increase with Harmonic

This is more informative than viewing the damping coefficient because in order to calculate the damping coefficient, the damping parameter is normalized by frequency. Figure 5-2 gives insight as to what are assumed to be the effects of material damping alone.

Because these data sets were collected in a vacuum, there are no effects of aerodynamic damping. Friction damping caused by the string rubbing on the nut or the saddle was assumed to be negligible. The fundamental frequency and first harmonic of the BW056 and PB056 strings each had contributions of linear damping which is the result of the friction forces incurred when the wrap-wire windings rub against each other. This was proved by the fact that the decay envelopes of the core-wire harmonics are purely exponential when placed in a vacuum. Since there are no windings, there is no Coulomb damping present in the filtered harmonics– leaving only material damping.

From Figure 5-2, it can be concluded that material damping may have similar properties to viscous damping. It is said to be viscous-like in that the damping force increases linearly with mode number similar to viscous damping, but there is no fluid-structure interaction for the data in Figure 5-2 because it was taken in a vacuum.

5.3.1. Brightness in Tone

Another conclusion that can be made from the data shown in Figure 5-2 is that the PB056 string quantitatively has less damping in the upper harmonics than the BW056 string. Initially it would appear that this material damping data contradicts what the musicians heard in that the string with 20% zinc wrap-wire (BW056) sounded “brighter” than the string with 8-10% zinc wrap-wire (PB056). More than likely, the musicians’ comments were based on playing with a full set of strings, not just one string at a time. Because the 80-20 bronze-wound low E string is more heavily damped than the phosphor bronze-wound low E string, the high frequency content from the other 80-20 strings would be more easily

perceived, resulting in an overall “brighter” sound. This shows that the method in this study confirms what the experienced guitarists are hearing when they play a set of strings.

5.4. Curve-fit Reliability

When curve-fitting the time-response data of each harmonic, the largest threat to validity was whether the curve-fit data could actually represent the physics that were occurring. It was proven in Appendices A, B, and C that a linear summation of damping functions given by Smith and Werely (1999) do in fact characterize the decay envelope for a SDOF system whose response is identical to that of a single string harmonic. Based on the results from this study, two obstacles still need to be addressed before this method can be considered reliable.

First, the sign of the calculated Coulomb damping coefficients are negative, which physically cannot occur in the SDOF model. Negative damping results in an unstable system, rendering the curve-fit and the model results meaningless. No matter what starting point or what range was defined when creating the curve-fit in Matlab, a positive damping coefficient could not be consistently contained. The curve-fit for the BW056 string in open air and in a vacuum for the first harmonic resulted in a positive Coulomb damping coefficient, but the remaining curve-fits resulted in negative Coulomb damping coefficients.

One reason why the damping coefficients never assumed the correct sign was because of the sensitivity of the curve-fitting algorithm; this is the second problem with the curve-fitting method. As mentioned in Chapter 4, the curve-fit was most sensitive to the aerodynamic damping parameter, and the viscous and Coulomb damping parameters could assume a wide range of values. It was expected that the curve-fitting algorithm would be more balanced in that each damping parameter could take on a small range of values that closely resembled the physics acting on the string as opposed to the wide range of values as

discussed in Section 4.3.3. This wide range of values makes it difficult to identify an optimal curve-fit that actually has physical relevance.

As discussed in Section 3.4, it appears that the curve-fit is largely influenced by the summation effect of the decay functions, in which the aerodynamic decay function is most significant. This function is the most significant because it has the fastest decay rate in the transient response due to the vertical asymptote at time 0. It would take the combination of an exponential function with a very fast decay rate along with a linear function with a very steep, negative slope to yield the same type of transient response. As time approaches infinity, the influence of this function may not be as significant, because the exponential or linear functions can now give nearly the identical steady-state response. This was demonstrated in Appendix D.

In summary, from the curve-fits, it is not possible to confirm that the calculated damping coefficients accurately describe the governing physics for the vibrating string.

5.5. Model Reliability

The SDOF model experienced some of the same sensitivity problems as the curve-fitting algorithm. While the SDOF model does accurately describe the response of a single string harmonic, it cannot accurately match the damping coefficients as calculated from the fitted damping parameters. The calculated damping coefficients cannot be used directly in these models; rather, they must be scaled significantly to match the fitted decay envelope. The scaling shown in Table 12 indicates that the aerodynamic damping coefficient is the most significant in matching the model's response to that of the data.

While the aerodynamic damping coefficients in the model and the data match well, the model still has difficulty matching the Coulomb and viscous damping coefficients. The model appears to be most sensitive to the aerodynamic damping parameter just as in the curve-fit. Again, this appears to

be out of mathematical convenience in that the 1/t function can fit the steep transient response as well as the flat steady state response.

5.6. Areas of Future Study

If this analysis method is to be used in the future, there are several areas that need to be researched before this method can be deemed as reliable.

5.6.1. Linear Electromagnetic Pickup Response

The first area of study lies in the nonlinear response of the electromagnetic pickup. Figure 3-19 showed that the decay rate of the fundamental frequency increases as the pickup is moved further away from the string. The amplitude of motion should decrease; however, the decay rate should not change. It is possible that the steel fixture altered the magnetic field in some way; for this, a magnetometer should be used to characterize the magnetic field around the string and pickup. If available, a modern laser vibrometer would be a more suitable instrument to measure the response of the string.

5.6.2. Effects of Boundary Contact Angle

If a similar type of fixture is used in the future, the effects of boundary contact angle in non-planar motion should be studied. If this contact angle significantly alters the rotational symmetry of the string then extra care should be taken in creating a satisfactory nut and saddle for mounting the string. Similarly, the effects of groove geometry on non-planar motion should also be studied. If the depth of cut or angle of cut in the nut (and potentially saddle) alters the rotational symmetry of the string, this could explain a source of variation in tonal differences in acoustic guitars. While changes in tonal variation in acoustic guitars caused by geometry, build materials, and soundboard bracing have been widely studied, the effects of groove geometry have not be heavily researched.

This area could also explain tonal differences in electric guitars to a certain extent; the type and location of the pickup is usually a larger contributor in tonal differences.

5.6.3. Friction Losses at the Boundaries

While the primary source of friction damping was assumed to come from the windings rubbing on each other, the effects of friction damping by the string rubbing on the nut and saddle are worth investigating in the future. A challenge in this avenue of study will be in measuring the longitudinal (or axial) motion of the string if conventional Coulomb damping is to be calculated. In trying to enforce high-impedance boundary conditions, it was clear that some vertical motion in the string at the boundaries was damped out when clamped. If this vertical motion is appreciable, then perhaps traditional Coulomb- sliding friction- damping is not the best way to describe the damping at the boundaries. If the string moves vertically and laterally at the boundaries then another type of damping model will need to be identified.

5.6.4. Partial Differential Equation Models

From this study, it was apparent that, while the SDOF and lumped parameter models are easy to solve and simple in nature, they are not sufficient for guitar string manufacturers to use in the near future. Instead, a partial differential equation model should be used if the time-responses of the harmonics are desired. A less numerically intensive approach would be to use transfer functions and modal parameters in the frequency domain, similar to that of Woodhouse (2004a).

If a partial differential equation model is to be used, then extra effort needs to be made in accounting for the wrap-wire for wound guitar strings. The most well known equations of motion for strings do not account for windings. Haselhoff (2010) derived an expression for the tension of a wound string which can be

used in the one-dimensional wave equation. This is a good first step for investigation in this avenue of study, but several assumptions made in this derivation should be addressed. Problematic assumptions may include:

1. The diameter of the wrap and core-wires are the same.
2. The density of the wrap and core-wires are the same.
3. Bending stiffness in the string is negligible.
4. String motion is limited to one direction.
5. No damping terms are included.

5.6.5. Hysteretic Damping Model

While the qualitative appearance of material damping was identified in this study (see Section 5.3), a valid material damping model needs to be identified. Chen and You (1999) and Inaudi (1995) used an integral-differential equation model to characterize temporal hysteretic damping via the Hilbert transform. While this may ultimately describe temporal hysteresis, it is numerically intensive to solve. If guitar manufacturers want a model that they can tune in order to achieve the desired amount of damping in their strings, they will most likely want something simpler to use. Currently, this seems to be the most physically relevant mathematical model; others violate the causality principle, contradict experimental results, or result in unstable systems as discussed in Section 2.5.

5.6.6. New Curve-fitting Algorithms

While the curve-fitting methods outlined in this study are numerically easy to use and understand, the sensitivity of the algorithms in Matlab must be addressed. It is understood that the aerodynamic decay function numerically drives the curve-fit; however, this obscures the Coulomb and viscous damping parameters. In order to remedy this, different curve-fitting routines should be investigated. It could be that the current curve-fitting algorithms in Matlab are the most efficient, but a weighting factor needs to be added to the Coulomb and

viscous damping parameters. To supplement this investigation, dynamic time-response data should be taken using a vacuum chamber at varying pressures. If only the aerodynamic damping parameter changes with pressure while the other damping parameters hold the same values, this indicates that the calculated damping coefficients actually reflect the physics of the system because only aerodynamic damping should be changing.

5.7. Summary

From this study the following two conclusions have been made:

- The decay functions given by Smith and Werely (1999) can be summed linearly in order to accurately curve-fit the decay envelope of a string harmonic with multiple types of damping. These functions can be used to calculate the damping coefficients for each harmonic; however, the physical accuracy of these coefficients is highly dependent on the sensitivity of the curve-fitting algorithm.
- The same algorithm sensitivity occurs when trying to match the response of the SDOF model to the data.

Because of these two conclusions, this method is not ready to be used in industry settings.

For the future, a laser vibrometer is the ideal choice of transducers to be used in this type of testing. The effects of contact angle and friction losses at the boundaries also need to be investigated. A valid and easy-to-use model for hysteretic damping is needed along with a partial differential equation model that accurately describes the physics of wound strings. Lastly, a different curve-fitting algorithm may be needed: one that either can apply weighting factors to fitted parameters, or one that is less sensitive to the aerodynamic damping function. After these areas of study have been investigated, this method could prove to provide accurate damping information on a harmonic basis that guitar string manufacturers could use some day to change the tone of their strings.

LIST OF REFERENCES

LIST OF REFERENCES

Adhikari, S. (2006). Damping modeling using generalized proportional damping, *Journal of Sound and Vibration, 293 (1-2),* p. 156-170

Adhikari, S., & Woodhouse, J. (2001a). Identification of Damping: Part 1, Viscous Damping. *Journal of Sound and Vibration, 243 (1),* p. 43-61.

Adhikari, S., & Woodhouse, J. (2001b). Identification of Damping: Part 2, Non-Viscous Damping. *Journal of Sound and Vibration, 243 (1),* p. 63-88.

Banks, H.T., & Inman, D.J. (1991). On Damping Mechanisms in Beams. *Journal of Applied Mechanics, 58,* p.716-723.

Beards, C. F. (1996). *Structural Vibration: Analysis and Damping*. New York, NY: Halsted Press.

Chen, J.T, & You, D.W., (1998). An Integral-Differential Equation Approach for the Free Vibration of a SDOF System with Hysteretic Damping. *Advances in Engineering Software, 30 (1),* p.43-48.

Dalton, W.K. (1994). *The Technology of Metallurgy.* New York, NY: Macmillian Publishing Company.

Elliott, J.A. (1980). Intrinsic Nonlinear Effects in Vibrating Strings. *American Journal of Physics, 48 (6),* p.478-480.

Ewins, D.J. (2000). *Modal Testing: Theory and Practice (2nd edition)*. Baldock, Hertfordshire, England: Research Studies Press LTD.

Fang, TS. (2007). *Analysis on Non-Resonance Standing Waves and Vibration Tracks of Strings, 28 (4),* p.665-672.

French, R.M. (2009). *Engineering the guitar: Theory and Practice*. New York, NY: Springer Science+Business Media, LLC 2009.

French, R.M. (1999). What Makes a Good Impact Function. *Experimental Techniques, 23 (6),* p.33-35.

Hanson, R.J., Anderson, J.M., & Macomber, H.K., (1994). Measurements of Nonlinear Effects in a Driven Vibrating Wire. *Journal of the Acoustic Society of America, 96 (3).* p.1549-1556

Hasselman, T.K. (1972). Method for Constructing a Full Modal Damping Matrix from Experimental Measurements. *AIAA Journal, 10 (4).* p.526-527.

Horton, N.G. & Moore, T.R. (2009). Modeling the Magnetic Pickup of an Electric . *American Journal of Physics, 77 (2)*. p.144-150.

Inaudi, J.A., & Kelly, J.M. (1995). Linear Hysteretic Damping and the Hilbert Transform. *Journal of Engineering Mechanics*, *121*, p.626-632

Johns, R. (1977). Musical String Vibrations. *The Physics Teacher, 15 (3)*, p.145-156

Giordano, N. (1998). The Physics of Vibrating Strings, *Computers in Physics, 12 (2),* p.138-145

Hanson, R.J., Anders, J.M., Macomber, H.K. (1994) Measurements of nonlinear effects in a driven vibrating wire, *Journal of the Acoustical Society of America, 96, (3),* p.1549-1556

Haselhoff, E. (2010). The String Equations for Solid and Wound Musical Instrument Strings. Retrieved from HTTP://WWW.ELTJOHASELHOFF.COM/MAIN/ARTICLES/ARTICLES.HTML

Minas, C. & Inman, D.J. (1991). Identification of a Nonproportional Damping Matrix from Incomplete Modal Information. *Journal of Vibration and Acoustics, 113, p.219-224.*

Nashif, A. D, Jones, D. I., Henderson, J. P. (1985). *Vibration Damping*. New York, NY: John Wiley & Sons, Inc.

Norton, M.P., & Karczub, D.G. (2003). Fundamentals of Noise and Vibration Analysis for Engineers (2^{nd} ed.). Cambridge, UK: Cambridge University Press.

Rao, S.S. (2004). *Mechanical Vibrations* (4^{th} ed.). Upper Saddle River, NJ: Pearson Prentice Hall.

Lord Rayleigh. (1897). *Theory of Sound* (2nd ed., 1945 re-issue). New York, NY: Dover Publications.

Silva, C. W. (2007). *Vibration Damping, Control and Design*. Boca Raton, FL: Taylor & Francis Group, LLC.

Smith, C.B., & Wereley, N.M. (1999). Nonlinear Damping Identification from Transient Data. *AIAA Journal, 37 (12).* p.1625-1632.

Stanbridge, A.B, & Ewins, D.J. (1999). Modal Testing Using a Scanning Laser Doppler Vibrometer*, Mechanical Systems and Signal Processing 13 (2)*. p.255-270.

Stokes, G.G. (1850). Proceedings from the Cambridge Philosophical Society

Woodhouse, J. (1998). Linear Damping Models for Structural Vibration. *Journal of Sound and Vibration, 215 (3),* p. 547-569.

Woodhouse, J. (2004a). Plucked Guitar Transients: Comparison of Measurements and Synthesis. *Acta Acustica United with Acustica, 90 (5),* p.945-965

Woodhouse, J. (2004b). On the Synthesis of Guitar Plucks. *Acta Acustica United with Acustica, 90 (5),* p.924-944

APPENDICES

Appendix A. Damping Solutions

OBJECTIVE: Verify the appropriate solutions to the 1D wave equation

$m := 1 \qquad K := 8 \qquad \omega := \sqrt{\frac{K}{m}} = 2.828 \qquad f := \omega \cdot \frac{180}{\pi} = 162.057$

Is the solution to aerodynamic damping really a double exponential function?

Aerodynamic Damping Coefficient: $a_a := 0.15$

Given

$x(0) = 1 \qquad x'(0) = 0$

$x''(t) + a_a \cdot |x'(t)| \cdot x'(t) + \frac{K}{m} \cdot x(t) = 0$

$x_a := \text{Odesolve}(t, 20)$

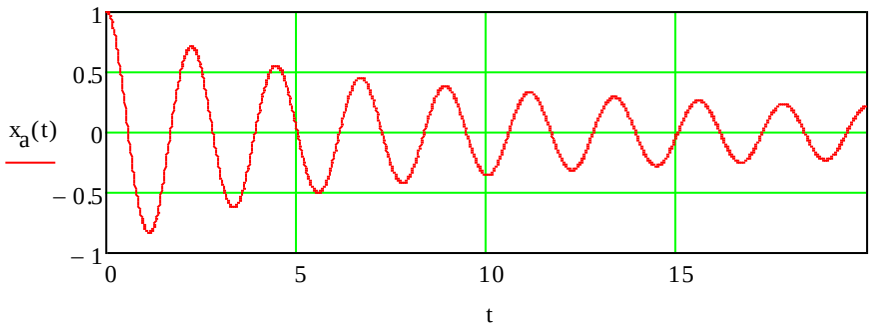

Is the solution to Coulomb damping really a linear function?

Coulomb Damping Coefficient: $a_c := 0.15$

Given

$x(0) = 1 \qquad x'(0) = 0$

$x''(t) + a_c \cdot \text{sign}(x'(t)) + \frac{K}{m} \cdot x(t) = 0$

$x_c := \text{Odesolve}(t, 20)$

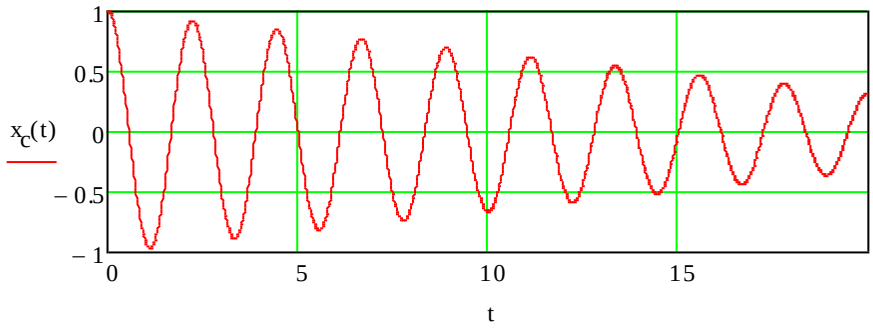

Is the solution to Viscous damping really an exponential function?

Viscous Damping Coefficient: $a_V := 0.15$

Given

$x(0) = 1 \qquad x'(0) = 0$

$x''(t) + a_V \cdot x'(t) + \frac{K}{m} \cdot x(t) = 0$

$x_V := \text{Odesolve}(t, 20)$

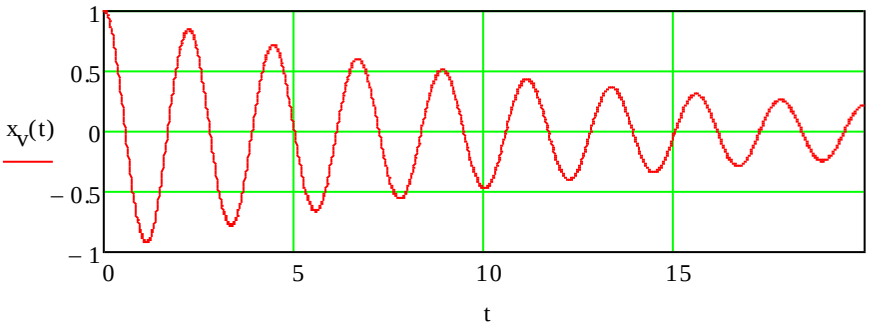

Export the data to Matlab and curve-fit the profiles

$t := 0, .1 .. 20$

$x_V(t) =$	$x_a(t) =$	$x_c(t) =$
1	1	1
0.96	0.96	0.961
0.846	0.845	0.847
0.666	0.667	0.667
0.436	0.441	0.436
0.176	0.189	0.172
-0.095	-0.068	-0.105
-0.354	-0.31	-0.372
-0.581	-0.52	-0.607
-0.759	-0.684	-0.793
...	...	...

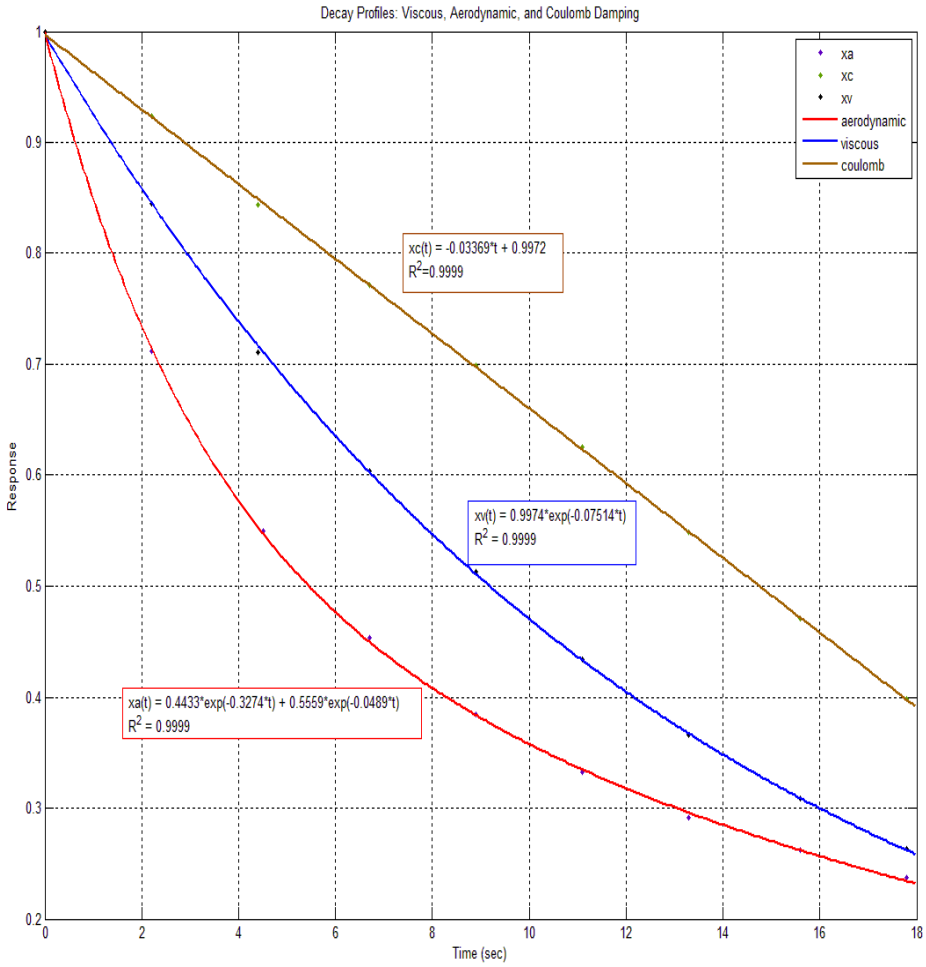

The curve-fits verify the theories:

1) Viscous damping exhibits an exponential decay profile
2) Aerodynamic damping exhibits a double exponential decay profile.

Note:
Smith and Werely (1999) indicate that it is a function of the form 1/t

3) Coulomb damping exhibits a linear decay profile

Appendix B. Smith and Werely Decay Envelopes

OBJECTIVE: Verify that the decay envelopes given by Smith and Werely (1999) are valid for the SDOF model at actual frequencies observed in the guitar string.

Smith and Werely gave the following decay envelopes for a SDOF spring-mass-damper system with three different types of damping:

	Equation of motion	*Decay Envelope*
Viscous Damping:	$x''(t) + 2\zeta\cdot\omega\cdot x'(t) + \omega^2\cdot x(t) = 0$	$a_V(t) = e^{-\zeta\cdot\omega\cdot t}$
Aerodynamic Damping:	$x''(t) + \varepsilon\cdot\lvert x'(t)\rvert\cdot x'(t) + \omega^2\cdot x(t) = 0$	$a_a(t) = \frac{2\cdot\pi\cdot a_0}{3\cdot\pi + 4\cdot\varepsilon\cdot\omega\cdot a_0\cdot t}$
Coulomb Damping:	$x''(t) + \mu\cdot\mathrm{sign}(x'(t)) + \omega^2\cdot x(t) = 0$	$a_c(t) = \frac{-2\cdot\mu}{\pi\cdot\omega}\cdot t + y_0$

Now verify that these profiles accurately describe the response of the SDOF model:

$\omega := 81.252\cdot\pi$ Fundamental frequency of the BW056 string

VISCOUS DAMPING: $\zeta := 0.000$

Given

$x(0) = 1 \qquad x'(0) = 0$ Give the spring-mass-damper system a unit displacement:

$x''(t) + 2\zeta\cdot\omega\cdot x'(t) + \omega^2\cdot x(t) = 0$

$x_V := \mathrm{Odesolve}(t, 20, 20000)$

$t := 0, \frac{20}{20000} .. 20$

Export the data to Matlab to curve fit it with the decay envelopes given by Smith and Werely (1999)

$t =$	$x_V(t) =$
0	1
$1\cdot10^{-3}$	0.873
$2\cdot10^{-3}$	0.523
$3\cdot10^{-3}$	0.039
...	...

If Smith and Werely are correct, then the decay envelope should be: $a_V(t) = e^{-\zeta\cdot\omega\cdot t}$

where: $-\zeta\cdot\omega = -0.1021$

From Matlab, the best fit decay envelope was found to be:

$f_V(t) := e^{-0.1024 t}$ $\quad R^2 = 1$

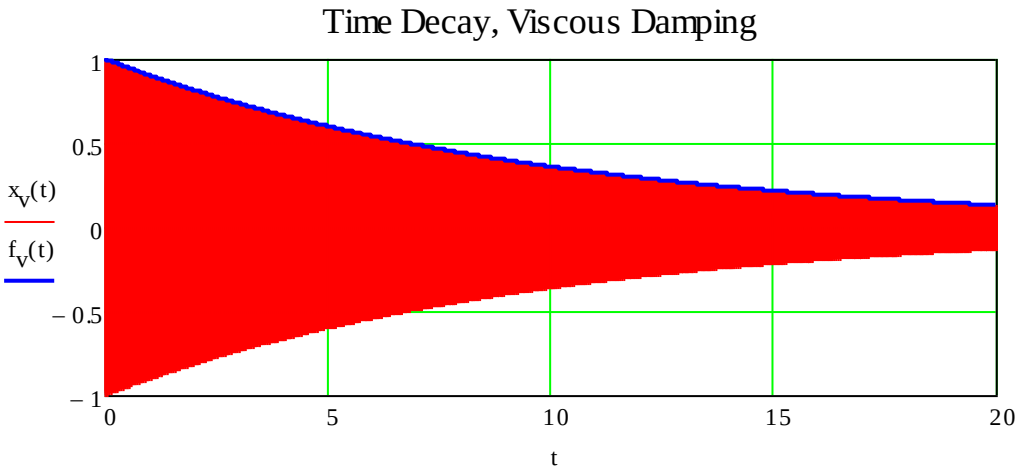

The % difference in the exponents are: $E_V := \left| \frac{.1021 - 0.1024}{.1021} \right| \cdot 100$ $\quad E_V = 0.294$

The decay profile for viscous damping has been validated, now move onto Aerodynamic Damping.

AERODYNAMIC DAMPING $\varepsilon := .002$

Aerodynamic damping is considered quadratic damping in that it is proportional to the velocity squared. Quadratic damping was mentioned in Smith and Wereley (1999); however, this is synonomous with Aerodynamic Damping.

Given

$x(0) = 1 \qquad x'(0) = 0$

$x''(t) + \varepsilon \cdot |x'(t)| \cdot x'(t) + \omega^2 \cdot x(t) = 0$

$x_a := \text{Odesolve}(t, 20, 20000)$

Export the data to Matlab to curve fit it with the decay envelopes given by Smith and Werely (1999)

$t =$	$x_a(t) =$
0	1
$1 \cdot 10^{-3}$	0.873
$2 \cdot 10^{-3}$	0.523
$3 \cdot 10^{-3}$	0.04
...	...

If Smith and Werely are correct, then the decay envelope should be: $a_a(t) = \frac{2\cdot\pi\cdot a_0}{3\cdot\pi + 4\cdot\varepsilon\cdot\omega\cdot a_0\cdot t}$

where: $a_0 := \frac{3}{2}$

$4\cdot\varepsilon\cdot\omega = 4.084$

From Matlab, the best fit decay envelope was found to be:

$f_a(t) := \frac{3\pi}{3\pi + 4.089t}$ $R^2 = 1$

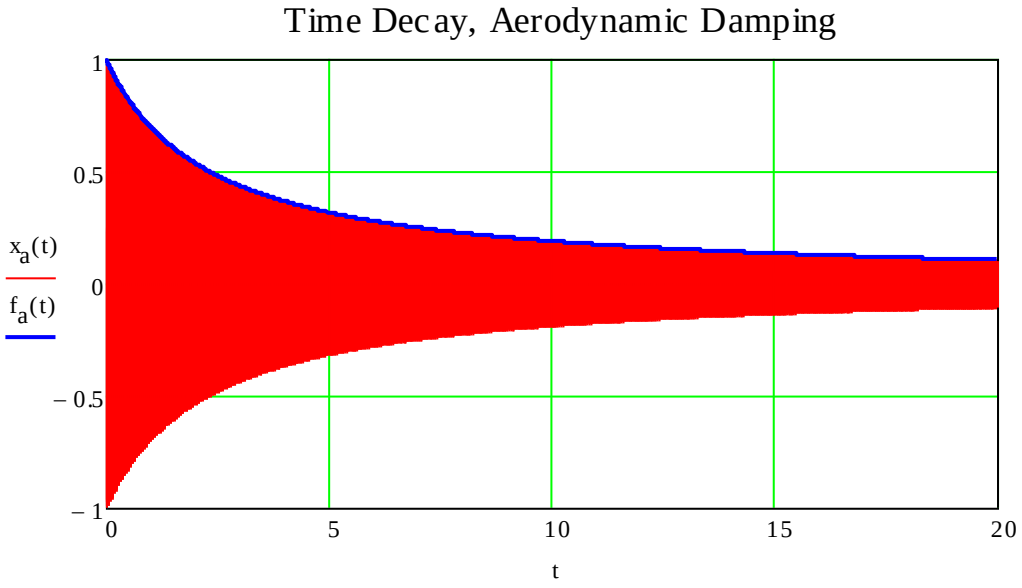

The % difference in the constants are: $E_a := \left|\frac{6.126 - 4.089}{6.126}\right|\cdot 100$ $E_a = 33.252$

This error is significant in magnitude and relevant because the damping coefficient is contained in this number. Try to see if a correction factor can be made to account for this.

First, see if this correction factor is constant for different damping coefficients:

$\varepsilon = 2\times 10^{-3}$ now let: $\varepsilon_1 := 0.001$ $\varepsilon_2 := 0.005$ $\varepsilon_3 := 0.01$

Given

$x(0) = 1 \qquad x'(0) = 0$

$x''(t) + \varepsilon_1 \cdot |x(t)| \cdot x'(t) + \omega^2 \cdot x(t) = 0$

$x_{a1} := \text{Odesolve}(t, 20)$

Given

$x(0) = 1 \qquad x'(0) = 0$

$x''(t) + \varepsilon_2 \cdot |x(t)| \cdot x'(t) + \omega^2 \cdot x(t) = 0$

$x_{a2} := \text{Odesolve}(t, 20)$

Given

$x(0) = 1 \qquad x'(0) = 0$

$x''(t) + \varepsilon_3 \cdot |x(t)| \cdot x'(t) + \omega^2 \cdot x(t) = 0$

$x_{a3} := \text{Odesolve}(t, 20)$

Export the data to Matlab and perform another series of curve fits

$x_{a1}(t) =$

1
0.886
0.772
0.659
0.548
0.438
...

$x_{a2}(t) =$

1
0.886
0.773
0.661
0.55
0.441
...

$x_{a3}(t) =$

1
0.887
0.775
0.663
0.553
0.444
...

The best fit curves are:

$f_{a1}(t) := \dfrac{3 \cdot \pi}{3 \cdot \pi + 2.045t}$ $\qquad$ $f_{a2}(t) := \dfrac{3 \cdot \pi}{3 \cdot \pi + 10.22t}$ $\qquad$ $f_{a3}(t) := \dfrac{3 \cdot \pi}{3 \cdot \pi + 20.43t}$

$R^2 = 1$ $\qquad$ $R^2 = 1$ $\qquad$ $R^2 = 1$

$4 \cdot \varepsilon_1 \cdot \omega \cdot a_0 = 3.063$ $4 \cdot \varepsilon_2 \cdot \omega \cdot a_0 = 15.315$ $4 \cdot \varepsilon_3 \cdot \omega \cdot a_0 = 30.631$

The % difference in the constants are: $E_{a1} := \left| \frac{3.063 - 2.045}{3.063} \right| \cdot 100$ $E_{a1} = 33.235$

The % difference in the constants are: $E_{a2} := \left| \frac{15.315 - 10.22}{15.315} \right| \cdot 100$ $E_{a2} = 33.268$

The % difference in the constants are: $E_{a3} := \left| \frac{30.631 - 20.43}{30.631} \right| \cdot 100$ $E_{a3} = 33.303$

The magnitude of the damping coefficient seems to be low by a constant factor. See if the same is true for different frequencies.

$\omega = 510.509$ $\omega_1 := 40 \cdot 2 \cdot \pi = 251.327$ $\omega_2 := 160 \cdot 2 \cdot \pi = 1.005 \times 10^3$ $\omega_3 := 800 \cdot 2 \cdot \pi = 5.027 \times 10^3$

Given

$x(0) = 1$ $x'(0) = 0$

$x''(t) + \varepsilon \cdot |x(t)| \cdot x(t) + \omega^2 \cdot x(t) = 0$

$x_{aw1} := \text{Odesolve}(t, 20)$

Given

$x(0) = 1$ $x'(0) = 0$

$x''(t) + \varepsilon \cdot |x(t)| \cdot x(t) + \omega^2 \cdot x(t) = 0$

$x_{aw2} := \text{Odesolve}(t, 20)$

Given

$x(0) = 1$ $x'(0) = 0$

$x''(t) + \varepsilon \cdot |x(t)| \cdot x(t) + \omega^2 \cdot x(t) = 0$

$x_{aw3} := \text{Odesolve}(t, 20)$

$x_{aw1}(t) =$

1
0.886
0.772
0.66
0.548
0.439
0.331
0.226
...

$x_{aw2}(t) =$

1
0.886
0.772
0.66
0.548
0.439
0.331
0.226
...

$x_{aw3}(t) =$

1
0.886
0.772
0.66
0.548
0.439
0.331
0.226
...

Export the data to Matlab and perform another series of curve fits

$$f_{aw1}(t) := \frac{3\cdot\pi}{3\cdot\pi + 4.089t} \qquad f_{aw2}(t) := \frac{3\cdot\pi}{3\cdot\pi + 4.089t} \qquad f_{aw2}(t) := \frac{3\cdot\pi}{3\cdot\pi + 4.089t}$$

$R^2 = 1$ $\qquad$ $R^2 = 1$ $\qquad$ $R^2 = 1$

Given the same constants in the denominator, this error seems to be a constant that is not associated with frequency, rather the magnitude of the damping coefficient.

$4\cdot\varepsilon\cdot\omega\cdot a_0 = 6.126$ $\qquad$ $4\cdot\varepsilon\cdot\omega\cdot a_0 = 6.126$ $\qquad$ $4\cdot\varepsilon\cdot\omega\cdot a_0 = 6.126$

$$E_w := \left|\frac{6.126 - 4.089}{6.126}\right|\cdot 100 \qquad E_w = 33.252$$

Going back to the original expression for the decay envelope $\qquad a_a(t) = \dfrac{2\cdot\pi\cdot a_0}{3\cdot\pi + 4\cdot\varepsilon\cdot\omega\cdot a_0\cdot t}$

where: $\qquad a_0 := \dfrac{3}{2}$

$4\cdot\varepsilon\cdot\omega\cdot a_0 = 6.126$

From Matlab, the best fit decay envelope was found to be:

$$f_a(t) := \frac{3\pi}{3\pi + 4.089t} \qquad \frac{6.126}{4.089} = 1.498$$ which is roughly = to a0

Try removing a0 from the denominator: $a_a(t) = \frac{2\cdot\pi\cdot a_0}{3\cdot\pi + 4\cdot\varepsilon\cdot\omega\cdot t}$

where: $4\cdot\varepsilon\cdot\omega = 4.084$

Recall, the best fit curves from varying the amplitude of the damping coefficient were:

$f_{a1}(t) := \frac{3\cdot\pi}{3\cdot\pi + 2.045t}$ $f_{a2}(t) := \frac{3\cdot\pi}{3\cdot\pi + 10.22t}$ $f_{a3}(t) := \frac{3\cdot\pi}{3\cdot\pi + 20.43t}$

$4\cdot\varepsilon_1\cdot\omega = 2.042$ $4\cdot\varepsilon_2\cdot\omega = 10.21$ $4\cdot\varepsilon_3\cdot\omega = 20.42$

The % difference in the constants are now: $E_{a1} := \left|\frac{2.042 - 2.045}{2.042}\right|\cdot 100$ $E_{a1} = 0.147$

The % difference in the constants are now: $E_{a2} := \left|\frac{10.21 - 10.22}{10.21}\right|\cdot 100$ $E_{a2} = 0.098$

The % difference in the constants are now: $E_{a3} := \left|\frac{20.42 - 20.43}{20.42}\right|\cdot 100$ $E_{a3} = 0.049$

It seems that this correction factor has now made the decay profile suitable for use. The actual decay envelope for aerodynamic will be considered as:

$$a_a(t) = \frac{2\cdot\pi\cdot a_0}{3\cdot\pi + 4\cdot\varepsilon\cdot\omega\cdot t}$$

Now move on to the last type of damping considered, Coulomb Damping.

COULOMB DAMPING $\mu := 25$ $\omega := 81.252\pi$

Given

$x(0) = 1$ $x'(0) = 0$

$x''(t) + \mu\cdot\text{sign}(x'(t)) + \omega^2\cdot x(t) = 0$

$x_c := \text{Odesolve}(t, 20, 20000)$

Export the data to Matlab to curve fit it with the decay envelopes given by Smith and Werely (1999)

$x_c(t) =$

1
0.873
0.523
0.039
...

If Smith and Werely are correct, then the decay envelope should be: $a_c(t) = \frac{-2\cdot\mu}{\pi\cdot\omega}\cdot t + y_0$

where: $\frac{-2\cdot\mu}{\pi\cdot\omega} = -0.0312$

While y0 is not formely defined in their article, it appears that y0 would be equivalent to a0

From Matlab, the best fit decay envelope was found to be:

$f_c(t) := -0.0313t + 0.9997$ $R^2 = 1$ Notice with the offset term, this is identical to a0

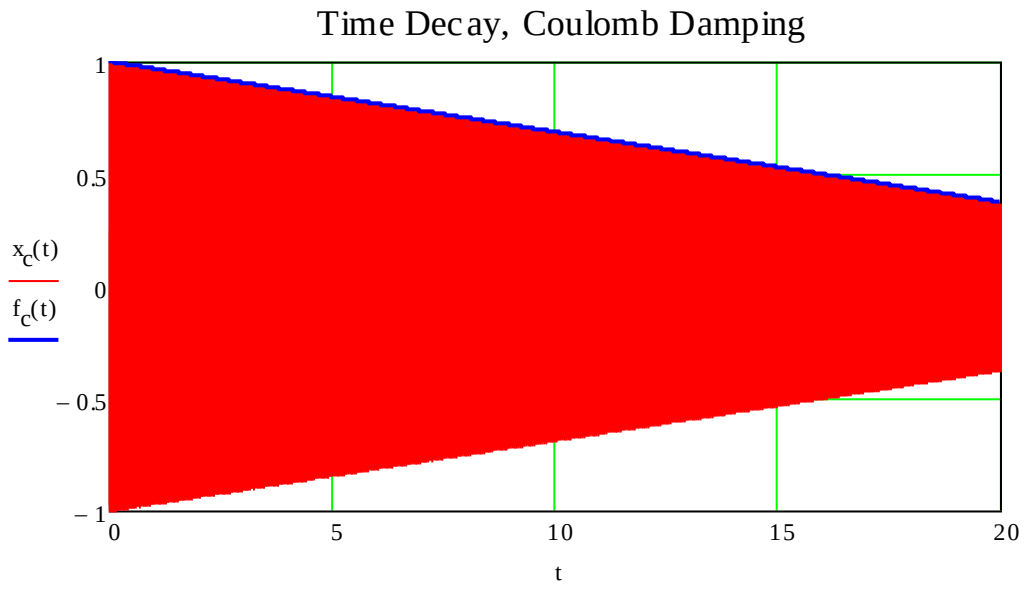

The % difference in the slope constant is: $E_{a3} := \left|\frac{-0.0312 - -0.0313}{-0.0312}\right|\cdot 100$

$E_{a3} = 0.321$

The decay profile for Coulomb damping has been validated. These three decay functions will be used to curve-fit the decay of the time signals of the data. From these functions, the damping coefficients that apply to the SDOF differential equation will be determined for each harmonic.

Viscous Damping

$$a_v(t) = e^{-\zeta\cdot\omega\cdot t}$$

Aerodynamic Damping

$$a_a(t) = \frac{2\cdot\pi\cdot a_0}{3\cdot\pi + 4\cdot\varepsilon\cdot\omega\cdot t}$$

Coulomb Damping

$$a_c(t) = \frac{-2\cdot\mu}{\pi\cdot\omega}\cdot t + y_0$$

Hysteretic Damping

Hysteretic Damping is not well characterized. It is used to describe the phase difference between stress and strain whereby the past deformation history in a member determines the strain experienced in the future. Most of the mathematical models are noncausal and do not have solutions that are easy to evaluate analytically.

The most common math model for a system with hysteretic damping is below:

$$x''(t) + \omega^2\cdot(1 + i\cdot\beta)\cdot x(t) = 0 \qquad \text{(Equation 1)}$$

This equation is used because it shows that the energy loss per cycle is independent of frequency (Inaudi & Kelly, 1995).

For the given system: $\beta := 0.0$ $\omega^2 = 1000$

$$x''(t) + \omega^2\cdot(1 + i\cdot\beta)\cdot x(t) = 0$$

Mathcad is unable to solve this equation using the Odesolve function, so this will be solved using Matlab's dsolve function.

Matlab code

```
>> t=linspace(0,20,20000);
>> eqt2='D2y+1000*(1+0.01*i)*y=0';inits='y(0)=1,Dy(0)=0';
>> y2=dsolve(eqt2,inits,'t');
>> z2=eval(vectorize(y2));
```

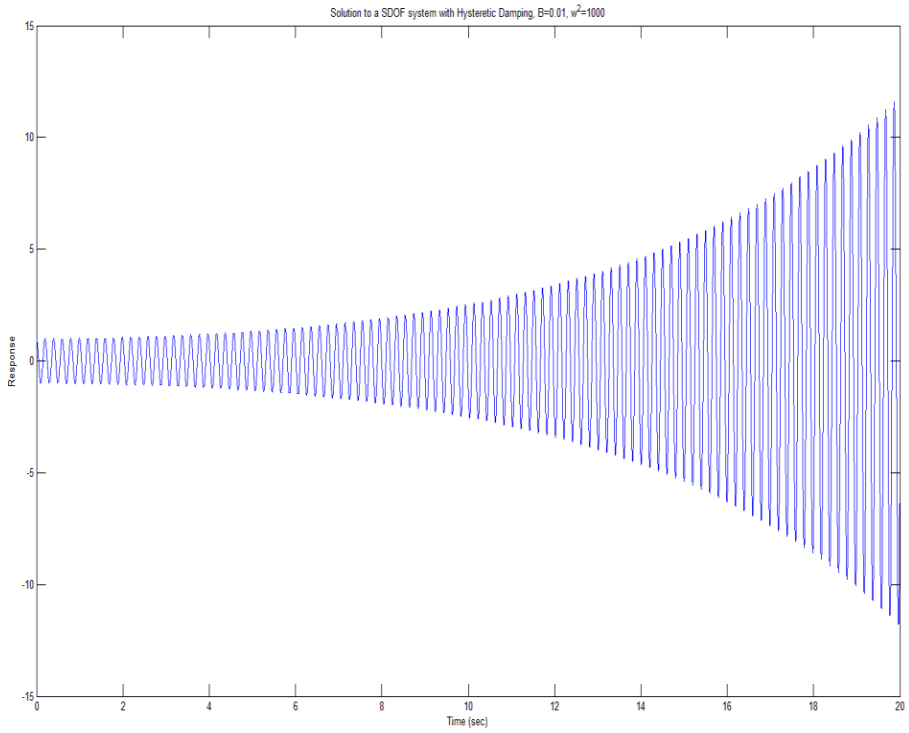

This system isn't stable. With this equation, there is negative damping, in the energy is being added to the system as time goes on. Another equation needs to be investigated.

The next common math model for a system with hysteretic damping is below:

$$x''(t) + \frac{h}{m \cdot \omega} \cdot x(t) + \omega^2 \cdot x(t) = 0 \qquad \text{(Equation 2)}$$

Given

$h := 1$ $\qquad m := \frac{7.02}{1000}$ mass of the BW056 string (kg)

$x(0) = 1$ $\qquad x'(0) = 0$

$$x''(t) + \frac{h}{m \cdot \omega} \cdot x'(t) + \omega^2 \cdot x(t) = 0$$

$x_h := \text{Odesolve}(t, 20, 20000)$

Best fit profile from Matlab: $f_h(t) := 0.9999e^{-0.1398 \cdot t}$ $\qquad R^2 = 1$

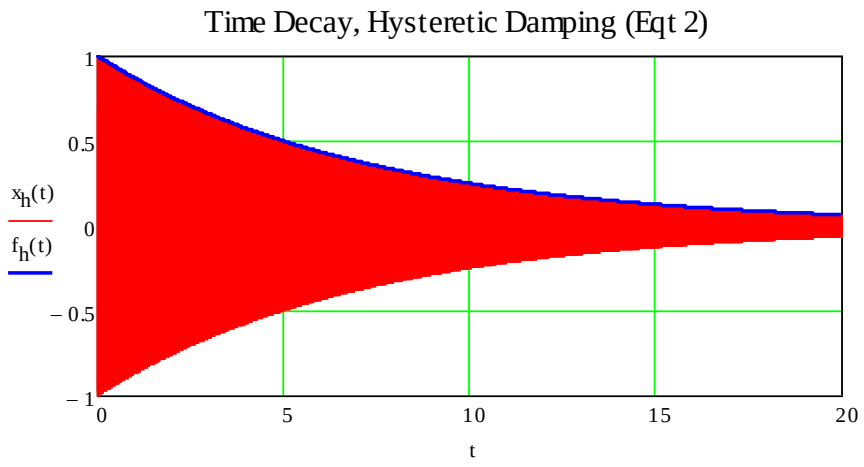

Given

$h := 1$ $\omega := 2\cdot\omega$ First Harmonic

$x(0) = 1$ $x'(0) = 0$

$$x''(t) + \frac{h}{m\cdot\omega}\cdot x'(t) + \omega^2\cdot x(t) = 0$$

$x_h := \text{Odesolve}(t, 20, 20000)$

Best fit profile from Matlab: $f_{h12}(t) := e^{-0.07001\cdot t}$ $R^2 = 1$

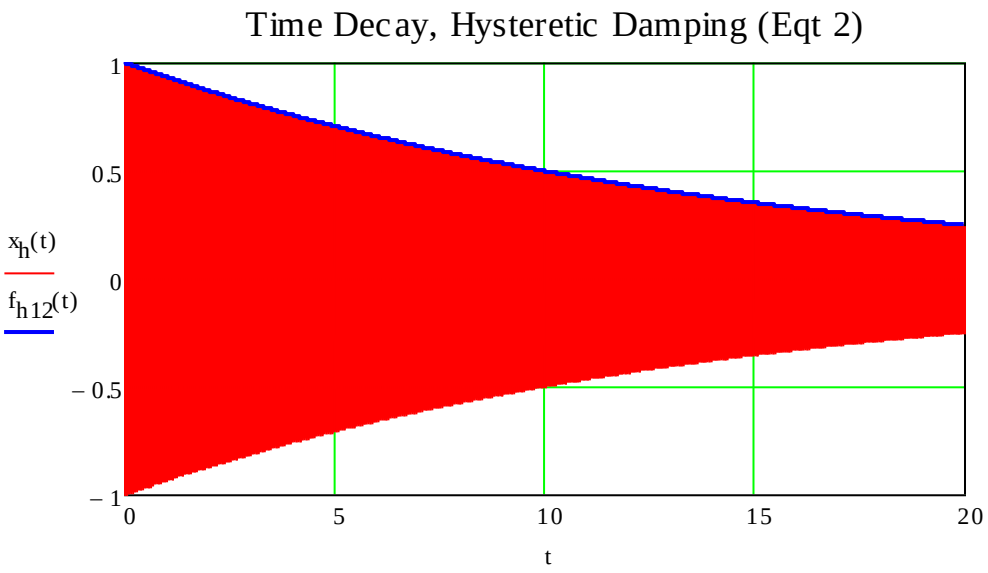

As opposed to the viscous damping model, as the frequency increases the decay rate decreases, implying that higher harmonics have less damping.

This model does not seem to be valid in the case of a vibrating guitar string. From the data, the higher harmonics have a faster decay rate implying that this type of damping is directly proportional to frequency, not inversely proportional as implied by this model. Try one more equation for hysteretic damping.

$$x''(t) + h \cdot i \cdot x(t) + \omega^2 \cdot x(t) = 0 \qquad \text{(Equation 3)}$$

For the given system:

$$h := 1 \qquad \omega := 81.252 \cdot \pi$$

$$x''(t) + h \cdot i \cdot x(t) + \omega^2 \cdot x(t) = 0$$

The solution (from Matlab) is:

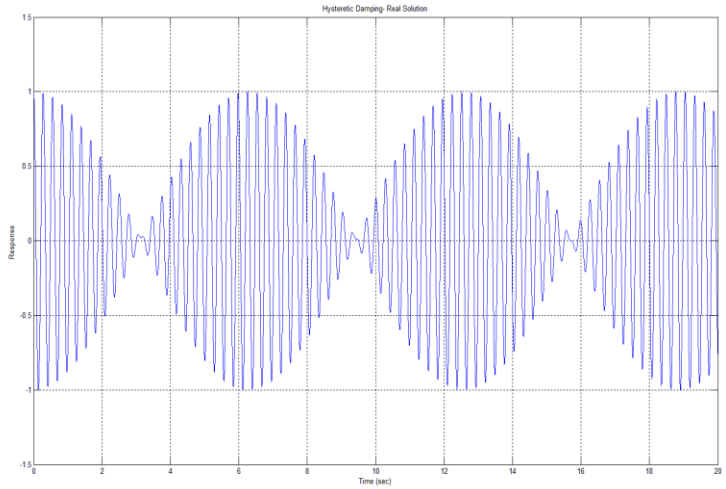

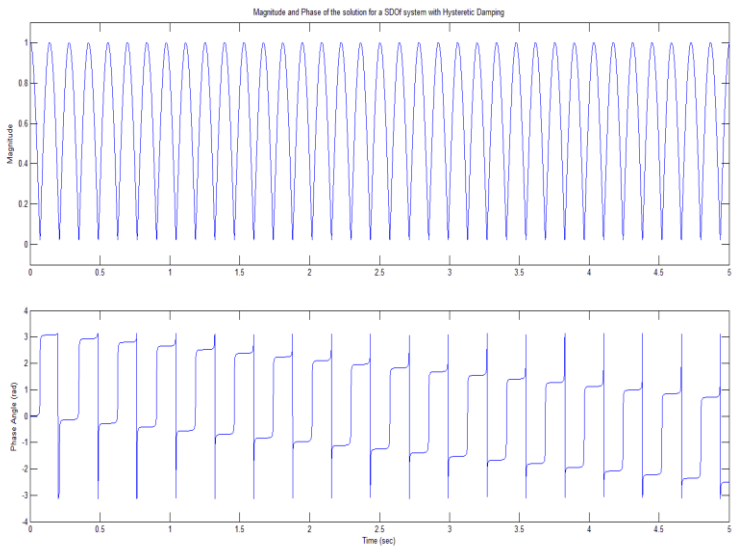

This solution does not seem to make any sense. For a SDOF system, there should not be any beating phenomenon, especially given the nature of material damping.

Appendix C. Combined Damping Solutions

OBJECTIVE: Verify that the decay envelopes for the SDOF math model with multiple types of damping are a LINEAR SUMMATION of the individual decay envelopes as given by Smith & Werely (1999)

Combined Damping: Viscous, Aerodynamic, Coulomb

$m := .5 \quad K := 8 \qquad \omega := \sqrt{\frac{K}{m}} = 4 \qquad f := \omega \cdot \frac{180}{\pi} = 229.183$

Viscous:	$\zeta := 0.01$	exponential decay
Aerodynamic:	$\varepsilon := 0.25$	double exponential decay
Coulomb:	$\mu := 0.09$	linear decay

Given

$x(0) = 1 \qquad x'(0) = 0$

$x''(t) + 2 \cdot \zeta \cdot \omega \cdot x'(t) + \varepsilon \cdot |x'(t)| \cdot x'(t) + \mu \cdot \text{sign}(x'(t)) + \omega^2 \cdot x(t) = 0$

$x_{vac} := \text{Odesolve}(t, 20)$

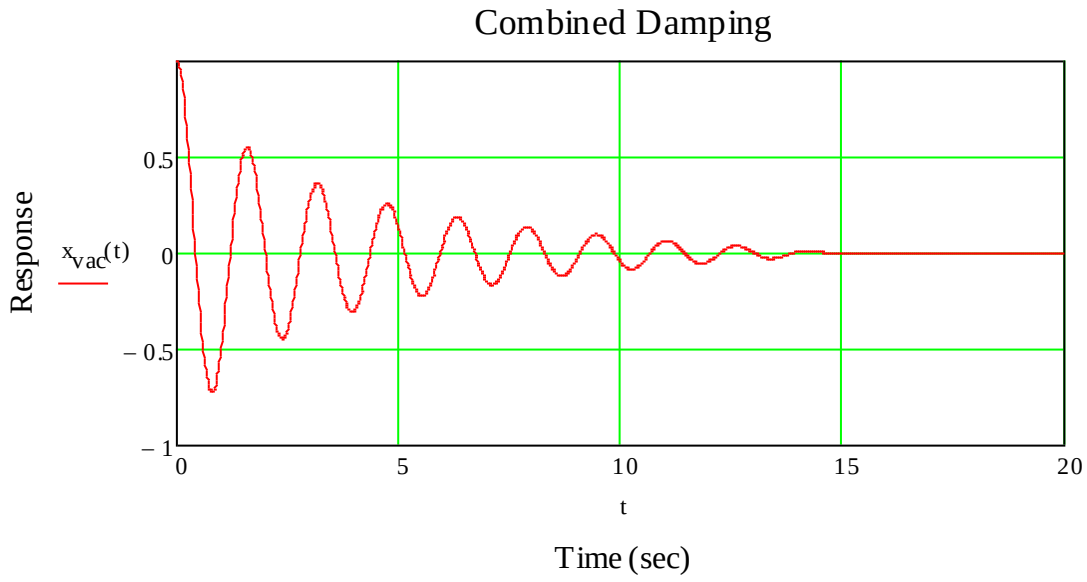

$t := 0, 0.01 .. 20$

Export the data to Matlab to obtain a curve fit of the decay profile:

t =	$x_{vac}(t)$ =
0	1
0.01	0.999
0.02	0.997
0.03	0.993
...	...

Using the decay profiles from Smith & Werely (1999):

Viscous Damping	Aerodynamic Damping	Coulomb Damping
$a_v(t) = e^{-\zeta\cdot\omega\cdot t}$	$a_a(t) = \frac{2\cdot\pi\cdot a_0}{3\cdot\pi + 4\cdot\varepsilon\cdot\omega\cdot t}$	$a_c(t) = \frac{-2\cdot\mu}{\pi\cdot\omega}\cdot t + y_0$

Purely Viscous, Decay: $f_v(t) := e^{-0.01\cdot 4\cdot t} - .492$ $R^2 = 0.636$

Purely Aerodynamic, Decay: $f_a(t) := \frac{3\cdot\pi}{3\cdot\pi + 6.197t}$ $R^2 = 0.973$

Purely Coulomb, Decay: $f_c(t) := -0.05586t + 0.668$ $R^2 = 0.763$

Linear Combination: $a := -0.510$ $c := 0.0226$ $b := 4.17$ $d := -0.489$

$F(t) := e^{-0.01\cdot 4\cdot t} + a + \frac{3\pi}{3\pi + b\cdot t} + c\cdot t + d$ $R^2 = 0.999$

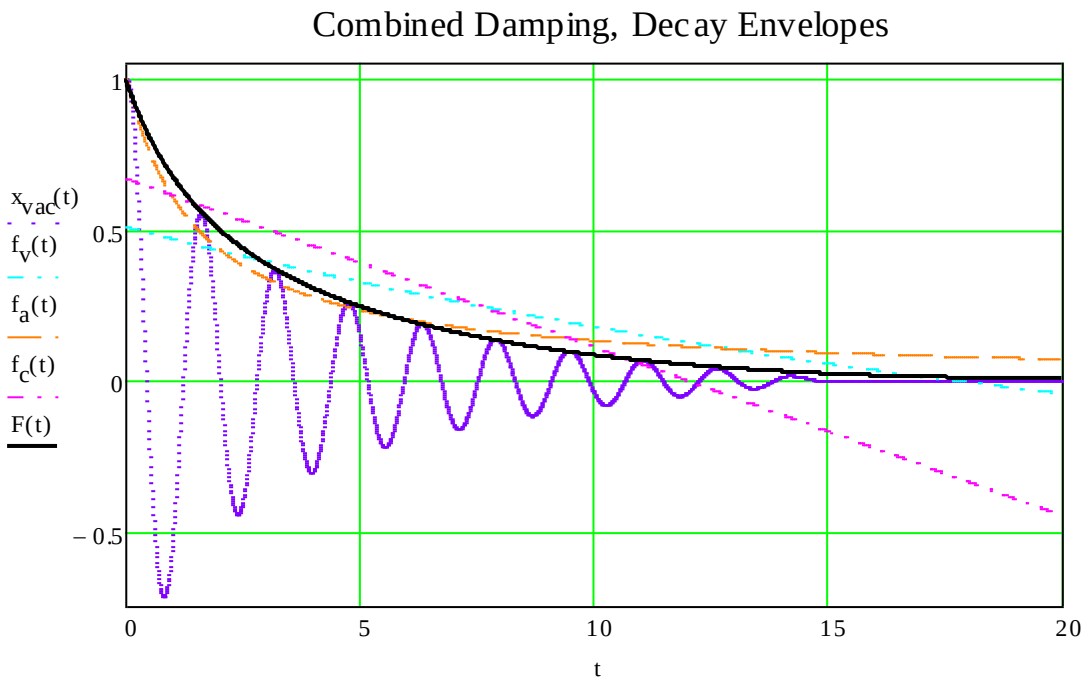

This proves that for the SDOF math model, the decay envelope can be accurately described as a LINEAR SUMMATION of the decay envelopes as given by Smith and Werely. Now this type of combined decay function will be used to back out the damping coefficients that correspond to the SDOF math model. Recall that when filtering each harmonic, the time response of this will be a damped sine wave as seen in this document.

Appendix D. Equivalent Decay Functions

OBJECTIVE: Identify why viscous damping is so often used to most damping cases

The decay envelope of a system with viscous damping is: $v(t) = e^{-t}$

The decay envelope of a system with aerodynamic damping is: $a(t) = \frac{1}{t}$

Viscous damping works very well as an approximate to aerodynamic damping because it quickly converges to emulate the steady state response of a system with aerodynamic damping. Usually a viscous damping factor can be identified to represent aerodynamic damping reasonably well.

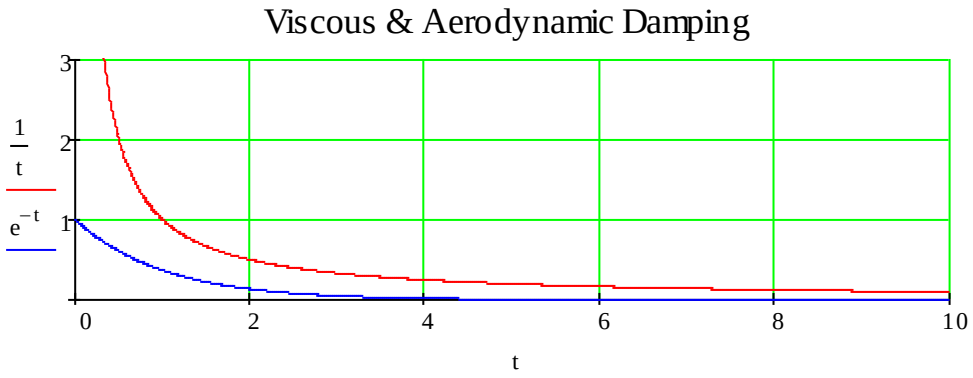

For the given functions, find a value for δ such that the error between the two damping functions is minimized.

$v(m,\delta,t) := m \cdot e^{-\delta \cdot t}$ $a(t) := \frac{1}{t}$

Decay Rate Amplitude

Initial Guesses $\delta := 0.1$ $m := 2$

Error Function $E(m,\delta) := \sum_{n=1}^{10} (v(m,\delta,n) - a(n))^2$

Given

$\delta < 1$

$\begin{pmatrix} m \\ \delta \end{pmatrix} := \text{Minimize}(E, m, \delta)$ $m = 1.38$ $\delta = 0.409$

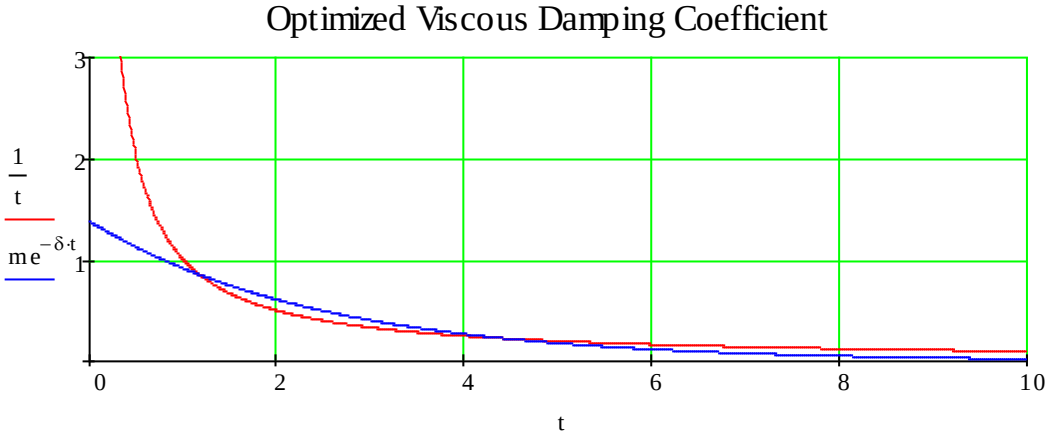

Notice that the primary difference now between viscous and aerodynamic damping is the transient response; the steady state responses are nearly identical. An exponential function will not be able to approximate the transient response because of the asymptote at t=0 for 1/t.

Another decay function that resembles these two types of damping is a logarithmic decay.

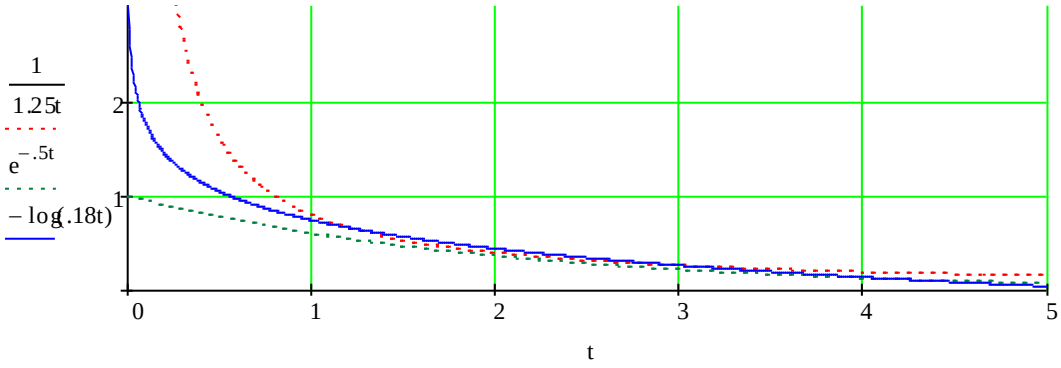

Performing the same type of exercise, find the optimal logarithmic damping coefficient to approximate the response of aerodynamic and viscous damping.

$v(t) := e^{-\delta \cdot t}$ $a(t) := \frac{1}{t}$ $L(\gamma, t) := -\log(\gamma \cdot t)$ Initial Guess $\gamma := 0.1$

Error Function $E(\gamma) := \sum_{n=1}^{10} \left[(v(n) - L(\gamma, n))^2 + (a(n) - L(\gamma, n))^2 \right]$

Given

$\gamma < 1$ $\gamma := \text{Minimize}(E, \delta)$ $\gamma = 0.126$ $E(\gamma) = 0.26$

Optimized Logarithmic Damping Coefficient

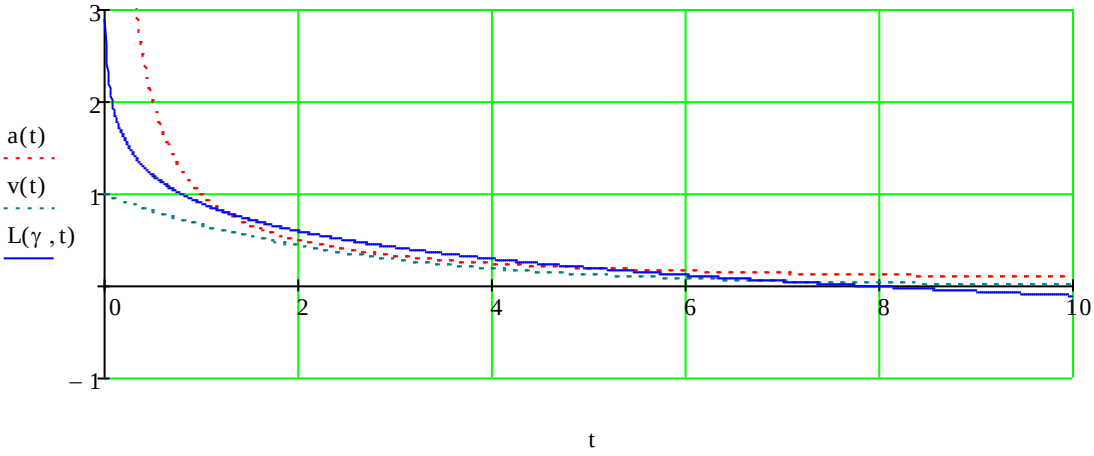

Notice that the viscous damping function most resembles the aerodynamic damping function at steady state; however, the logarithmic damping function closer resembles the aerodynamic damping function in the transient response. The transient response of 1/t and log(t) both have asymptotes at t=0; thus, their transient responses are similar.

Appendix E. Power Spectral Density Plots

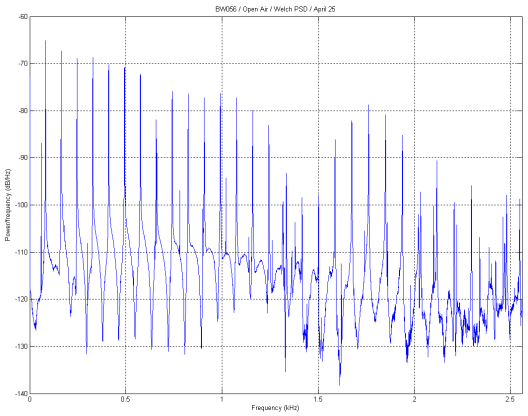

BW056, Open Air

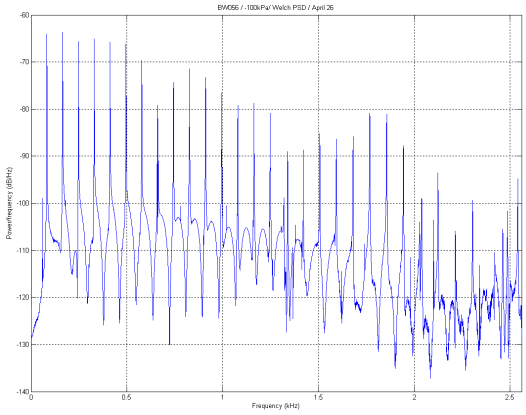

BW056 Vacuum

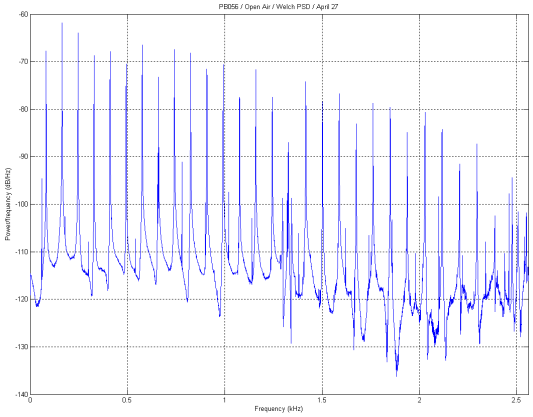

PB056, Open Air

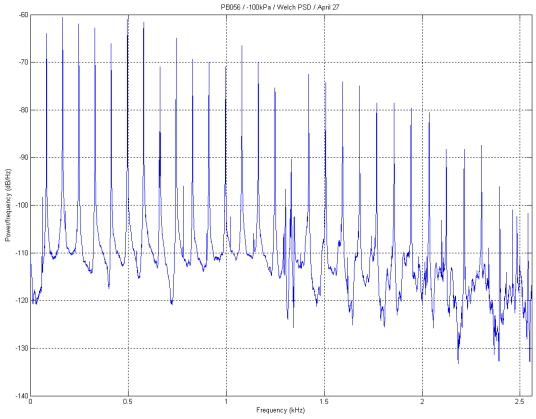

PB056, Vacuum

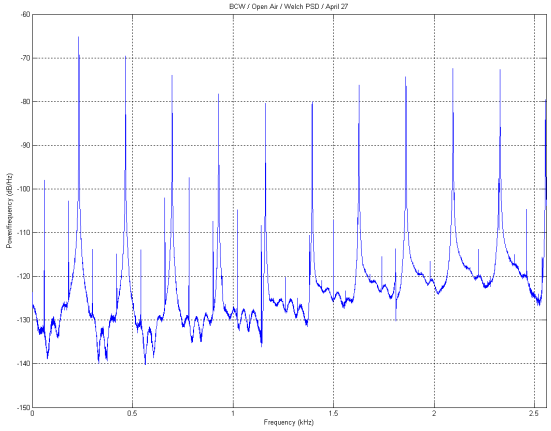

Core Wire, Open Air

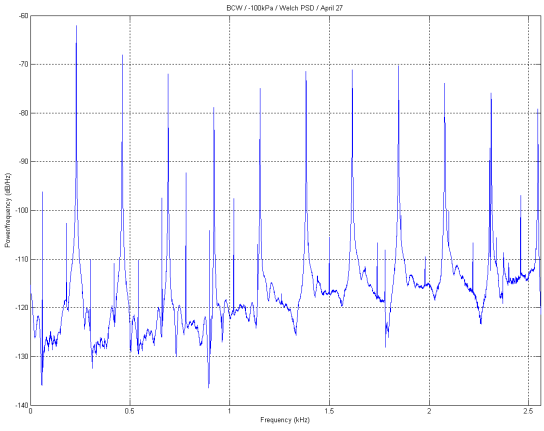

Core Wire, Vacuum

Appendix F. Sample Filters

Samples of 3rd Order Band-pass Butterworth Filters: Magnitude and Phase

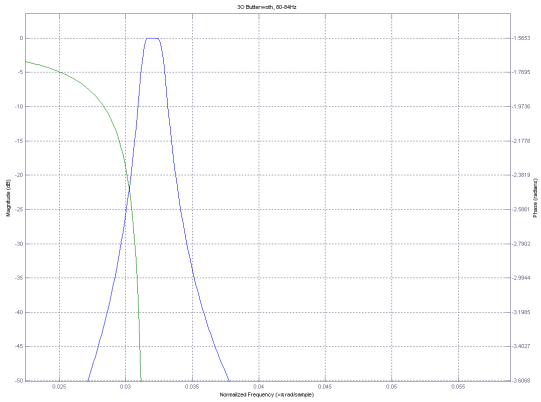

80-84Hz, Harmonic 0

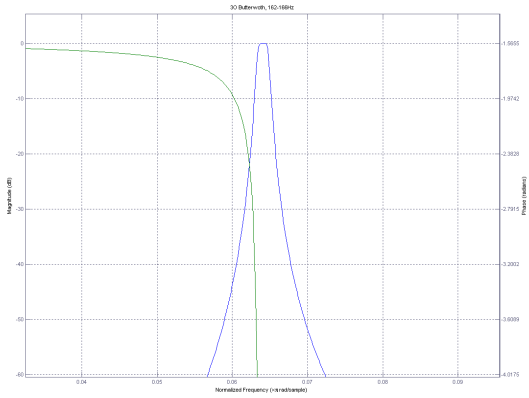

162-166 Hz, Harmonic 1

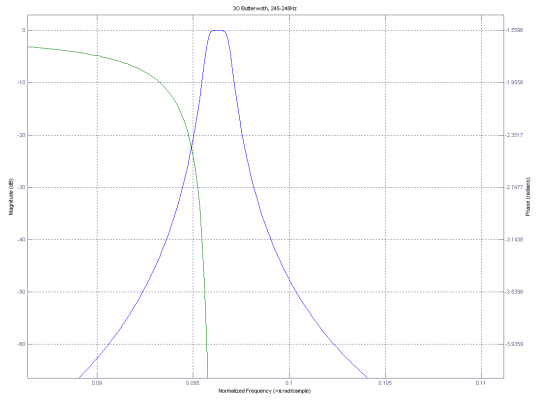

245-248 Hz, Harmonic 2

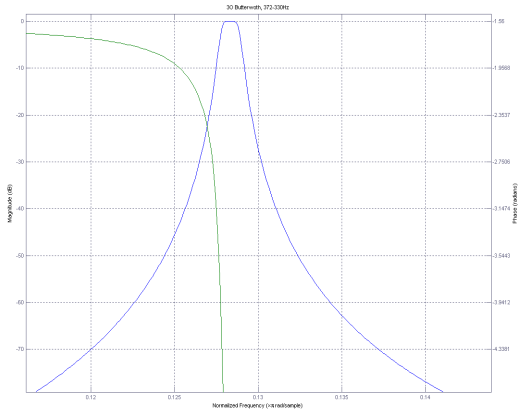

327-330 Hz, Harmonic 3

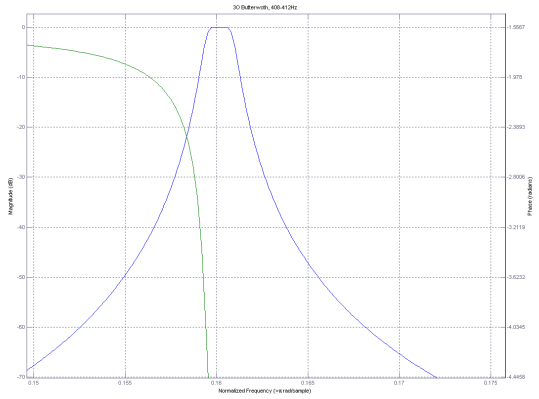

408-412 Hz, Harmonic 4

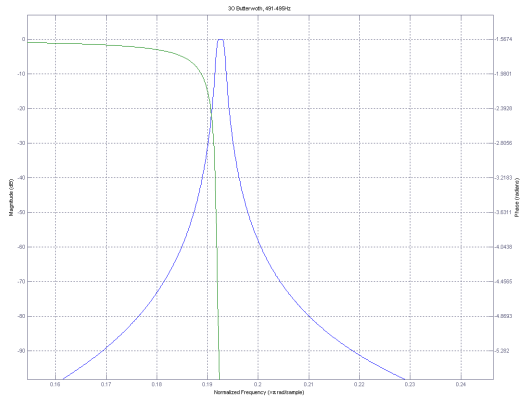

491-496 Hz, Harmonic 5

Appendix G. Time Waveforms

BW056, Open Air, Filtered Time Waveforms: Harmonics 0, 1, 12, 14, 21

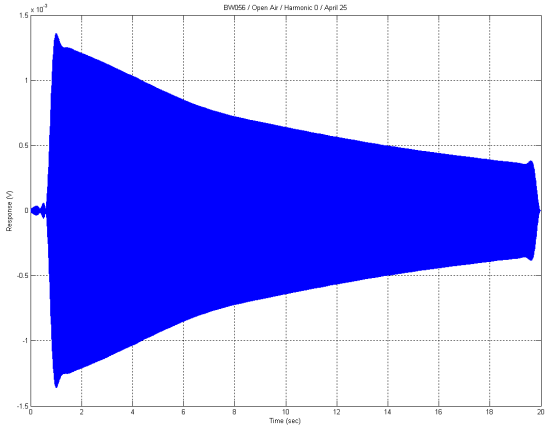

BW056, Open Air, Harmonic 0

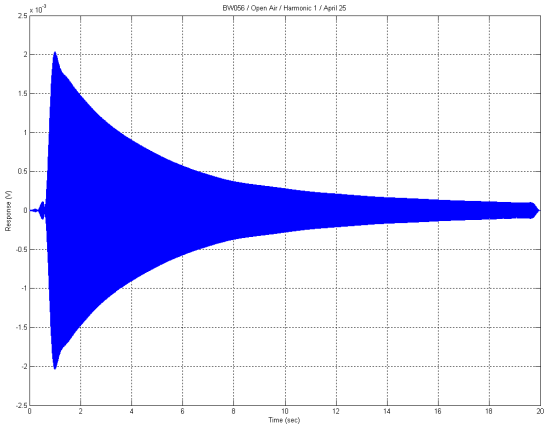

BW056, Open Air, Harmonic 1

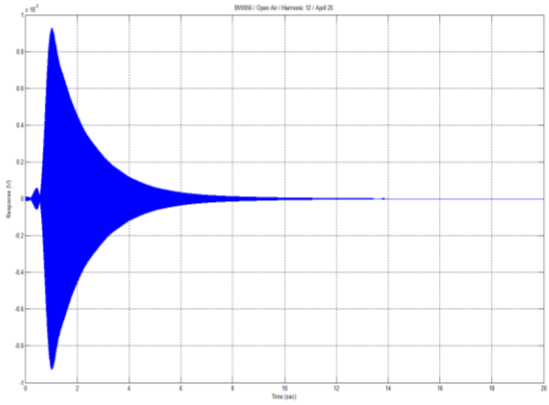

BW056, Open Air, Harmonic 12

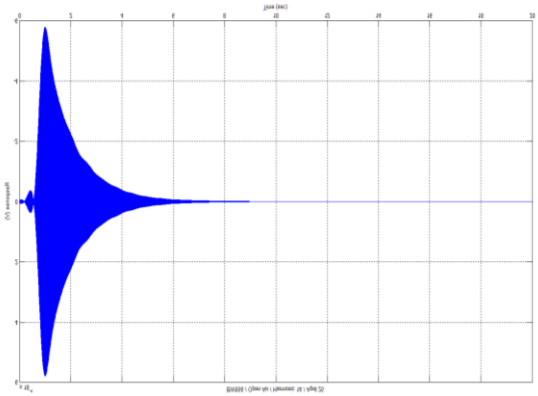

BW056, Open Air, Harmonic 14

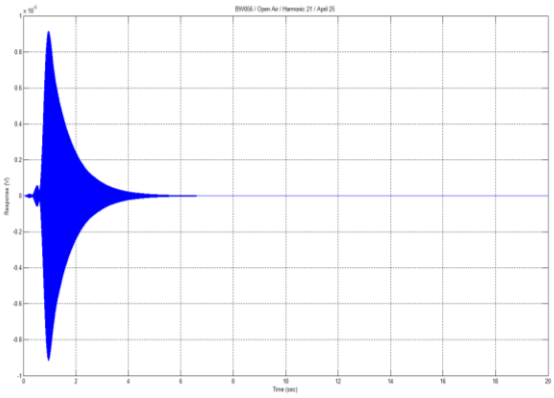

BW056, Open, Harmonic 21

BW056, Vacuum, Filtered Time Waveforms: Harmonics 0, 1, 12, 14, 21

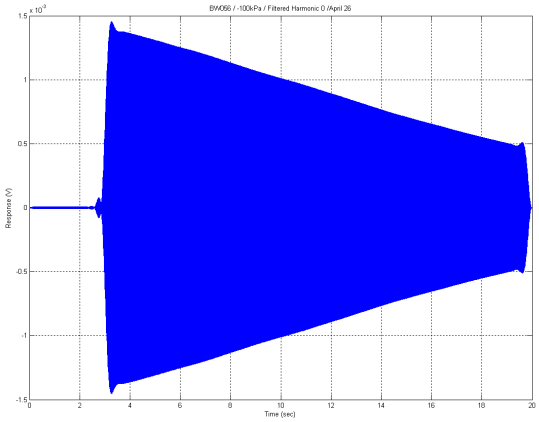

BW056, Vacuum, Harmonic 0

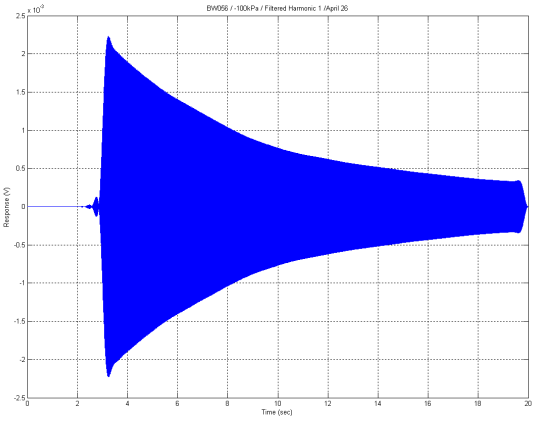

BW056, Vacuum, Harmonic 1

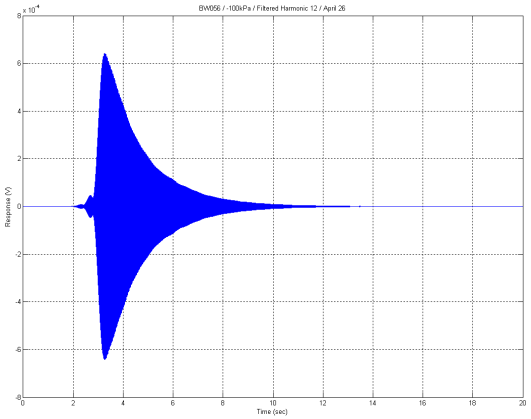

BW056, Vacuum, Harmonic 12

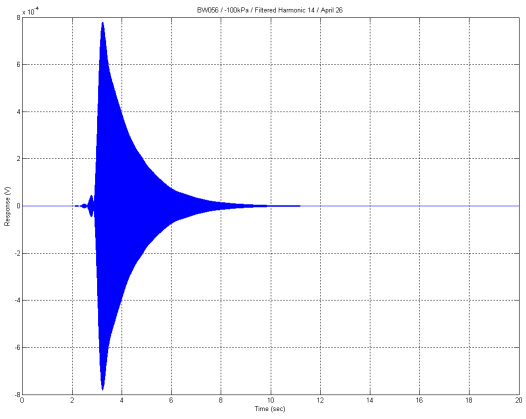

BW056, Vacuum, Harmonic 14

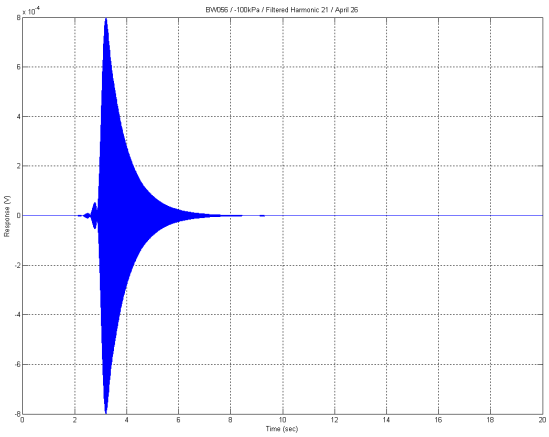

BW056, Vacuum, Harmonic 21

PB056, Open Air, Filtered Time Waveforms: Harmonics 0, 1, 12, 17, 21

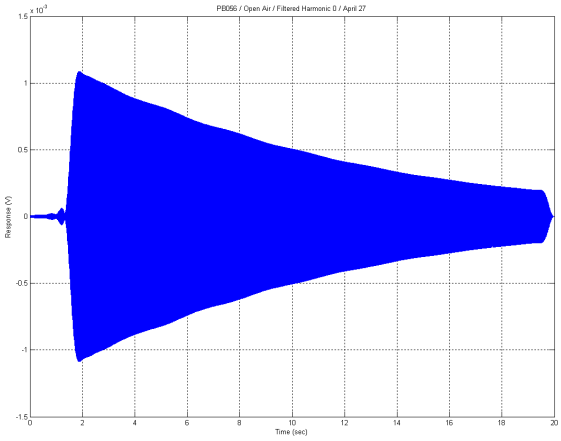

PB056, Open Air, Harmonic 0

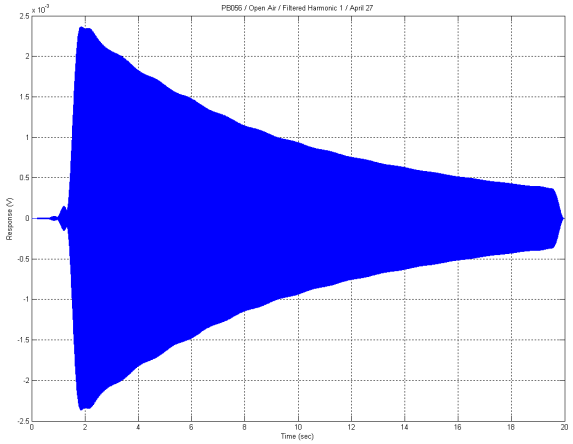

PB056, Open Air, Harmonic 1

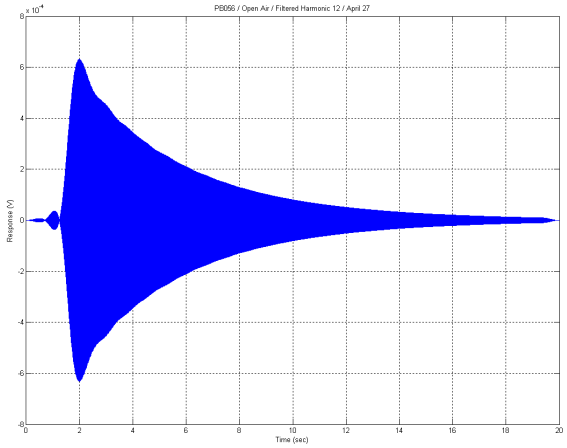

PB056, Open Air, Harmonic 12

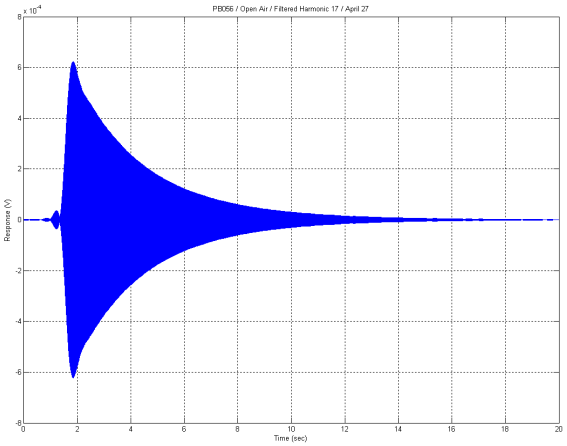

PB056, Open Air, Harmonic 17

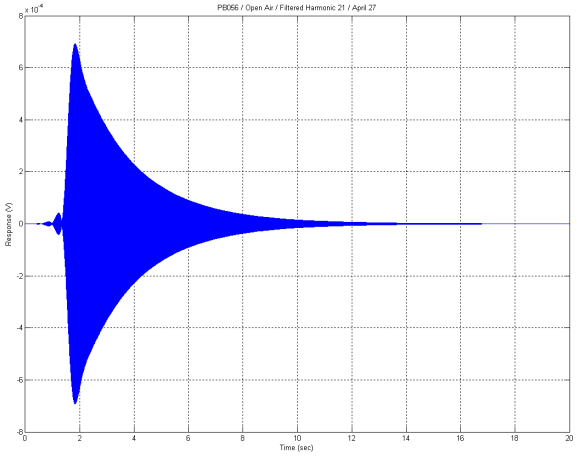

PB056, Open Air, Harmonic 21

PB056, Vacuum, Filtered Time Waveforms: Harmonics 0, 1, 12, 17, 21

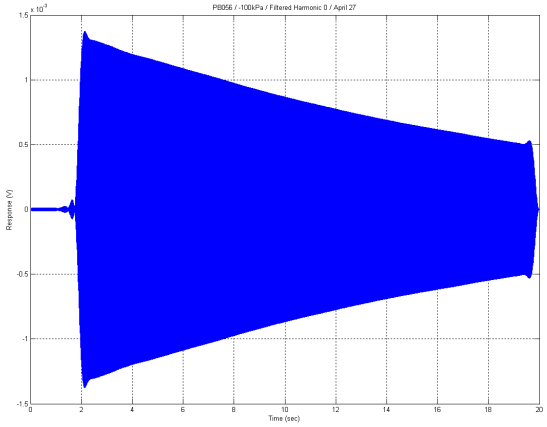

PB056, Vacuum, Harmonic 0

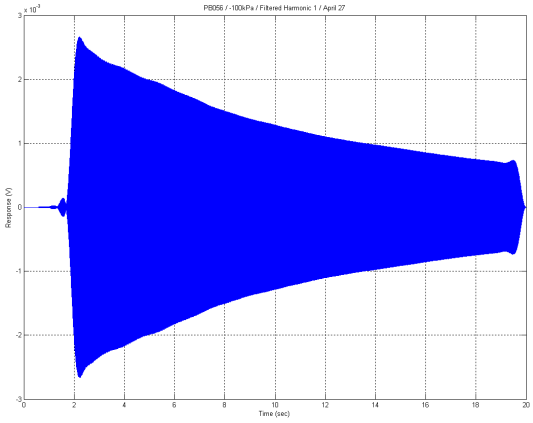

PB056, Vacuum, Harmonic 1

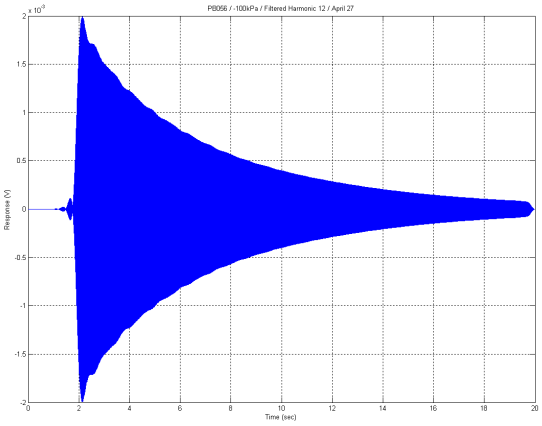

PB056, Vacuum, Harmonic 12

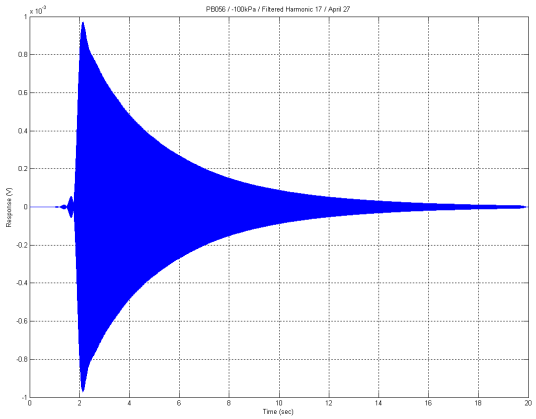

PB056, Vacuum, Harmonic 17

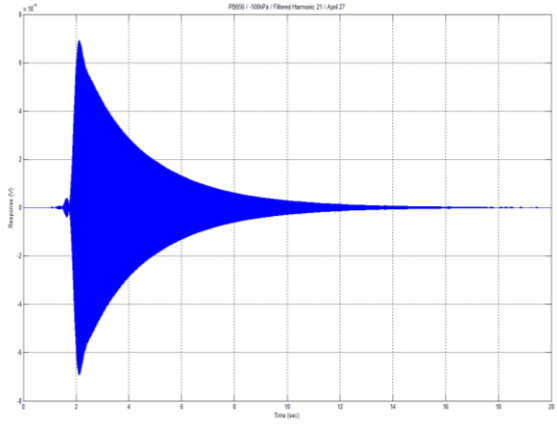

PB056, Vacuum, Harmonic 21

Core Wire, Open Air, Filtered Time Waveforms: Harmonics 0, 1, 2, 3, 7

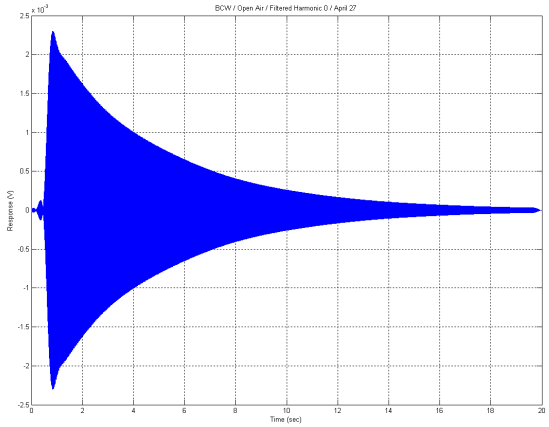

Core Wire, Open Air, Harmonic 0

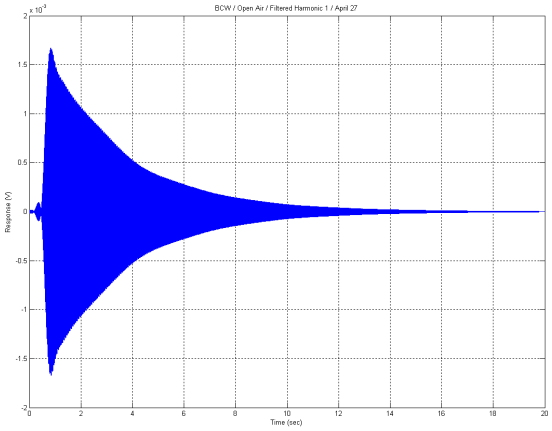

Core Wire, Open Air, Harmonic 1

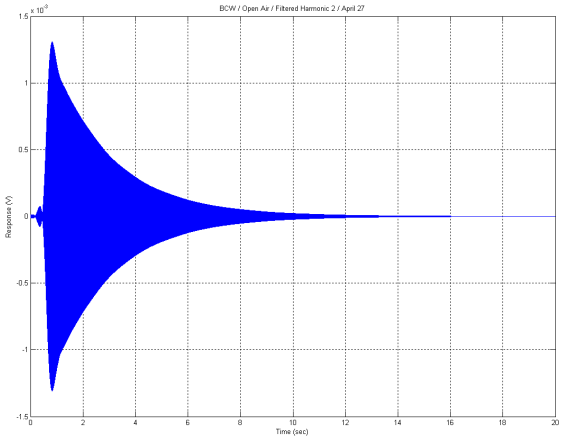

Core Wire, Open Air, Harmonic 2

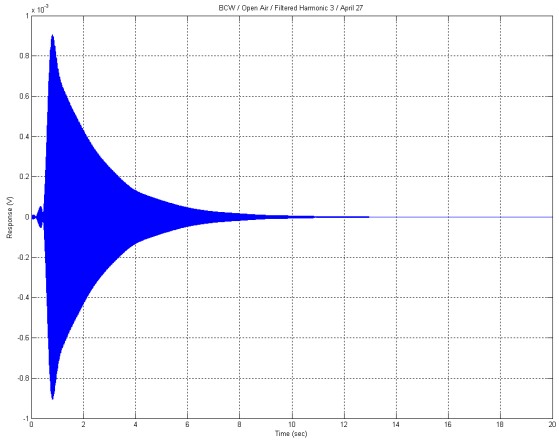

Core Wire, Open Air, Harmonic 3

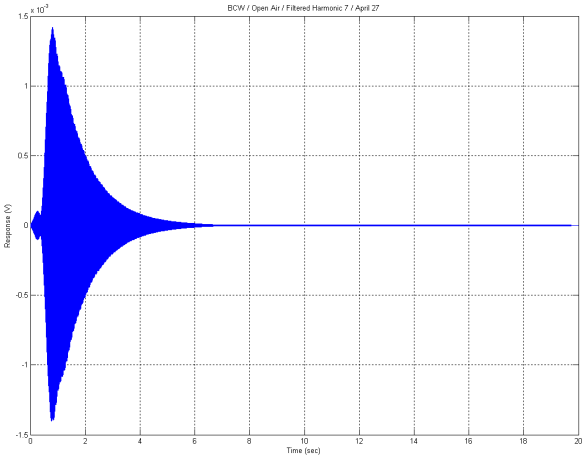

Core Wire, Open Air, Harmonic 7

Core Wire, Vacuum, Filtered Time Waveforms: Harmonics 0, 1, 2, 7

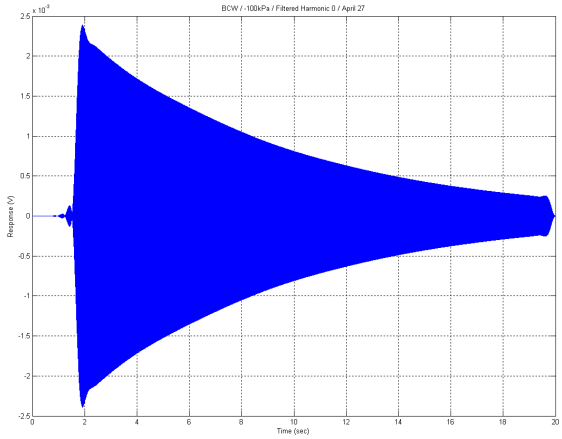

Core Wire, Vacuum, Harmonic 0

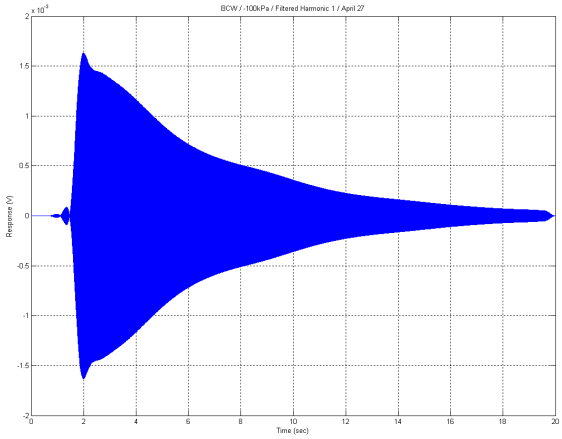

Core Wire, Vacuum, Harmonic 1

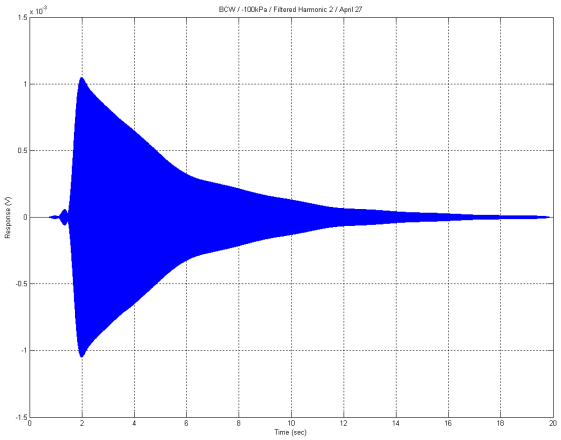

Core Wire, Vacuum, Harmonic 2

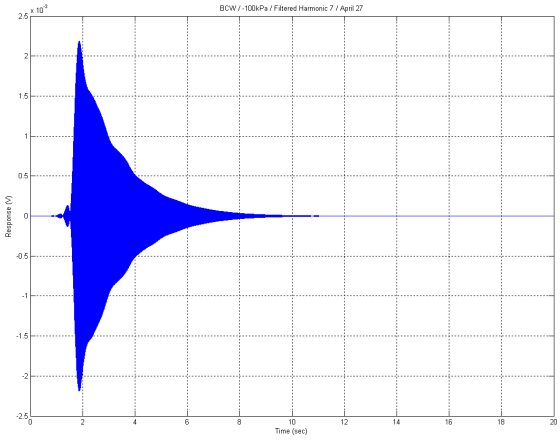

Core Wire, Vacuum, Harmonic 7

Ten BW056 Strings, Open Air, Filtered Fundamental Frequency

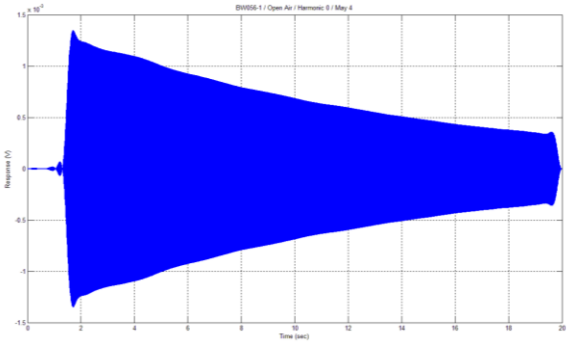

BW056, String 1

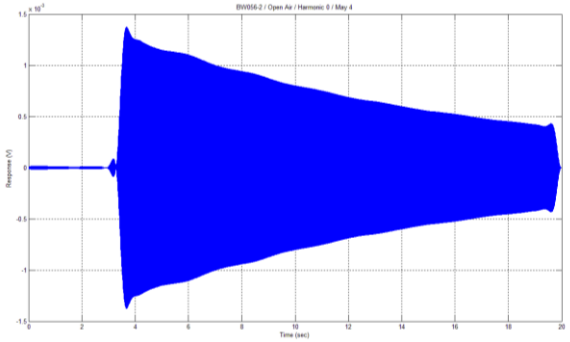

BW056, String 2

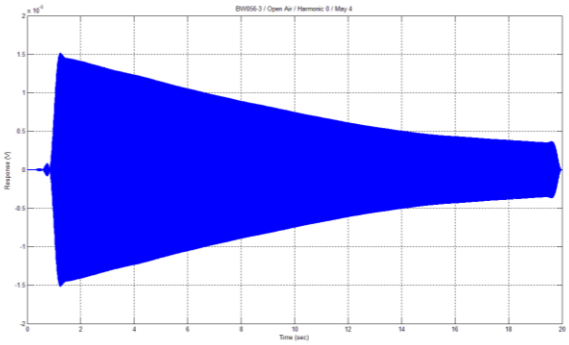

BW056, String 3

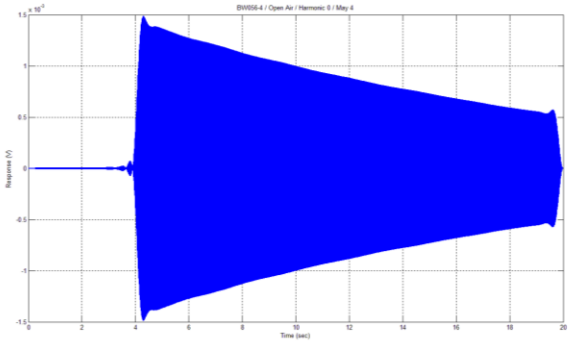

BW056, String 4

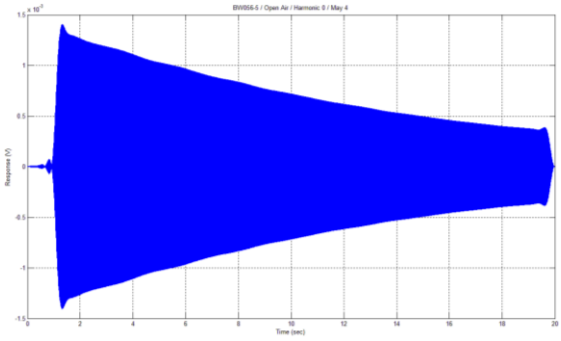

BW056, String 5

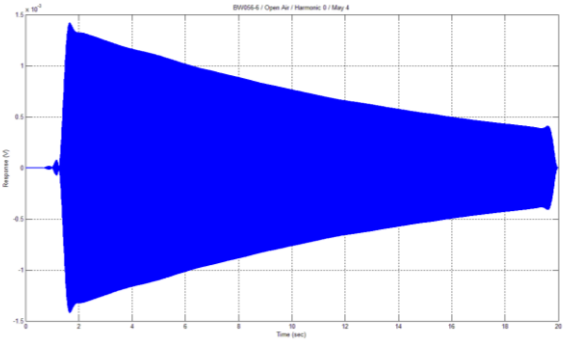

BW056, String 6

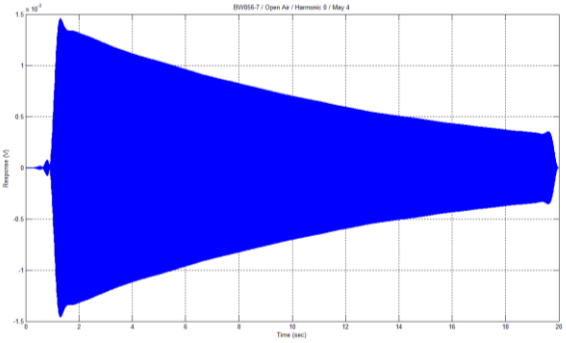

BW056, String 7

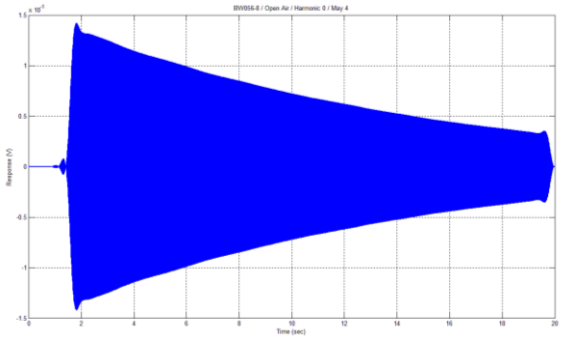

BW056, String 8

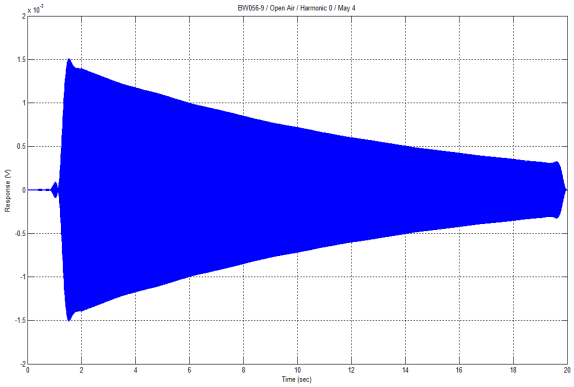

BW056, String 9

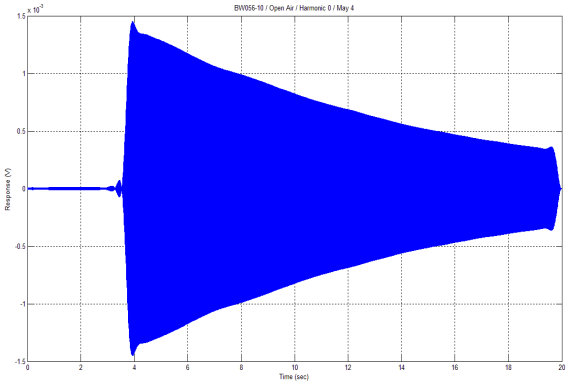

BW056, String 10

Appendix H. Curve Fits

BW056 - First Pass Curve Fits, April 25

[Harmonic 0]

General model:
f(t) = (2*pi*a0)/(3*pi+c*t) + d*t+e
Coefficients (with 95% confidence bounds):
a0 = 0.002583 (0.0006711, 0.004494)
c = 1.054 (-0.2198, 2.328)
d = -6.158e-007 (-3.206e-005, 3.083e-005)
e = -0.0001755 (-0.001609, 0.001258)

Goodness of fit:
SSE: 1.167e-009
R-square: 0.9985
Adjusted R-square: 0.9978
RMSE: 1.291e-005

[Model Harmonic 0]
General model:
f(t) = (2*pi*a0)/(3*pi+c*t) + d*t+e
Coefficients (with 95% confidence bounds):
a0 = 0.002366 (0.00224, 0.002492)
c = 1.095 (1.019, 1.171)
d = -4.638e-006 (-6.779e-006, -2.497e-006)
e = -3.157e-005 (-0.0001194, 5.629e-005)

Goodness of fit:
SSE: 3.818e-011
R-square: 1
Adjusted R-square: 1
RMSE: 1.784e-006

[Harmonic 1]

General model:
f(t) = (2*pi*a0)/(3*pi+c*t) + d*t+e
Coefficients (with 95% confidence bounds):
a0 = 0.005537 (0.005296, 0.005778)
c = 2.822 (2.126, 3.518)
d = 2.324e-005 (1.288e-005, 3.359e-005)
e = -0.0008806 (-0.001191, -0.0005701)

Goodness of fit:
SSE: 1.235e-009
R-square: 0.9996
Adjusted R-square: 0.9995
RMSE: 1.171e-005

[Model Harmonic 1]

General model:
f(t) = (2*pi*0.005537)/(3*pi+c*t) +d*t-0.0008806
Coefficients (with 95% confidence bounds):
c = 2.892 (2.693, 3.091)
d = 2.791e-005 (2.047e-005, 3.534e-005)

Goodness of fit:
SSE: 2.477e-008
R-square: 0.9957
Adjusted R-square: 0.9953
RMSE: 4.977e-005

[Harmonic 12]

General model:
f(t) = (2*pi*a0)/(3*pi+c*t) + d*t+e
Coefficients (with 95% confidence bounds):
a0 = 0.005118 (0.004494, 0.005743)
c = 11.32 (7.478, 15.17)
d = 4.012e-005 (2.94e-005, 5.083e-005)
e = -0.0006256 (-0.0007666, -0.0004846)

Goodness of fit:
SSE: 1.43e-010
R-square: 0.9998
Adjusted R-square: 0.9997
RMSE: 4.228e-006

[Model Harmonic 12]

General model:
f(t) = (2*pi*0.005118)/(3*pi+c*t) +d*t-0.0006256
Coefficients (with 95% confidence bounds):
c = 11.97 (11.17, 12.78)
d = 5.653e-005 (3.578e-005, 7.728e-005)

Goodness of fit:
SSE: 2.139e-008
R-square: 0.9957
Adjusted R-square: 0.9952
RMSE: 4.876e-005

[Harmonic 14]

General model Exp1: <--Exponential Fits Better than AC
f(t) = a*exp(-b*t)
Coefficients (with 95% confidence bounds):
a = 0.001373 0 (0.001221, 0.001525)
b = 0.8903 (-0.9642, -0.8163)

Goodness of fit:
SSE: 1.127e-009
R-square: 0.9966
Adjusted R-square: 0.9962
RMSE: 1.119e-005

(Best I could get with the AC fit was R^2 = 0.966)
General model:
f(t) = (2*pi*a0)/(3*pi+c*t) + d*t+e
Coefficients (with 95% confidence bounds):
a0 = 0.006402 (-0.1038, 0.1166)
c = 60 (-1223, 1343)
d = -1.15e-005 (-0.0001255, 0.0001025)
e = -5.717e-005 (-0.001094, 0.0009793)

Goodness of fit:
SSE: 1.132e-008
R-square: 0.966
Adjusted R-square: 0.9514
RMSE: 4.022e-005

[Harmonic 21]

General model Exp1:
f(t) = a*exp(-b*t)
Coefficients (with 95% confidence bounds):
a = 0.002842 (0.002504, 0.003181)
b = 1.207 (-1.295, -1.119)

Goodness of fit:

SSE: 1.508e-009
R-square: 0.9979
Adjusted R-square: 0.9976
RMSE: 1.373e-005

[Model Harmonic 21]

General model Exp1:
f(x) = a*exp(-b*x)
Coefficients (with 95% confidence bounds):
a = 0.001409 (0.001383, 0.001434)
b = 0.9479 (-0.9762, -0.9196)

Goodness of fit:
SSE: 2.394e-009
R-square: 0.9989
Adjusted R-square: 0.9989
RMSE: 1.357e-005

BW056: Second Pass Curve-Fits

Note: m not included in the VAC fits because the fits are very insensitive to it, see: BW056-Open-DiffSenstv.txt

Note: all these d values should be negative, even when trying to make d negative in the equation, the fit will always give the wrong sign of d

---

[Harmonic 0] w=81.88

General model:
f(t) = exp(-a*t)+ (2*pi*a0)/(3*pi+c*t) + d*t+e
Coefficients (with 95% confidence bounds):
a = 7.025 (-553.3, 567.4)
a0 = 0.002977 (-0.0006689, 0.006623)
c = 0.84 (-0.7009, 2.381)
d = 5.29e-006 (-4.57e-005, 5.628e-005)81.88
e = -0.0004654 (-0.003162, 0.002232)

Goodness of fit:
SSE: 7.832e-010
R-square: 0.999
Adjusted R-square: 0.9983
RMSE: 1.143e-005

[MODEL-0 FIT]

General model:
f(t) = exp(-a*t)+ (2*pi*a0)/(3*pi+c*t) + d*t+e
Coefficients (with 95% confidence bounds):
a = 19.32 (17.9, 20.75)
a0 = 0.002806 (0.002653, 0.002958)
c = 0.8581 (0.8012, 0.9149)
d = 1.8e-006 (-4.422e-007, 4.042e-006)
e = -0.0003555 (-0.0004624, -0.0002486)

Goodness of fit:
SSE: 6.046e-012
R-square: 1
Adjusted R-square: 1
RMSE: 8.694e-007

[Harmonic 1] w=163.8

General model:
f(t) = exp(-a*t)+ (2*pi*a0)/(3*pi+c*t) + d*t+e
Coefficients (with 95% confidence bounds):
a = 9.238 (-198.1, 216.5)
a0 = 0.00554 (0.005281, 0.0058)
c = 2.943 (1.761, 4.125)
d = 2.208e-005 (8.513e-006, 3.565e-005)
e = -0.0008396 (-0.001263, -0.0004162)

Goodness of fit:
SSE: 1.266e-009
R-square: 0.9996
Adjusted R-square: 0.9994
RMSE: 1.258e-005

[Harmonic 12] w=1075

General model Exp1:
f(x) = a*exp(b*x)
Coefficients (with 95% confidence bounds):
a = 0.001679 (0.001579, 0.00178)
b = -0.6401 (-0.6718, -0.6084)

Goodness of fit:
SSE: 1.049e-009
R-square: 0.9985
Adjusted R-square: 0.9984
RMSE: 1.024e-005

[Harmonic 21] w=1849

General model Exp1:
f(x) = a*exp(b*x)
Coefficients (with 95% confidence bounds):
a = 0.002842 (0.002504, 0.003181)
b = -1.207 (-1.295, -1.119)

Goodness of fit:
SSE: 1.508e-009
R-square: 0.9979
Adjusted R-square: 0.9976
RMSE: 1.373e-005

[Harmonic 0] - Trying Different Functions for Best Curve-Fit

..Exponential
General model Exp1:
f(x) = a*exp(b*x)
Coefficients (with 95% confidence bounds):
a = 0.001343 (0.001283, 0.001404)
b = -0.07063 (-0.07639, -0.06487)

Goodness of fit:
SSE: 6.679e-009
R-square: 0.9912
Adjusted R-square: 0.9902
RMSE: 2.724e-005

...Linear
Linear model Poly1:
f(x) = p1*x + p2
Coefficients (with 95% confidence bounds):
p1 = -4.759e-005 (-5.621e-005, -3.898e-005)
p2 = 0.001185 (0.001087, 0.001282)

Goodness of fit:
SSE: 4.134e-008
R-square: 0.9455
Adjusted R-square: 0.9394
RMSE: 6.777e-005

...Aero
General model:
f(t) = (2*pi*a0)/(3*pi+c*t)
Coefficients (with 95% confidence bounds):
a0 = 0.002477 (0.002318, 0.002637)
c = 1.524 (1.323, 1.725)

Goodness of fit:
SSE: 4.338e-009
R-square: 0.9943
Adjusted R-square: 0.9936
RMSE: 2.195e-005

...Aero-Viscous
General model:

f(t) = a*exp(-b*t)+(2*pi*a0)/(3*pi+c*t)
Coefficients (with 95% confidence bounds):
a = 9.85 (-7.878e+008, 7.878e+008)
a0 = 0.002489 (0.00196, 0.003018)
b = 7.873 (-3.347e+007, 3.347e+007)
c = 1.603 (1.021, 2.184)

Goodness of fit:
SSE: 6.599e-009
R-square: 0.9913
Adjusted R-square: 0.9876
RMSE: 3.07e-005

...Aero-Viscous-Coul
General model:
f(t) = m*exp(-a*t)+ (2*pi*a0)/(3*pi+c*t) + d*t+e
Coefficients (with 95% confidence bounds):
a = 8 (-4.464e+007, 4.464e+007)
a0 = 0.002643 (-0.001475, 0.006761)
c = 1 (-2.244, 4.244)
d = 3.401e-007 (-6.625e-005, 6.693e-005)
e = -0.0002206 (-0.003631, 0.00319)
m = 1 (-1.066e+008, 1.066e+008)

Goodness of fit:
SSE: 7.517e-010
R-square: 0.999
Adjusted R-square: 0.998
RMSE: 1.226e-005

Curve fitting is not sensitive to c from 0.9-1.3 (d and e change moderately)

...General model:
f(t) = m*exp(-a*t)+ (2*pi*a0)/(3*pi+c*t) + d*t+e
Coefficients (with 95% confidence bounds):
a = 8 (-2.205e+007, 2.205e+007)
a0 = 0.002834 (-0.002219, 0.007887)
c = 0.9 (-2.011, 3.811)
d = 3.243e-006 (-7.125e-005, 7.774e-005)
e = -0.0003617 (-0.004343, 0.003619)
m = 1 (-5.265e+007, 5.265e+007)

Goodness of fit:
SSE: 7.653e-010

R-square: 0.999
Adjusted R-square: 0.998
RMSE: 1.237e-005

...General model:
f(t) = m*exp(-a*t)+ (2*pi*a0)/(3*pi+c*t) + d*t+e
Coefficients (with 95% confidence bounds):
a = 8 (-2.279e+007, 2.279e+007)
a0 = 0.002495 (-0.0009352, 0.005925)
c = 1.1 (-2.53, 4.73)
d = -2.062e-006 (-6.307e-005, 5.894e-005)
e = -0.0001089 (-0.003122, 0.002904)
m = 1 (-5.442e+007, 5.442e+007)

Goodness of fit:
SSE: 7.536e-010
R-square: 0.999
Adjusted R-square: 0.998
RMSE: 1.228e-005

...General model:
f(t) = m*exp(-a*t)+ (2*pi*a0)/(3*pi+c*t) + d*t+e
Coefficients (with 95% confidence bounds):
a = 8 (-4.687e+007, 4.687e+007)
a0 = 0.002379 (-0.0005192, 0.005277)
c = 1.2 (-2.873, 5.273)
d = -4.087e-006 (-6.108e-005, 5.291e-005)
e = -1.826e-005 (-0.002746, 0.00271)
m = 1 (-1.119e+008, 1.119e+008)

Goodness of fit:
SSE: 7.678e-010
R-square: 0.999
Adjusted R-square: 0.998
RMSE: 1.239e-005

...General model:
f(t) = m*exp(-a*t)+ (2*pi*a0)/(3*pi+c*t) + d*t+e
Coefficients (with 95% confidence bounds):
a = 8 (-4.843e+007, 4.843e+007)
a0 = 0.002286 (-0.0001808, 0.004753)
c = 1.3 (-3.274, 5.874)
d = -5.82e-006 (-5.988e-005, 4.824e-005)
e = 5.665e-005 (-0.00246, 0.002574)
m = 1 (-1.156e+008, 1.156e+008)

Goodness of fit:
SSE: 7.914e-010
R-square: 0.999
Adjusted R-square: 0.9979
RMSE: 1.258e-005

Curve fitting is not sensitive to m from 0.1-40 (d and e change slightly)

...General model:
f(t) = m*exp(-a*t)+ (2*pi*a0)/(3*pi+c*t) + d*t+e
Coefficients (with 95% confidence bounds):
a = 8
a0 = 0.002149
c = 1.5
d = -8.634e-006
e = 0.0001732
m = 0.1

Goodness of fit:
SSE: 8.591e-010
R-square: 0.9989
Adjusted R-square: 0.9977
RMSE: 1.311e-005

...General model:
f(t) = m*exp(-a*t)+ (2*pi*a0)/(3*pi+c*t) + d*t+e
Coefficients (with 95% confidence bounds):
a = 8 (-5.21e+007, 5.21e+007)
a0 = 0.002149 (0.000364, 0.003934)
c = 1.5 (-4.253, 7.253)
d = -8.634e-006 (-5.889e-005, 4.162e-005)
e = 0.0001732 (-0.002061, 0.002408)
m = 0.5 (-6.219e+007, 6.219e+007)

Goodness of fit:
SSE: 8.592e-010
R-square: 0.9989
Adjusted R-square: 0.9977
RMSE: 1.311e-005

...General model:
f(t) = m*exp(-a*t)+ (2*pi*a0)/(3*pi+c*t) + d*t+e
Coefficients (with 95% confidence bounds):
a = 8 (-2.605e+007, 2.605e+007)

a0 = 0.002149 (0.000364, 0.003934)
c = 1.5 (-4.254, 7.254)
d = -8.634e-006 (-5.889e-005, 4.163e-005)
e = 0.0001733 (-0.002061, 0.002408)
m = 1 (-6.219e+007, 6.219e+007)

Goodness of fit:
SSE: 8.592e-010
R-square: 0.9989
Adjusted R-square: 0.9977
RMSE: 1.311e-005

...General model:
f(t) = m*exp(-a*t)+ (2*pi*a0)/(3*pi+c*t) + d*t+e
Coefficients (with 95% confidence bounds):
a = 8 (-1.303e+007, 1.303e+007)
a0 = 0.002149 (0.0003634, 0.003935)
c = 1.5 (-4.255, 7.255)
d = -8.635e-006 (-5.891e-005, 4.164e-005)
e = 0.0001733 (-0.002062, 0.002408)
m = 4 (-1.245e+008, 1.245e+008)

Goodness of fit:
SSE: 8.597e-010
R-square: 0.9989
Adjusted R-square: 0.9977
RMSE: 1.311e-005

...General model:
f(t) = m*exp(-a*t)+ (2*pi*a0)/(3*pi+c*t) + d*t+e
Coefficients (with 95% confidence bounds):
a = 8 (-4.345e+006, 4.345e+006)
a0 = 0.002149 (0.0003624, 0.003935)
c = 1.5 (-4.259, 7.259)
d = -8.638e-006 (-5.893e-005, 4.166e-005)
e = 0.0001734 (-0.002063, 0.00241)
m = 10 (-1.038e+008, 1.038e+008)

Goodness of fit:
SSE: 8.605e-010
R-square: 0.9989
Adjusted R-square: 0.9977
RMSE: 1.312e-005

...General model:
f(t) = m*exp(-a*t)+ (2*pi*a0)/(3*pi+c*t) + d*t+e

Coefficients (with 95% confidence bounds):
a = 8 (-9.067e+006, 9.067e+006)
a0 = 0.002148 (0.0003572, 0.003939)
c = 1.5 (-4.275, 7.275)
d = -8.652e-006 (-5.907e-005, 4.176e-005)
e = 0.0001738 (-0.002068, 0.002415)
m = 40 (-8.667e+008, 8.667e+008)

Goodness of fit:
SSE: 8.646e-010
R-square: 0.9989
Adjusted R-square: 0.9977
RMSE: 1.315e-005

Curve Fitting is not sensitive to a from 7-40

...General model:
f(t) = m*exp(-a*t)+ (2*pi*a0)/(3*pi+c*t) + d*t+e
Coefficients (with 95% confidence bounds):
a = 7 (-3.894e+006, 3.894e+006)
a0 = 0.001979 (0.001192, 0.002766)
c = 2 (-7.737, 11.74)
d = -1.318e-005 (-5.958e-005, 3.321e-005)
e = 0.0003506 (-0.001552, 0.002253)
m = 0.8892 (-8.271e+006, 8.271e+006)

Goodness of fit:
SSE: 1.095e-009
R-square: 0.9986
Adjusted R-square: 0.9971
RMSE: 1.48e-005

...General model:
f(t) = m*exp(-a*t)+ (2*pi*a0)/(3*pi+c*t) + d*t+e
Coefficients (with 95% confidence bounds):
a = 8 (-6.285e+007, 6.285e+007)
a0 = 0.001979 (0.001192, 0.002766)
c = 2 (-7.73, 11.73)
d = -1.319e-005 (-5.954e-005, 3.317e-005)
e = 0.0003506 (-0.00155, 0.002252)
m = 0.8892 (-1.335e+008, 1.335e+008)

Goodness of fit:
SSE: 1.094e-009
R-square: 0.9986
Adjusted R-square: 0.9971
RMSE: 1.479e-005

...General model:
f(t) = m*exp(-a*t)+ (2*pi*a0)/(3*pi+c*t) + d*t+e
Coefficients (with 95% confidence bounds):
a = 9
a0 = 0.001979
c = 2
d = -1.319e-005
e = 0.0003506
m = 0.8892

Goodness of fit:
SSE: 1.094e-009
R-square: 0.9986
Adjusted R-square: 0.9971
RMSE: 1.479e-005

...General model:
f(t) = m*exp(-a*t)+ (2*pi*a0)/(3*pi+c*t) + d*t+e
Coefficients (with 95% confidence bounds):
a = 10
a0 = 0.001979
c = 2
d = -1.319e-005
e = 0.0003506
m = 0.8892

Goodness of fit:
SSE: 1.094e-009
R-square: 0.9986
Adjusted R-square: 0.9971
RMSE: 1.479e-005

...General model:
f(t) = m*exp(-a*t)+ (2*pi*a0)/(3*pi+c*t) + d*t+e
Coefficients (with 95% confidence bounds):
a = 11
a0 = 0.001979
c = 2
d = -1.319e-005
e = 0.0003506

m = 0.8892

Goodness of fit:
SSE: 1.094e-009
R-square: 0.9986
Adjusted R-square: 0.9971
RMSE: 1.479e-005

...General model:
f(t) = m*exp(-a*t)+ (2*pi*a0)/(3*pi+c*t) + d*t+e
Coefficients (with 95% confidence bounds):
a = 12
a0 = 0.001979
c = 2
d = -1.319e-005
e = 0.0003506
m = 0.8892

Goodness of fit:
SSE: 1.094e-009
R-square: 0.9986
Adjusted R-square: 0.9971
RMSE: 1.479e-005

...General model:
f(t) = m*exp(-a*t)+ (2*pi*a0)/(3*pi+c*t) + d*t+e
Coefficients (with 95% confidence bounds):
a = 20
a0 = 0.001979
c = 2
d = -1.319e-005
e = 0.0003506
m = 0.8892

Goodness of fit:
SSE: 1.094e-009
R-square: 0.9986
Adjusted R-square: 0.9971
RMSE: 1.479e-005

...General model:
f(t) = m*exp(-a*t)+ (2*pi*a0)/(3*pi+c*t) + d*t+e
Coefficients (with 95% confidence bounds):
a = 40
a0 = 0.001979
c = 2

d = -1.319e-005
e = 0.0003506
m = 0.8892

Goodness of fit:
SSE: 1.094e-009
R-square: 0.9986
Adjusted R-square: 0.9971
RMSE: 1.479e-005

Appendix I. SDOF Model Matching

OBJECTIVE: Using the decay envelopes from Smith and Werely (1999), obtain the damping coefficients for each harmonic of the BW056 string.

Smith and Werely gave the following decay envelopes for a SDOF spring-mass-damper system with three different types of damping:

	Equation of motion	*Decay Envelope*
Viscous Damping:	$x''(t) + 2\zeta\cdot\omega\cdot x'(t) + \omega^2\cdot x(t) = 0$	$a_v(t) = e^{-\zeta\cdot\omega\cdot t}$
Aerodynamic Damping:	$x''(t) + \varepsilon\cdot\lvert x(t)\rvert\cdot x'(t) + \omega^2\cdot x(t) = 0$	$a_a(t) = \frac{2\cdot\pi\cdot a_0}{3\cdot\pi + 4\cdot\varepsilon\cdot\omega\cdot t}$
Coulomb Damping:	$x''(t) + \mu\cdot\mathrm{sign}(x'(t)) + \omega^2\cdot x(t) = 0$	$a_c(t) = \frac{-2\cdot\mu}{\pi\cdot\omega}\cdot t + y_0$

Recall that for multiple types of damping, the resulting decay envelope is a linear summation of these individual decay functions.

BW056 - Open Air - Fundamental Frequency

$\omega_0 := 81.882\pi$ Fundamental frequency of the BW056 string $\omega := \omega_0$

Best Curve-Fit from data is Aerodynamic + Coulomb Damping:

$a := 7.02$ $a_0 := 0.00297$ $c := 0.8$ $d := 5.291\cdot10^{-6}$ $f := -0.000465$

$f_0(t) := e^{-a\cdot t} + \frac{2\cdot\pi\cdot a_0}{3\cdot\pi + c\cdot t} + d\cdot t + f$ $R^2 = 0.999$ $\varepsilon := \frac{c}{4\cdot\omega}$ $\varepsilon = 4.082\times10^{-4}$

$\mu := \frac{-\pi\cdot\omega\cdot d}{2}$ $\mu = -4.275\times10^{-3}$

scaling the damping coefficients $\zeta := \frac{a}{\omega}$ $\zeta = 0.014$

$\varepsilon_0 := 600\varepsilon$ $\mu_0 := \frac{\lvert\mu\rvert}{175}$ $\zeta_0 := \frac{\zeta}{245}$ $n := 15000$

Given

$x(0) = f_0(0) - 1$ $x'(0) = 0$

$x''(t) + 2\cdot\zeta_0\cdot\omega\cdot x'(t) + \varepsilon_0\cdot\lvert x(t)\rvert\cdot x'(t) + \mu_0\cdot\mathrm{sign}(x'(t)) + \omega^2\cdot x(t) = 0$

$x_0 := \mathrm{Odesolve}(t, 20, n)$

$t := 0, \frac{20}{n}..20$

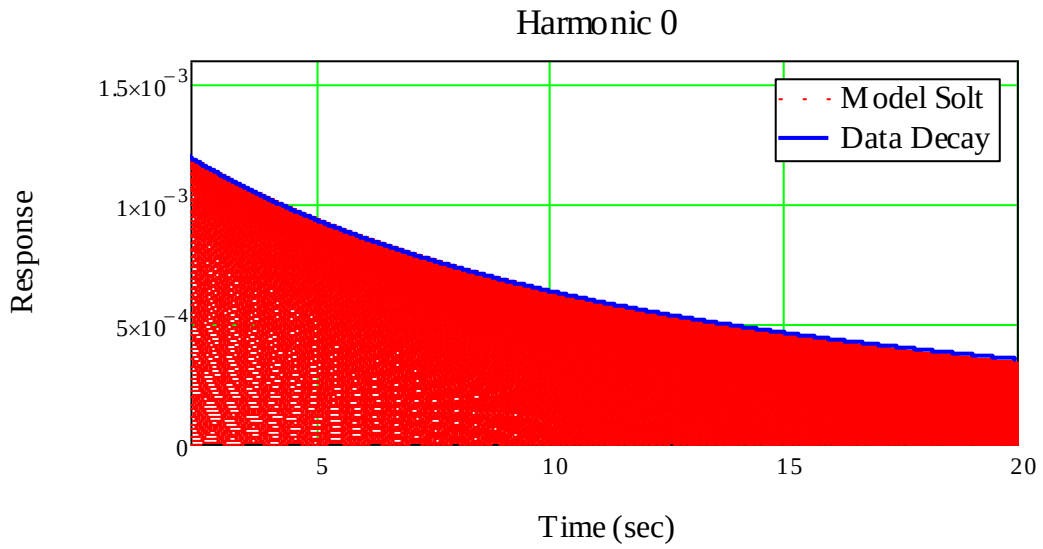

Note: the first fitted data point was at t=2.4

	Aerodynamic	Coulomb	Viscous
Calculated Damping Coefficients:	$\varepsilon = 4.082\times 10^{-4}$	$\mu = -4.275\times 10^{-3}$	$\zeta = 0.014$
Scaled Damping Coefficients:	$\varepsilon_0 = 0.245$	$\mu_0 = 2.443\times 10^{-5}$	$\zeta_0 = 5.573\times 10^{-5}$

Export the data to Matlab to curve-fit the response of the model, then calculate the error between the two fits.

t =
19.999
19.999
19.999
19.999
20
20
20
...

$x_0(t)$ =
$-3.374\cdot10^{-4}$
$-3.321\cdot10^{-4}$
$-3.253\cdot10^{-4}$
$-3.17\cdot10^{-4}$
$-3.072\cdot10^{-4}$
$-2.959\cdot10^{-4}$
$-2.832\cdot10^{-4}$
...

Model Decay Profile:

$a := 19.3$ $a_0 := 0.00280$ $c := .858$ $d := 1.810^{-6}$ $f := -0.000355$

$f_{0m}(t) := e^{-a \cdot t} + \frac{2 \cdot \pi \cdot a_0}{3 \cdot \pi + c \cdot t} + d \cdot t + f$ $R^2 = 0.999$ $\varepsilon_{0m} := \frac{c}{4 \cdot \omega}$ $\varepsilon = 4.082 \times 10^{-4}$

$\mu_{0m} := \frac{-\pi \cdot \omega \cdot d}{2}$ $\mu = -4.275 \times 10^{-3}$

$\zeta_{0m} := \frac{a}{\omega}$ $\zeta = 0.014$

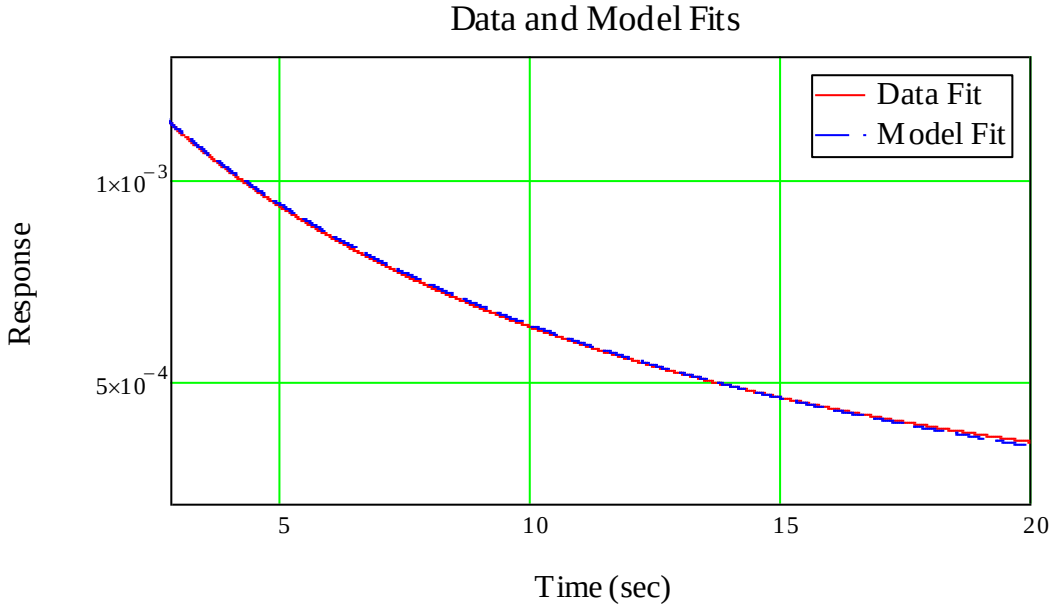

Ratio of the area between the curves to the area underneath the decay profile.

$$E := \sum_{n=0}^{20} \frac{\left(f_0(n) - f_{0m}(n)\right)^2}{f_0(n)} \qquad E = 3.532 \times 10^{-4}$$

Compare the differences between the calculated damping coefficients and the model damping coefficients.

$E_{\varepsilon 0} := \left| \frac{\varepsilon - \varepsilon_{0m}}{\varepsilon} \right| \cdot 100$ $E_{\varepsilon 0} = 2.155$

$\varepsilon = 4.082 \times 10^{-4}$ calculated from the fitted data

$\varepsilon_{0m} = 4.17 \times 10^{-4}$ calculated from the fitted model

$E_{\mu 0} := \left| \frac{\mu - \mu_{0m}}{\mu} \right| \cdot 10($ $E_{\mu 0} = 65.974$ $\mu = -4.275 \times 10^{-3}$ calculated from the fitted data

$\mu_{0m} = -1.455 \times 10^{-3}$ calculated from the fitted model

$E_{\zeta 0} := \left| \frac{\zeta - \zeta_{0m}}{\zeta} \right| \cdot 10($ $E_{\zeta 0} = 175.018$ $\zeta = 0.014$ calculated from the fitted data

$\zeta_{0m} = 0.038$ calculated from the fitted model